TECHNICAL REPORT

Naval Facilities Engineering Service Center, Port Hueneme, CA 93043-4328

TR-2019-ENV

May 1994

by: C. A. Kodres

Sponsored by:
Office of Naval Research

MOISTURE INDUCED PRESSURES IN CONCRETE AIRFIELD PAVEMENTS

ABSTRACT The erosion of military concrete airfield pavements by jet exhausts is an expensive problem expected to get worse. Scaling of pavements is being observed beneath the auxiliary power units (APUs) of F/A-18 and B-1 aircraft. The AV-8B Harrier and future vertical takeoff and landing aircraft will generate a concrete environment much more severe than that generated by the low power APUs.

In order to develop pavements impervious to this form of erosion, the failure mechanism must be known. One plausible culprit, suggested by the apparent role of heating, is moisture. To examine this hypothesis, a mathematical model was developed to predict pore pressures caused by water vapor and air migrating through the pores of a heated section of concrete.

The foundation of this model is a constitutive relationship developed to characterize the flow of high velocity, compressible, heated gases through concrete. This relationship equates a nondimensional flow parameter with pressure and temperature ratios across the medium. The key premise is that the resistance to flow through a high resistance porous medium can be modeled with friction coefficients analogous to the method used for simpler geometries.

Pore pressures predicted using this model show that moisture in the pores of the cement is unlikely to be the primary cause of material failure in airfield pavements heated by the F/A-18 APU. Moisture is a probable cause of failure, however, when the cement is being heated by the exhaust of a Harrier during takeoff and landing. For an initial pore saturation of 90 percent or greater, extremely high pore pressures and pressure gradients result from air being compressed by the thermal expansion of liquid water. Concrete temperatures beneath a VSTOL reach 300°C in about 2 minutes. For a lesser pore saturation, the water vapor pressure could eventually be sufficient to cause a tensile failure in Portland cement concrete.

METRIC CONVERSION FACTORS

Approximate Conversions to Metric Measures

Symbol	When You Know	Multiply by	To Find	Symbol
		LENGTH		
in	inches	*2.5	centimeters	cm
ft	feet	30	centimeters	cm
yd	yards	0.9	meters	m
mi	miles	1.6	kilometers	km
		AREA		
in^2	square inches	6.5	square centimeters	cm^2
ft^2	square feet	0.09	square meters	m^2
yd^2	square yards	0.8	square meters	m^2
mi^2	square miles	2.6	square kilometers	km^2
	acres	0.4	hectares	ha
		MASS (weight)		
oz	ounces	28	grams	g
lb	pounds	0.45	kilograms	kg
	short tons (2,000 lb)	0.9	tonnes	t
		VOLUME		
tsp	teaspoons	5	milliliters	ml
Tbsp	tablespoons	15	milliliters	ml
fl oz	fluid ounces	30	milliliters	ml
c	cups	0.24	liters	l
pt	pints	0.47	liters	l
qt	quarts	0.95	liters	l
gal	gallons	3.8	liters	l
ft^3	cubic feet	0.03	cubic meters	m^3
yd^3	cubic yards	0.76	cubic meters	m^3
		TEMPERATURE (exact)		
°F	Fahrenheit temperature	5/9 (after subtracting 32)	Celsius temperature	°C

*1 in = 2.54 (exactly). For other exact conversions and more detailed tables, see NBS Misc. Publ. 286, Units of Weights and Measures, Price $2.25, SD Catalog No. C13.10:286.

Approximate Conversions from Metric Measures

Symbol	When You Know	Multiply by	To Find	Symbol
		LENGTH		
mm	millimeters	0.04	inches	in
cm	centimeters	0.4	inches	in
m	meters	3.3	feet	ft
m	meters	1.1	yards	yd
km	kilometers	0.6	miles	mi
		AREA		
cm^2	square centimeters	0.16	square inches	in^2
m^2	square meters	1.2	square yards	yd^2
km^2	square kilometers	0.4	square miles	mi^2
ha	hectares (10,000 m^2)	2.5	acres	
		MASS (weight)		
g	grams	0.035	ounces	oz
kg	kilograms	2.2	pounds	lb
t	tonnes (1,000 kg)	1.1	short tons	
		VOLUME		
ml	milliliters	0.03	fluid ounces	fl oz
l	liters	2.1	pints	pt
l	liters	1.06	quarts	qt
l	liters	0.26	gallons	gal
m^3	cubic meters	35	cubic feet	ft^3
m^3	cubic meters	1.3	cubic yards	yd^3
		TEMPERATURE (exact)		
°C	Celsius temperature	9/5 (then add 32)	Fahrenheit temperature	°F

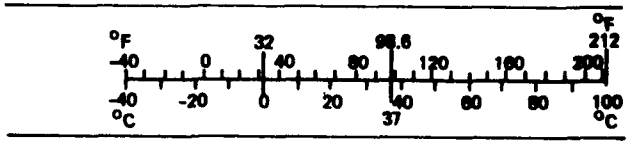

PREFACE

On 1 October 1993, the Naval Civil Engineering Laboratory (NCEL) and the Naval Energy and Environmental Support Activity (NEESA) were consolidated with four other Naval Facilities Engineering Command (NAVFAC) components into the Naval Facilities Engineering Service Center (NFESC). Due to publishing timeframes, this document may have references to NEESA or NCEL instead of NFESC.

REPORT DOCUMENTATION PAGE

Form Approved
OMB No. 0704-018

1. AGENCY USE ONLY (Leave blank)	2. REPORT DATE	3. REPORT TYPE AND DATES COVERED
	May 1994	Final, 1 Oct 1990 - 30 Sep 1993

4. TITLE AND SUBTITLE

MOISTURE INDUCED PRESSURES IN CONCRETE AIRFIELD PAVEMENTS

5. FUNDING NUMBERS

PR - R000-NO-211
WU - DN661002

6. AUTHOR(S)

C. A. Kodres

7. PERFORMING ORGANIZATION NAME(S) AND ADDRESSE(S)

Naval Facilities Engineering Service Center
560 Center Drive
Port Hueneme, CA 93043-4328

8. PERFORMING ORGANIZATION REPORT NUMBER

TR-2019-ENV

9. SPONSORING/MONITORING AGENCY NAME(S) AND ADDRESSES

Office of Naval Research
Arlington, VA 22217-5000

10. SPONSORING/MONITORING AGENCY REPORT NUMBER

11. SUPPLEMENTARY NOTES

12a. DISTRIBUTION/AVAILABILITY STATEMENT

Approved for public release; distribution is unlimited.

12b. DISTRIBUTION CODE

13. ABSTRACT *(Maximum 200 words)*

The erosion of military concrete airfield pavements by jet exhausts is an expensive problem expected to get worse. Scaling of pavements is being observed beneath the auxiliary power units (APUs) of F/A-18 and B-1 aircraft. The AV-8B Harrier and future vertical takeoff and landing aircraft will generate a concrete environment much more severe than that generated by the low power APUs.

In order to develop pavements impervious to this form of erosion, the failure mechanism must be known. One plausible culprit, suggested by the apparent role of heating, is moisture. To examine this hypothesis, a mathematical model was developed to predict pore pressures caused by water vapor and air migrating through the pores of a heated section of concrete.

The foundation of this model is a constitutive relationship developed to characterize the flow of high velocity, compressible, heated gases through concrete. This relationship equates a nondimensional flow parameter with pressure and temperature ratios across the medium. The key premise is that the resistance to flow through a high resistance porous medium can be modeled with friction coefficients analogous to the method used for simpler geometries.

Pore pressures predicted using this model show that moisture in the pores of the cement is unlikely to be the primary cause of material failure in airfield pavements heated by the F/A-18 APU. Moisture is a probable cause of failure, however, when the cement is being heated by the exhaust of a Harrier during takeoff and landing. For an initial pore saturation of 90 percent or greater, extremely high pore pressures and pressure gradients result from air being compressed by the thermal expansion of liquid water. Concrete temperatures beneath a VSTOL reach 300°C in about 2 minutes. For a lesser pore saturation, the water vapor pressure could eventually be sufficient to cause a tensile failure in portland cement concrete.

14. SUBJECT TERMS	15. NUMBER OF PAGES
Concrete, moisture, erosion of airfield pavements, computer program	103
	16. PRICE CODE

17. SECURITY CLASSIFICATION OF REPORT	18. SECURITY CLASSIFICATION OF THIS PAGE	19. SECURITY CLASSIFICATION OF ABSTRACT	20. LIMITATION OF ABSTRACT
Unclassified	Unclassified	Unclassified	UL

CONTENTS

INTRODUCTION

Scaling of U.S. Navy and Marine Corps concrete airfield parking and run-up aprons is becoming a multimillion dollar problem. A scaling airfield pavement is an immediate threat to jet engines, generating loose cement and aggregate that is easily ingested.

The age of the failing pavements ranges from a few years to over 15 years. Yet, the damage has been observed only recently, always following the arrival of the F/A-18. Figures 1 and 2 show examples of run-up apron scaling. This particular damage occurred at the Naval Air Station (NAS) North Island, California.

Unlike its predecessors, the auxiliary power unit (APU) of the F/A-18 tilts away from the aircraft centerline. The APU is a low power gas turbine that provides compressed air, from a load driven compressor, for starting the main engines and for operating auxiliary systems during ground maintenance. Exhaust from the APU strikes the pavement at about a 45-degree angle approximately below the tail section of the plane as illustrated in Figure 3.

While starting the main engines, the APU nozzle velocity reaches about 125 m/sec at a temperature slightly above 500°C (Houck, 1990). The concrete surface is heated to roughly 100°C during a 30-second main engine start (Houck, 1990; Bier et al., 1991; Houck et al., 1992). A typical run-up apron is subjected to the APU blast three to five times a day, five days a week, throughout the year. During ground maintenance, the APU runs for a much longer duration.

Failure does not happen immediately, nor does it occur explosively. Scaling occurs slowly, beginning in those areas that have the most usage. The depth and extent of the damage varies with the location of the airfield. In general, scaling occurs to the top 1/2 to 1 cm of the pavement. The extent of the damage ranges from only a few square centimeters up to an area of more than 2 meters in diameter. With only one exception, scaling is limited to the cement; at NAS Cecil Field, Florida, fracturing occurred through some of the limestone aggregates.

Future erosion problems will be more severe. The APU exhaust temperature of the new A-12 attack aircraft is about 40°C hotter than the APU of the F/A-18. V-22 tiltrotor jets will strike the pavement at temperatures in excess of 500°C. The AV-8B Harrier and future vector thrust aircraft will generate a concrete environment much more severe than that induced by the relatively low velocity, low temperature APUs. Perhaps the main runways will be affected.

The damage suggests a fatigue failure (Houck, 1990). Failure mechanisms involving chemical degradation of the cement are also being proposed (McVay et al., 1993). The most plausible cause of the scaling, however, is the simplest. These same failure characteristics would be present if the tensile strength of the concrete was being exceeded intermittently, and in very small regions, by the thermal expansion of water or some other fluid trapped in the pores of the concrete. This report discusses the theoretical and experimental examination of this hypothesis.

Cement Pore Structure

The term concrete as used in this work can be interpreted to mean a mixture of portland cement, water, and some inert mineral aggregate. Portland cement is a calcium silicate compound predominantly containing tricalcium and dicalcium silicates. The development of strength is the result of chemical reactions between the cement silicates and the added water,

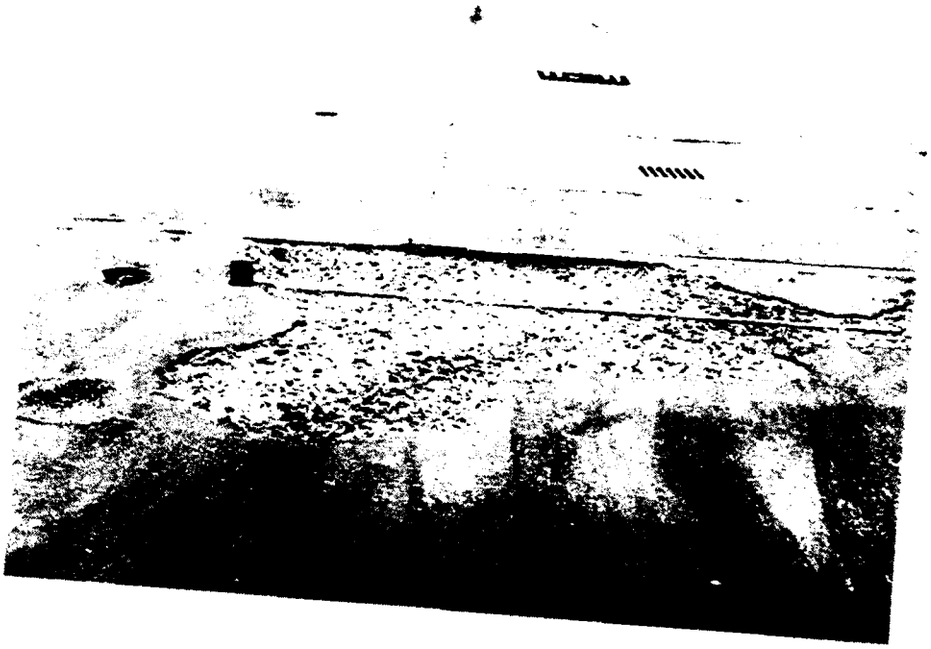

Figure 1
Pavement scaling due to F/A-18 exhaust at NAS North Island.

Figure 2
Close-up of NAS North Island damage.

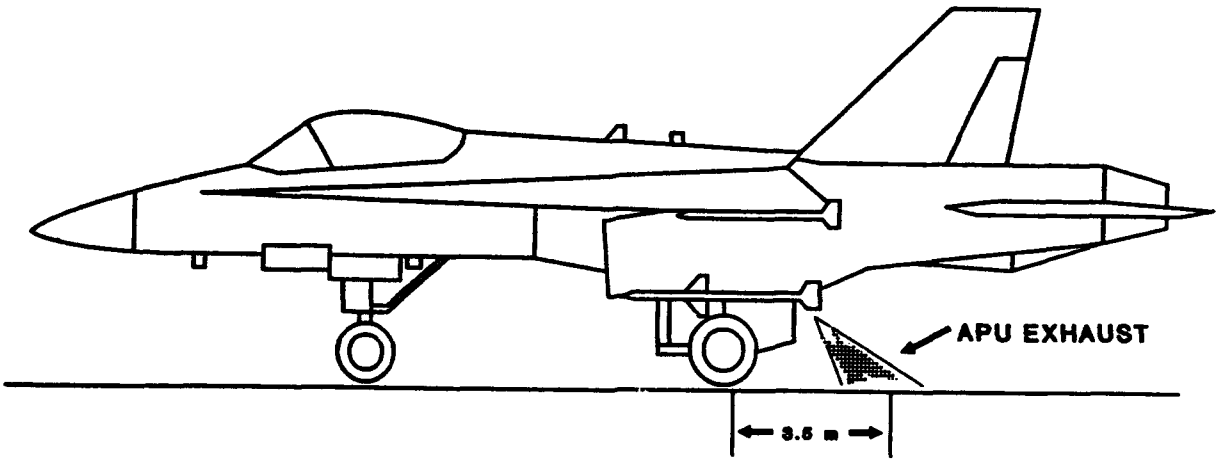

Figure 3
F/A-18 APU exhaust profile.

forming a fibrillar calcium-silicate-hydrate gel (Collepardi, 1973; Neville, 1973; Double and Hellawell, 1977). Aggregate, which is cheaper than the cement, was originally dispersed throughout the cement paste for economic reasons (Neville, 1973). Aggregate is not completely inert, however, and it is equally plausible to view concrete as an aggregate framework held together by the cement paste.

Pores formed in the cement are initially either water or gas filled. As the cement and water react, the resulting mixture expands into the volume originally filled with water. The final volume of the cement paste is less than the sum of the original volumes of cement and water (Verbeck, 1966). Voids remain in the concrete, called capillary pores to differentiate from the smaller pores inherent in the gel. Some of these pores remain filled with water.

Water reacting with the cement is usually designated "non-evaporable" to distinguish from evaporable, or free, water. About 20 percent of the weight of fully hydrated portland cement is non-evaporable water (Powers, 1949; Harmathy and Berndt, 1966; Neville, 1973). Evaporable water is primarily water in capillary and gel pores but also includes adsorbed water (Lankard et al., 1971) so the distinction is largely for reference. Much of the evaporable water in concrete was part of the original mix, and is a function of mix conditions such as temperature, water-cement ratio, and degree of hydration. Evaporable water is also transferred to and from the environment, the mass transfer induced by humidity and rainfall. Thus, the amount of evaporable water in cement or concrete is highly variable. Without including rainfall, values around 5 percent by weight are representative (Copeland and Hayes, 1953).

The porosity of cement is largely a function of the initial evaporable water. Cement is porous. The gel porosity of hardened portland cement reaches about 28 percent (Powers, 1949), and, although capillary pores should eventually disappear if the original water-cement ratio is not above approximately 0.39 by weight (Powers, 1949), even cement mixed under optimum conditions will contain some capillary pores. For a fully hydrated cement paste mixed with a water-cement ratio of 0.4, Diamond (1973) measured a total porosity of about 37 percent. If the aggregate is included, porosities are commonly in the range 6 to 10 percent (Dullien, 1979).

Figure 4 is a pore size distribution of Secar 250 hydrated cement measured by M. Jung (1973) using mercury penetration (Winslow and Diamond, 1970; Auskern and Horn, 1973). At 100°C, pore radii range between 10^{-5} and 10^{-3} mm with the largest total volume of pores formed with a radius between 10^{-4} and 10^{-3} mm. Other published pore distributions are of the same orders of magnitude (Verbeck, 1966; Diamond, 1973; Chekhovsky et al., 1973). Figure 5 is perhaps more enlightening. It shows pore distribution in terms of number of pores rather than pore volume. Gel pores are by far the most numerous, formed with a radius less than 10^{-5} mm.

As would be expected from the way pores are formed, intrusion measurements show both porosity and average pore size to increase with an increase in the water-cement mix ratio and to decrease with hydration time (Diamond, 1973; Jung, 1973). The average pore size decreases with increase in the curing temperature (Chekhovsky et al., 1973) although not significantly (Diamond, 1973).

Cement also contains voids formed from air, accidently trapped or purposely entrained, dispersed throughout the cement paste. These voids range in size up to a maximum of about 2 mm (Verbeck, 1966).

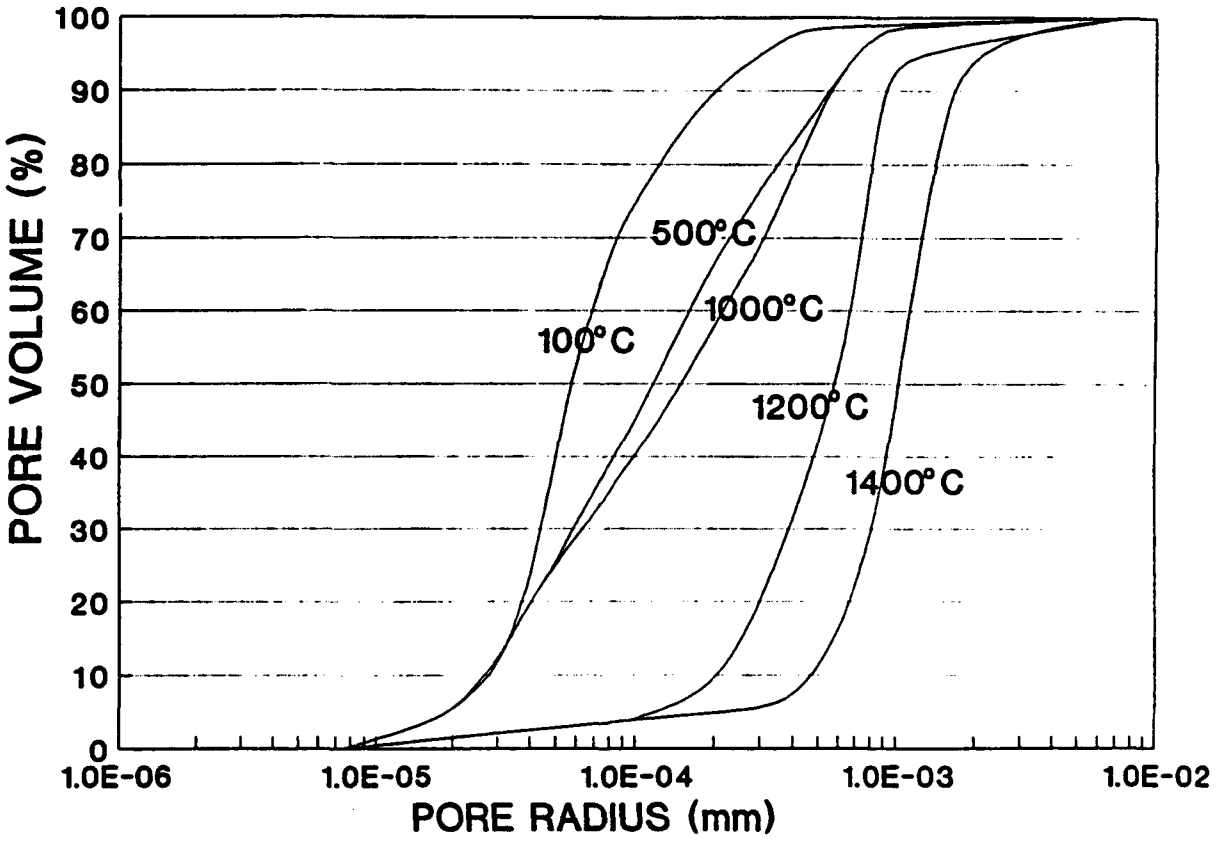

Figure 4
Pore size distribution of secar 250 hydrated cement
as a function of firing temperature (Jung, 1973).

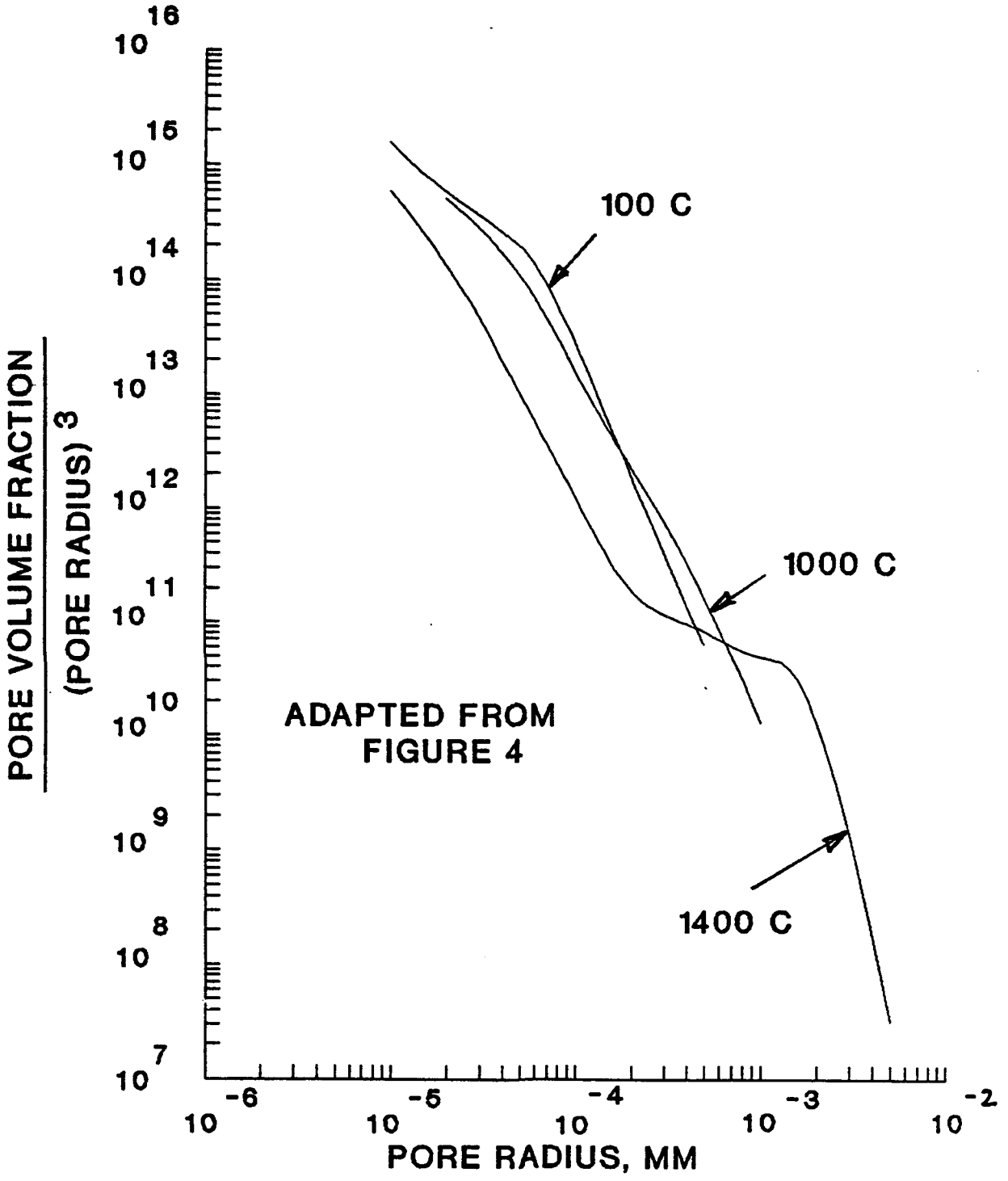

Figure 5
Number of pores in cement at different temperatures.

Cement is porous, yet, the permeability[1] of even moderate quality portland cement is very low. Most of the porosity is accounted for by the very small gel pores (see Figure 4). Capillary pores are much fewer in number and spread throughout the cement. The dominant resistance to flow is the resistance provided by the smaller pores. Therefore, mix conditions that affect pore size distribution will also affect permeability. For example, permeability of cement paste is increased approximately a thousandfold by an increase in water-cement ratio from 0.4 to 0.8; permeability is decreased approximately a thousandfold between the curing ages of 7 days and 1 year (Verbeck, 1966).

The pore structure of fully hydrated portland cement is altered by heating. Hydrated cement dehydrates at higher temperatures, 100°C to perhaps 500°C, and the total pore volume which had been decreasing with hydration, increases again (Jung, 1973). Bazant and Thonguthal (1978) have observed that the permeability of concrete to water increases over two orders of magnitude between 95°C and 105°C. They attribute this increase to evaporation plus a "smoothing" of the pore necks providing the dominant resistance. Further heating can be expected to induce hydrate phase transformations and the formation of new mineral phases. Above 1,000°C, with beginning sintering, smaller pores combine to form larger pores (Jung, 1973) as shown in Figure 5.

Thermodynamics of Pore Moisture

Consider a single isolated concrete capillary pore such as illustrated in Figure 6. To simplify explanation of the behavior of pore moisture when heated, suppose, for the moment, this pore contains only water and water vapor. Assume the water, its vapor, and the surrounding cement are in equilibrium. Finally, neglect any effects that temperature or pressure might have on the pore dimensions; the volume of this pore remains constant.

When water trapped in these pores is heated, the quality of the liquid-vapor mixture is changed. The net phase change can go in either direction, depending upon the initial liquid and vapor fractions in the pore (i.e., on the initial quality of the liquid-vapor mixture). The phenomena is best shown on the pressure-volume (P-V) diagram for water (Figure 7). If there is very little liquid water in the pore (a high specific volume of the contents of the pore), heating the concrete will evaporate the remaining water, leaving only the saturated vapor. Further increases in temperature will superheat the vapor. Shown on the P-V diagram, the mixture in the pore is changing from the state at A1 to the state at A2. Conversely, if the pore is nearly filled with liquid water (a low specific volume), heating the concrete will expand the liquid phase faster than it is being vaporized. The pore becomes filled with the saturated liquid phase. Further heating compresses the water. This process is illustrated on the P-V diagram by a change from state B1 to state B2. With less heating, both water and vapor, in equilibrium, remain in the pore, and the pressure of the liquid is equal to its vapor pressure. Observe that, at any given temperature, the pressure of the compressed liquid is much higher than the vapor pressure or the pressure of the superheated vapor. Figure 7, which is not drawn to scale, does not accurately show the tremendous pressures generated when water is compressed in this manner.

---

[1]Constant proportional to flow through porous media, see Equation 1.

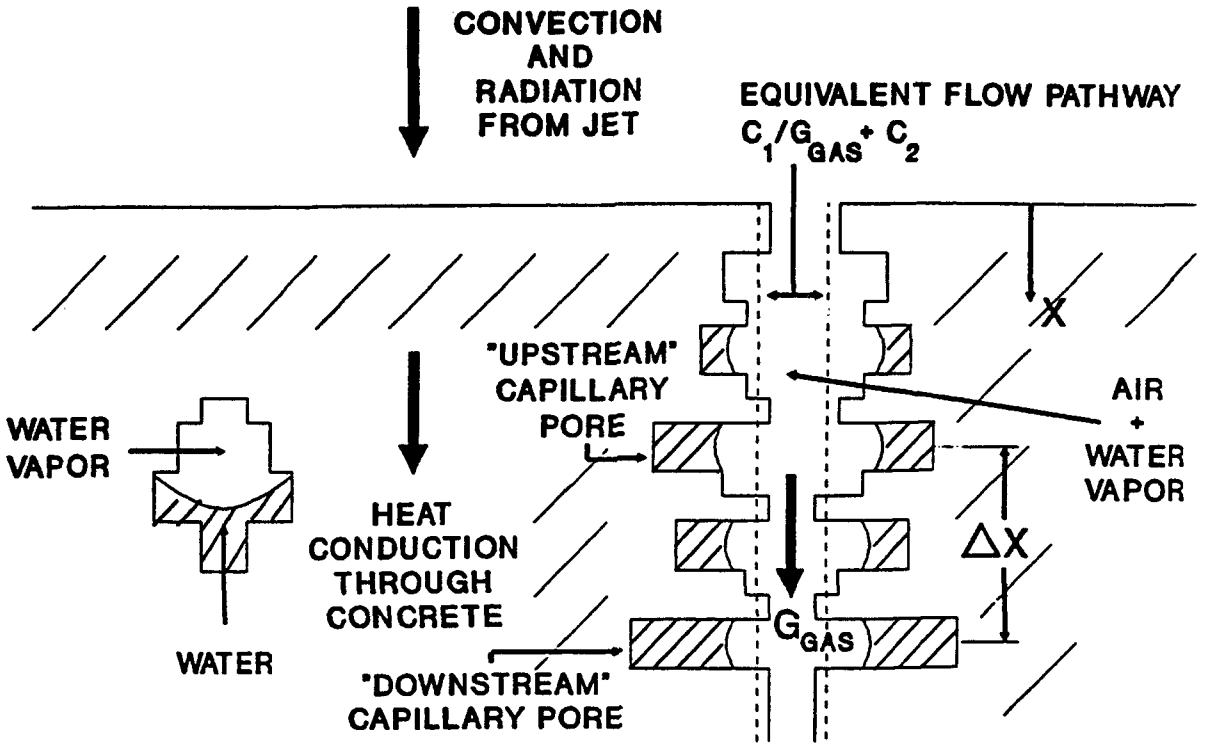

Figure 6
Concrete pores are heated by an impinging jet.

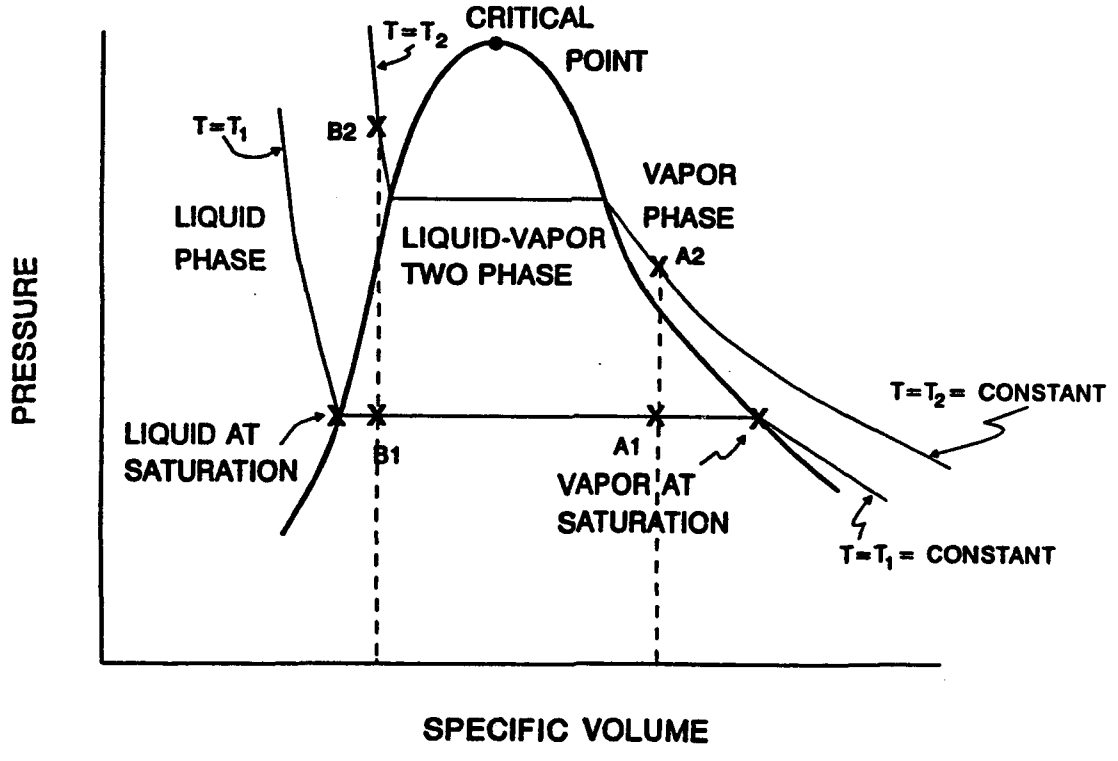

Figure 7
Pressure-volume diagram for water.

Recall that no transport of water between pores was allowed. If the pores are connected, which they normally are, the specific volume of the water in the pores will change, illustrated, for example, by a change of state from B1 to A2 on the P-V diagram. Furthermore, if the pore is near the surface of the cement, the gas pressure inside the pore could be less than the saturation pressure of the water. Under these conditions, the water would boil.

Also recall that the pore was assumed to contain only water. Air is present in the pores of cement and has a major influence on pore pressure. The solubility of air in water is low. Therefore, when heated, water does not expand into the gas phase as it does if only water vapor is present. Air acts as a shock absorber; the water expands against the mass of the air rather than against the solid walls of the pore. The pore pressure will never reach the magnitudes it would if only water were present. However, compression of the liquid phase occurs with less water in the pores.

The effect of air on pore pressure is illustrated by Figures 8 and 9. These figures were developed by assuming:

1. Air is an ideal gas; air is insoluble in water.

2. Liquid water is in equilibrium with its vapor.

3. Completely mixed gases and water.

4. Air and water vapor occupy the same space only.

5. No capillary effects.

6. No deformation of the pore other than thermal expansion.

Curve fits of the Steam Table data (Keenan and Keyes, 1936) were used as equations of state for water and water vapor. The equations of state for air and water were solved simultaneously for pressures while conserving the mass of water plus water vapor and the mass of air and constraining the total volume of the pore.

In Figure 8, a closed cement pore has been heated from 15°C up to 180°C. The fraction of pore volume occupied by liquid water (percent of saturation) when the cement was cold is used as the independent variable. Pore pressure, the dependent variable, is the sum of the air and water vapor pressures, or equivalently, since capillarity is being neglected, the pressure of the liquid water phase.

As more water is enclosed by the pore, the decrease in air volume due to the expansion of the water becomes fractionally more significant, and the air compression increases. As the pore approaches 100 percent saturation, the expanding water occupies so much of the pore volume that the air pressure becomes very high. Under the conditions assumed to develop Figure 8, pore pressures will exceed the tensile strength of cement heated to 180°C when pore saturation is greater than about 85 percent.

Volumetric expansion of the pore water is proportional to the rise in temperature. Thus, the hotter the cement, the higher the pore pressure and, more importantly, the lower the "critical" saturation. Figure 9 is a similar plot of pore pressures but with the final cement temperature as a parameter. For example, if the cement is heated further to 230°C, the tensile strength of the material is exceeded in pores with only 75 percent saturation.

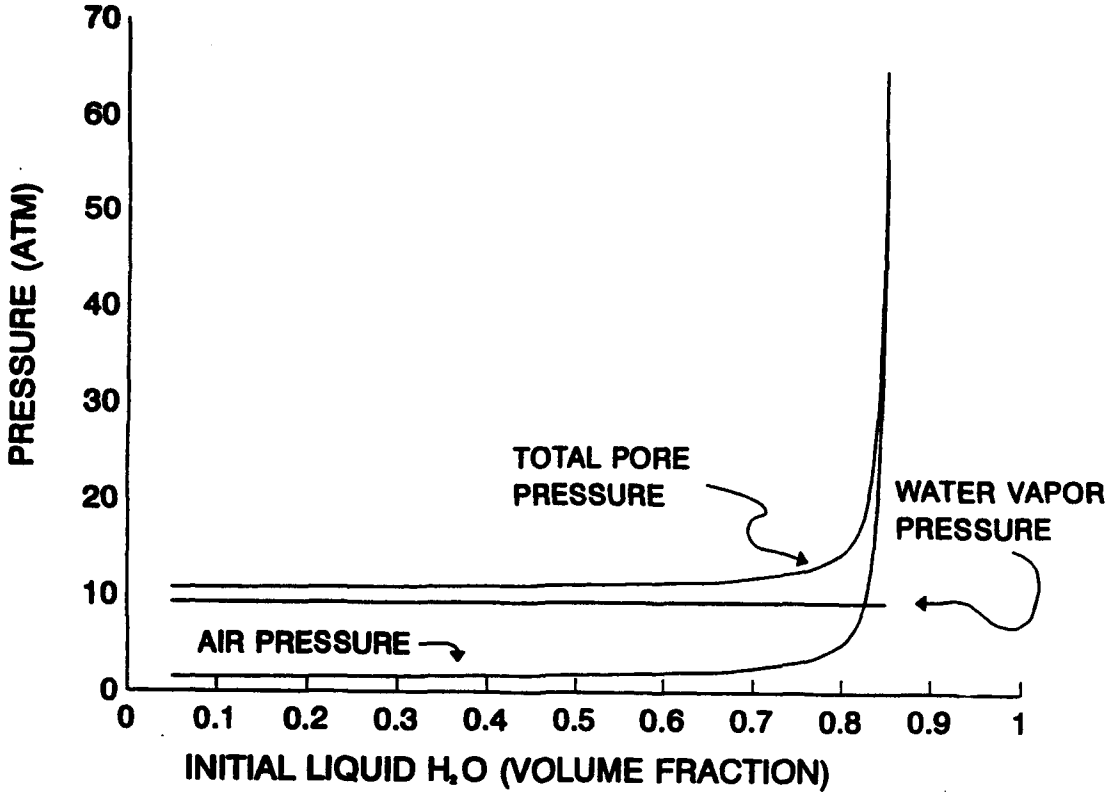

Figure 8
Effect of saturation on concrete pore pressure (isolated pore heated to 180°C).

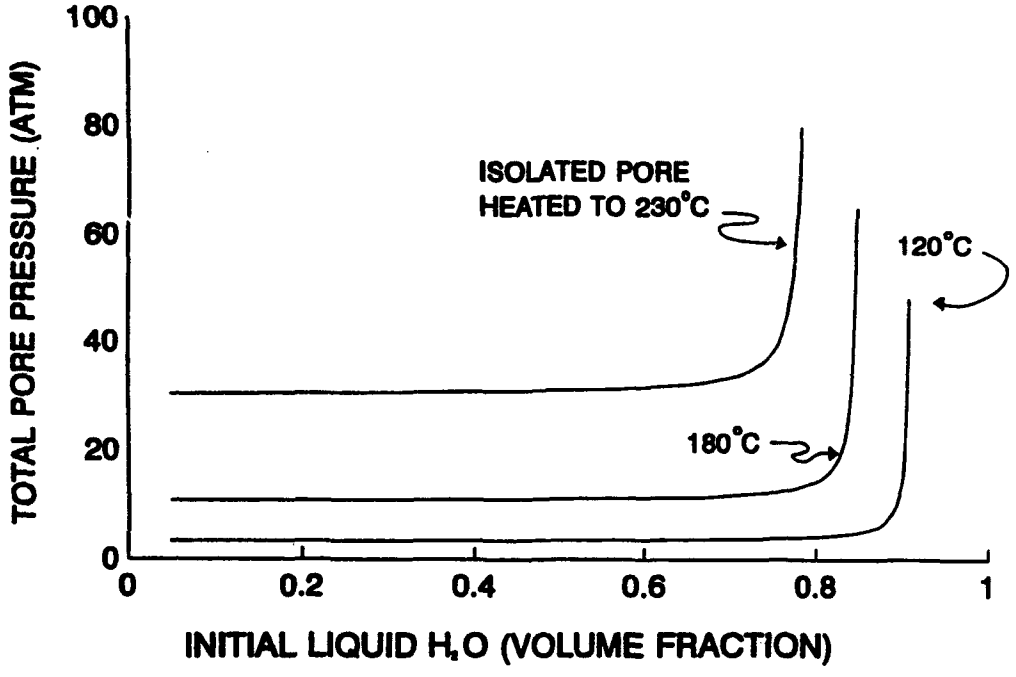

Figure 9
Effect of temperature on concrete pore pressure.

Because most of the pores in cement are interconnected, as also shown schematically in Figure 6, mass is transferred from pore to pore, pressure differences induced by local differences in saturation and temperature. Such mass flows tend to equalize pore pressures. Although the air is still compressed in the manner described above, maximum pore pressures will be decreased because of the air and water flowing out of the highest pressure pores.

Hypothesis

Yet, the resistance to flow through cement is very high. If the concrete is heated rapidly, for example, by the APU of an F/A-18, flow rates out of the pores might not be sufficient to relieve the pressures generated by water expansion.

The work presented here is based upon this hypothesis. Somehow the water gets into the pores of the concrete pavement. The pavement surface is likely to be the wettest, with rainfall entering the pores, adding to evaporable water remaining from the original mix. The surface also has the highest heating rate and reaches the highest temperatures. The concrete is then heated intermittently by the jet of the APU. Occasionally, a pore is hot enough and saturated enough to produce a state of compressed water. Pore pressures are increased beyond the tensile strength of the cement. Material failure results, beginning with a few single pores near the pavement surface. Over a period of time, the damage spreads to the extent that scaling is visually observed.

Plan of Attack

The procedure followed to confirm this hypothesis is to first theoretically determine pore pressures induced by the APU. Then, if these pressures are predicted to exceed the tensile strength of the cement, results will be confirmed by saturating and heating samples of airfield concrete pavement.

This work is limited to moderate temperatures. There are no reactions affecting the chemical structure of the cement. The concrete expands and contracts with temperature changes, and the evaporable water migrates from pore to pore, but hydration is complete and temperatures are too low for dehydration.

Scaling characteristics suggest that the affected pores are located in the cement rather than the aggregate. The aprons are made of concrete, however, and much of the published related work examines concrete rather than cement. Thus, these analyses have been made as general as possible, distinguishing between cement and concrete where necessary.

RELATED WORK

The effects of moisture plus high temperature on concrete are also important to fire researchers and to nuclear engineers, and much of their work is published. Heating rates are somewhat slower, however, and the quantitative contribution of this work to runway erosion analyses is limited.

Most of the available literature is theoretical. There are three different approaches to the analyses. The first approach is to assume the mass flow of the liquid phase is negligible and treat the problem as a flow of gases through a porous concrete. Two arguments for this approach are given. Resistance to the flow of liquids through concrete is several orders of

magnitude greater than the resistance to gases. In addition, the liquid phase is unlikely to be continuous from pore to pore. Sahota and Pagni (1979) use this approach to examine the thermodynamics of moisture in the pores of a concrete structure subjected to fire. This work is particularly pertinent because many of their assumptions are adopted to theoretically study the runway erosion problem. In addition to neglecting the movement of liquid water, Sahota and Pagni assume:

1. Local thermal equilibrium exists.

2. Local phase equilibrium exists, and therefore, water vapor pressure is equal to the water saturation pressure at the pore temperature.

3. Dehydration is neglected.

4. Air and water vapor are ideal gases.

Sahota and Pagni solved the conservation equations for energy and species, employing a finite difference scheme. Permeability was used as a parameter; however, they stopped the parametric study when pore pressures reached 10 atmospheres. Pressures above 10 atmospheres "are not expected due to microcracking and cracking."

An empirical approach was adopted by Bazant and Thonguthal (1978) to study the heating of concrete. By fitting test data, they developed relationships between pore saturation and pore pressure and between permeability and pore pressure. They did not distinguish between mass flux phases. These equations were coupled with conservation of energy and mass and solved employing a finite element technique. An unsealed concrete slab was examined (Bazant and Thonguthal, 1979) with surface temperature increasing at the rate of 80°C. /in. At this rate, the surface temperature reaches 150°C in slightly less than 2 minutes, similar to the rate at which an APU heats an airfield pavement. The corresponding maximum pore pressure is about 5 atmospheres. Huang and Ahmed (1991) used the same empirical model to make a similar study. A 40-cm concrete slab was subjected to fire. The slab had an initial saturation of about 10 percent. They found the moisture front to move rapidly in the early stages, and to slow as the fire progressed, requiring approximately 2 hours to dry completely.

The third approach to calculating moisture migration through high resistance porous media is to use the methods developed to study the migration of moisture through more permeable media such as soil. The flow of both liquid and gaseous phases is accounted for, applying theoretical correlations between capillary pressure and pore saturation and relative permeability and pore saturation (Fatt and Klikoff, 1959; Brooks and Corey, 1964; van Genuchten, 1980; Verma, 1985). Doughty and Pruess (1990) employed this method to determine the feasibility of constructing a geologic repository for high-level nuclear waste.

While theoretical studies of moisture migration in concrete are plentiful, experimental studies are scarce. Difficulties in measuring moisture and pressure on a pore scale are manifest. The most cited experimental study is still the work of England and Ross (1970), and England and Sharp (1971), completed in 1971. They heated one end of a 0.6-meter cylindrical concrete specimen and recorded pressure and, using resistance meters, moisture along its length. The sides of the specimen were insulated to ensure one-dimensional heat and mass transfer. The hot end reached 150°C, although time and space gradients of temperature were very small. This work is of special interest because it provides, in part, an experimental confirmation of the

hypothesis behind the runway scaling analyses. Initially, all pore total pressures were greater than the water vapor pressures at the measured temperatures, the difference being the contribution of air also in the pores. Over time, and sequentially, as moisture migrated away from the hot end, pore pressures fell to values less than the saturated vapor pressure of water alone. There was not enough water left in the pores to support two phases, demonstrating the change of state from B1 to A2 in Figure 7.

Implicit in the hypothesis upon which this work is based is that moisture in contact with the surface of a concrete runway will enter the pores. Fagerlund (1982) and Haynes and Rail (1986) have shown experimentally that external water will be absorbed by concrete. The work of Fagerlund is of the most interest. In his tests, water absorption is induced only by capillarity. He includes the water-cement ratio of the mix as a parameter and comes up with an interesting result. "Resistance to water absorption decreases rapidly with increase in water-cement ratio," and therefore, increase in porosity, "decreasing about one order of magnitude between water-cement ratios of 0.42 and 0.70."

Very little consideration has been given to the possibility of compressing water in the pores. Bazant (1982) discusses the phenomenon, but intuitively concludes that the "water is not significantly compressed due to an increase in pore space," and that "pore pressures are pr[illegible]y several orders of magnitude less than the pressure enclosed in a rigid container." Lankard [illegible]. (1971) also dismisses any significant compression of pore water which "if real" is "minimal."

Applied Research Associates (Dass, 1990) funded by the Air Force, conducted a series of tests that consisted of heating the surface of saturated concrete slabs with a propane torch. Temperatures of the hot surface reached 500°C, somewhat higher than temperatures generated by an APU. This surface was severely damaged, however, and the source of the damage was apparently the expansion of water in the pores of the concrete. They also succeeded in inducing mass transfer of water through the pores of the specimens. Moisture was clearly visible on the cold surface of the slabs.

Similar tests were conducted at the Naval Civil Engineering Laboratory (Tomita, 1960) using an afterburning J34WE32. Severe spalling of the test specimens was observed to occur about 1 minute into the afterburning cycle. Surface temperatures also reached about 500°C. A water-cement mix ratio of 0.4 was employed. The specimens were air cured. No moisture was added prior to the tests.

HIGH VELOCITY FLOW THROUGH CONCRETE

All of the theoretical work referenced above is based on the premise that Darcy's law applies. Darcy's law is used as a constitutive relationship which, when coupled with continuity and an equation of state, is an "empirical equivalent to the Navier-Stokes equations as averaged over very large numbers of individual pores" (Muskat, 1937).

Darcy's Law

Henry Darcy, in 1856, was interested in flow characteristics through the sand filters of the fountains of the city of Dijon, France. The inherent difficulties in representing the problem mathematically forced him to resort to an experimental study, which led to the fundamental relationship for flow through a porous media now known as Darcy's law (Muskat, 1937; Bear, 1972). Darcy found that the volumetric flow of water through a sand bed was directly

proportional to the cross-sectional area of the bed and to the head, and inversely proportional to the length of the bed,

$$Q = -KA \frac{P_2 - P_1}{L}$$

The constant of proportionality, K, usually called hydraulic conductivity, is a function of both the fluid and porous media. Subsequent experiments with different fluids and with different media led to an expression eliminating fluid properties from the constant,

$$\bar{V} = \frac{Q}{A} = -\frac{k}{\mu} \frac{P_2 - P_1}{L} \qquad (1)$$

where $\bar{V}$ is an average flow velocity, μ is the viscosity of the fluid, and k is a permeability of the media and independent of the fluid (Temeng, 1988). "The various extensions of Darcy's law, e.g., to three dimensional flow, to unsteady flow, etc., were first suggested as heuristic generalizations, and were then justified a posteriori by numerous planned experiments as well as by their success in predicting the flow in porous media systems of practical interest" (Bear, 1972).

It soon became apparent that Darcy's law had limitations. At higher velocities, Equation 1 did not fit the flow data. Darcy's flow was laminar, and the departure from linearity was initially thought to be caused by turbulence. By analogy with the turbulence phenomena occurring in pipes, Forchheimer (Scheidegger, 1974), in 1901, added a $\bar{V}^2$ term to Equation 1,

$$\alpha \bar{V} + \beta \bar{V}^2 = -\frac{P_2 - P_1}{L} \qquad (2)$$

Universal correlations for the constants α and β have proven to be elusive.

Most researchers now believe that inertial effects, not turbulence, are responsible for the onset of nonlinear flow through porous media (Ahmed and Sunada, 1969; Firoozabadi and Katz, 1979; Noman and Archer, 1988; Geertsma, 1974). Bear (1972) and Wright (1968) both postulate a transition regime, still laminar, where inertial forces begin to dominate, followed by a turbulent flow regime. Other opinions exist. Hassanizadeh and Gray (1987) do an order of magnitude study and conclude that nonlinearities are due to the effects of increased drag forces on the pore walls. Temeng (1988) suggests that fluid properties are varying. Although there have been relatively successful modifications to Darcy's law to account for inertial effects, none of these relationships are valid when the flow is compressible or when it is heated.

Porous Media Friction Factors

Some thought has been given to extending Darcy's law to higher velocities by employing a variable friction factor analogous to the Fanning friction factor of pipe flow. Fancher and Lewis (1933) measured the flow of air, oil, and water through different types of sand, and, from these data, developed friction factor versus Reynolds number charts. These charts closely resemble those for flow through pipes. There is a definite change from viscous to turbulent flow as flow rate increases. Each type of sand has a different "roughness" and, therefore, plots as a separate curve. Green and Duwez (1951), Cornell and Katz (1953), and others carried this approach further. By defining friction factor and Reynolds number in terms of the constants in Forchheimer's equation, they were able to develop a single friction factor versus Reynolds number function, valid for several media.

The success of Green and Duwez and of Cornell and Katz in developing friction factor charts for sintered metals and for sandstone, respectively, plus the common use of friction and expansion coefficients to predict compressible flow through pipes, suggests that resistance to flow through concrete might be defined in a similar manner. There remains the additional problem of accounting for the role of heating.

Derivation of the Flow Equation

Consider a finite segment of a single passageway through a hot slab of concrete such as illustrated in Figure 10. A gas, consisting of a mixture of air and water vapor, is flowing through this passage, induced by a difference in pressure between the two ends of the segment. The ends of this segment are each formed by one of the larger (i.e., capillary) pores although the length of this segment is such that it contains many capillary pores and many more smaller gel pores. Thus, the fluid velocity at the upstream end of the segment is negligible compared with the average velocity through the segment. This flow is being heated, a condition that would occur near the top surface of the airfield pavement, but the flow direction is arbitrary. Make the following assumptions:

1. Energy and mass transport are one-dimensional.

2. All gases are ideal.

3. The porous structure of the concrete is homogeneous.

4. Steady state exists.

The one-dimensionality of the phenomena will become apparent when the results of the analyses are presented. Resistance to heat conduction into the segment is substantial. Over the few minutes of interest here, the depth of pavement influenced by the hot jet is very small compared to the "footprint" of the jet.

An air/water vapor mixture at the moderate pavement temperatures stipulated remains close to ideal.

The assumption of homogeneity is made so that passage cross-sectional area and friction losses are constants. This is certainly not true, but experimental input will ultimately be necessary, and this input will be the sum of flows through many such passages. Thus,

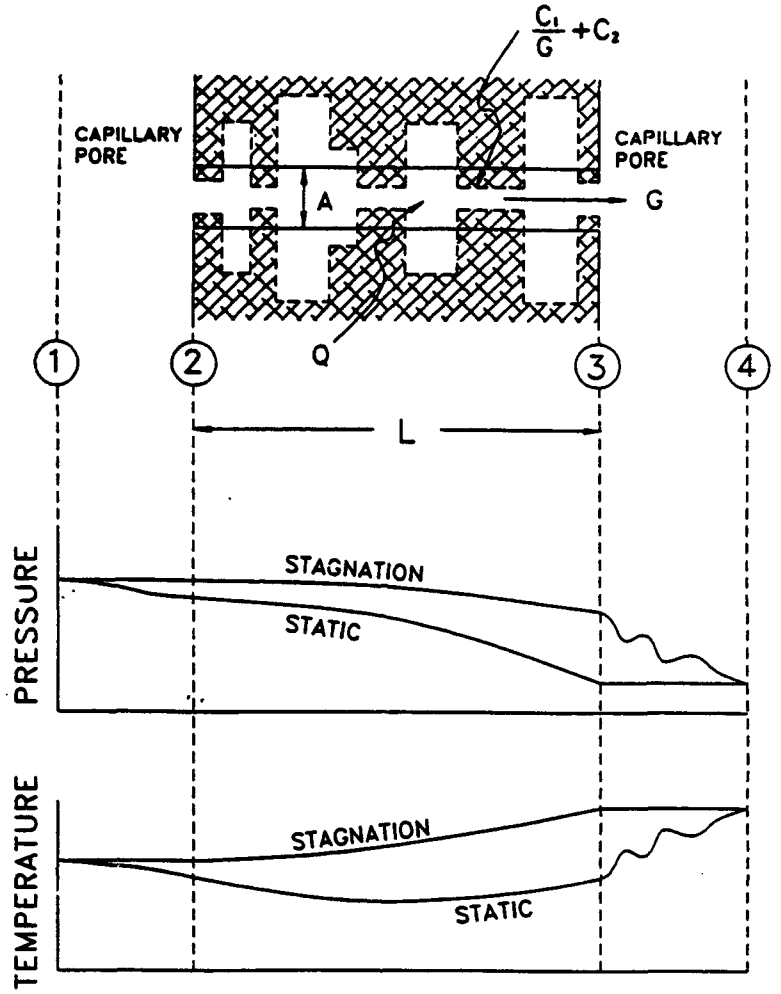

Figure 10
Qualitative pressure and temperature profiles through a single concrete flow passage.

homogeneity is necessarily built into the simulation. This will become clear when the derivation is complete.

Although the relationship being developed here is constitutive, it is derived over a finite region. Therefore, steady state does not necessarily always apply. For the airfield pavement problem, however, this is moot. The time frame associated with flow rates is several orders of magnitude shorter than the time frame associated with the heating of the fluids.

Also shown in Figure 10 are qualitative pressure and temperature profiles through the slab and numbers designating slab locations used in the derivation.

Applying continuity,

$$\frac{\dot{m}}{A} = \rho V \equiv G \qquad (3)$$

where $\dot{m}$ is the mass flow rate of gases through the passage, A the effective cross-sectional area of the passage, ρ the density of the gases, and V the gas velocity. G is the mass flux of the air/water vapor mixture.

Conserving momentum of the gases,

$$dP + \rho V dV + C_f \frac{\rho V^2}{2} dx = 0 \tag{4}$$

The coefficient C_f can be considered a concrete wall friction coefficient. It is defined as the ratio of the wall shearing stress to the dynamic head of the flow, a technique employed in elementary fluid mechanics and in several other approaches to modeling non-Darcy flow (Fancher and Lewis, 1933; Green and Duwez, 1951; Cornell and Katz, 1953).

Applying conservation of energy,

$$dh + d\left(\frac{V^2}{2}\right) = dq \tag{5}$$

The variable h is the specific enthalpy of the gases; q is the heat transfer per unit mass between the gases and concrete.

The equation of state for an ideal gas can be written:

$$P = \rho R T \tag{6}$$

where R is the gas constant.

Integrating Equation 5 from the first capillary pore to some arbitrary location x,

$$\int_1^x dh + \int_1^x d\left(\frac{V^2}{2}\right) = \int_1^x dq$$

$$h_x - h_1 = -\frac{V_x^2}{2} + {}_1Q_x$$

or, for an ideal gas,

$$c_p T_1 = \text{constant} = c_p T_x + \frac{V_x^2}{2} - {}_1Q_x \qquad (7)$$

where c_p is the specific heat of the gases, and ${}_1Q_x$ is the total heat transferred to the flow between "1" and "x."

Combining Equations 3, 6, and 7, dropping the "x" subscript,

$$c_p T_1 = \frac{c_p P}{\rho R} + \frac{G^2}{2\rho^2} - Q$$

and rearranging,

$$P = \rho R T_1 - \frac{R G^2}{2 \rho c_p} + \frac{\rho Q R}{c_p}$$

Differentiating, assuming constant specific heat,

$$dP = R T_1 d\rho + \frac{R G^2}{2 \rho^2 c_p} d\rho + \frac{Q R}{c_p} d\rho + \frac{\rho R}{c_p} dQ \qquad (8)$$

Combining Equations 3, 4, and 6,

$$\frac{2\rho}{G^2} dP + 2\frac{dV}{V} + C_f dx = 0$$

$$\frac{2\rho}{G^2} dP - 2\frac{d\rho}{\rho} + C_f dx = 0$$

Integrating across the concrete slab,

$$\frac{2}{G^2}\int_2^3 \rho\, dP - 2\int_2^3 \frac{d\rho}{\rho} + \int_2^3 C_f\, dx = 0$$

$$\frac{2}{G^2}\int_2^3 \rho\, dP - 2\ln\left(\frac{\rho_3}{\rho_2}\right) + \bar{C}_f L = 0 \qquad (9)$$

The friction coefficient $\bar{C}_f$ is the mean value over the length L.

Using Equation 8 to evaluate the integral in Equation 9,

$$\frac{2}{G^2}\int_2^3 \rho\, dP = \frac{2RT_1}{G^2}\int_2^3 \rho\, dp + \frac{R}{c_p}\int_2^3 \frac{d\rho}{\rho} + \frac{2R}{G^2 c_p}\int_2^3 \rho Q\, d\rho + \frac{2R}{G^2 c_p}\int_2^3 \rho^2\, dQ$$

$$\frac{2}{G^2}\int_2^3 \rho\, dP = \frac{RT_1}{G^2}\left(\rho_3^2 - \rho_2^2\right) + \frac{R}{c_p}\ln\left(\frac{\rho_3}{\rho_2}\right) + \frac{2R}{G^2 c_p}\left[\int_2^3 \rho Q\, d\rho + \int_2^3 \rho^2\, dQ\right]$$

Therefore,

$$\frac{RT_1}{G^2}\left(\rho_3^2 - \rho_2^2\right) + \left(\frac{R}{c_p} - 2\right)\ln\left(\frac{\rho_3}{\rho_2}\right) + \bar{C}_f L + \left(\frac{RT_1}{G^2}\right) f_1(\rho, Q) = 0$$

$$f_1(\rho, Q) = \frac{2}{c_p T_1}\left[\int_2^3 \rho Q\, d\rho + \int_2^3 \rho^2\, dQ\right] \qquad (10)$$

Solving for the mass flux,

$$G = \frac{[R T_1]^{1/2}\left[\rho_2^2 - \rho_3^2 - f_1\right]^{1/2}}{\left[\left(\frac{2c_p - R}{c_p}\right)\ln\left(\frac{\rho_2}{\rho_3}\right) + \bar{C}_f L\right]^{1/2}} \qquad (11)$$

A theoretical closed form relationship between gas density and heat transfer, necessary to determine the function f_1, is not normally available. The integrals are retained in the flow equation and evaluated numerically. This leads to a function of the form,

$$f_1 = \frac{2\bar{Q}}{c_p T_1}\left(C_4 \rho_2^2 + C_5 \rho_3^2\right) \qquad (10a)$$

$\bar{Q}$ is the total heat transferred to the gases as they pass through the segment. C_4 and C_5 are constants dependent upon the integration scheme employed. The techniques used in this work are discussed in Appendix A. Equation 11 then becomes:

$$G = \frac{[R T_1]^{1/2}\left[C_6 \rho_2^2 - C_7 \rho_3^2\right]^{1/2}}{\left[\left(\frac{2c_p - R}{c_p}\right)\ln\left(\frac{\rho_2}{\rho_3}\right) + \bar{C}_f L\right]^{1/2}} \qquad (11a)$$

$$C_6 \equiv 1 - \frac{2\bar{Q}C_4}{c_p T_1}$$

$$C_7 \equiv 1 + \frac{2\bar{Q}C_5}{c_p T_1}$$

The total heat transferred to the gases is determined from the overall problem. For an ideal gas,

$$\bar{Q} = c_p(T_{04} - T_{01}) = c_p(T_{03} - T_1)$$

$$\frac{\bar{Q}}{c_p T_1} = \frac{T_{03}}{T_1} - 1$$

and

$$C_6 = 1 - 2C_4\left(\frac{T_{03}}{T_1} - 1\right)$$

$$C_7 = 1 + 2C_5\left(\frac{T_{03}}{T_1} - 1\right)$$

The temperature T_{03} is the stagnation temperature at location 3.

The equation of state can be used to eliminate the densities in Equation 11:

$$C_6 \rho_2^2 - C_7 \rho_3^2 = C_6\left[\frac{P_2}{RT_2}\right]^2 - C_7\left[\frac{P_3}{RT_3}\right]^2$$

$$C_6 \rho_2^2 - C_7 \rho_3^2 = \left(\frac{P_1}{RT_1}\right)^2\left[C_6\left(\frac{P_2}{P_1}\right)^2\left(\frac{T_1}{T_2}\right)^2 - C_7\left(\frac{P_3}{P_1}\right)^2\left(\frac{T_1}{T_3}\right)^2\right] \quad (12)$$

$$\ln\left(\frac{\rho_2}{\rho_3}\right) = \ln\left[\left(\frac{P_2}{P_3}\right)\left(\frac{T_3}{T_2}\right)\right]$$

$$\ln\left(\frac{\rho_2}{\rho_3}\right) = \ln\left[\left(\frac{P_1}{P_3}\right)\left(\frac{P_2}{P_1}\right)\left(\frac{T_3}{T_1}\right)\left(\frac{T_1}{T_2}\right)\right] \quad (13)$$

At this stage of the derivation, the unknowns are the flow rate, the pressure and temperature at station 2, the friction coefficient, and the temperature at station 3. If the losses between stations 1 and 2 are neglected, two unknowns are eliminated, and the mathematics of the derivation are greatly simplified. The accuracy of the flow equation is not changed significantly. The length of the segment, L, is huge compared to the size of even the largest pores. "Moving" the ends of the segment a few pore diameters to diminish losses will not

noticeably change predicted flows through the segment. Regardless, the loss from station 1 to station 2 can be assumed lumped into the mean friction coefficient $\bar{C}_f$. Equations 12 and 13 now become,

$$C_6 \rho_2^2 - C_7 \rho_3^2 = \left(\frac{P_1}{R T_1}\right)^2 \left[C_6 - C_7 \left(\frac{P_3}{P_1}\right)^2 \left(\frac{T_1}{T_3}\right)^2\right] \tag{14}$$

$$\ln\left(\frac{\rho_2}{\rho_3}\right) = \ln\left[\left(\frac{P_1}{P_3}\right)\left(\frac{T_1}{T_3}\right)^{-1}\right] \tag{15}$$

Combining Equations 11, 14, and 15,

$$G = \frac{[R T_1]^{1/2} \left(\frac{P_1}{R T_1}\right) \left[C_6 - C_7 \left(\frac{P_1}{P_3}\right)^{-2} \left(\frac{T_1}{T_3}\right)^2\right]^{1/2}}{\left\{\left(\frac{2 c_p - R}{c_p}\right) \ln\left[\left(\frac{P_1}{P_3}\right)\left(\frac{T_1}{T_3}\right)^{-1}\right] + \bar{C}_f L\right\}^{1/2}}$$

or, in nondimensional form,

$$\Psi \equiv \frac{G[R T_1]^{1/2}}{P_1} = \frac{\left[C_6 - C_7 \left(\frac{P_1}{P_3}\right)^{-2} \left(\frac{T_1}{T_3}\right)^2\right]^{1/2}}{\left\{\left(\frac{2 c_p - R}{c_p}\right) \ln\left[\left(\frac{P_1}{P_3}\right)\left(\frac{T_1}{T_3}\right)^{-1}\right] + \bar{C}_f L\right\}^{1/2}} \tag{16}$$

The unknowns are now the flow parameter, Ψ, the mean friction coefficient, and the temperature ratio, T_1/T_3. Use of the nondimensional form of the flow equation simplifies the numerical procedures required for a solution. This form also makes the effects of heating and friction easier to evaluate. Therefore, even though the extra step of calculating the flow rate from Ψ is necessary, the nondimensional form of the flow equation is employed.

A second relationship is acquired by applying conservation of energy between the static and stagnation states at location 3,

$$\frac{T_{03}}{T_3} = 1 + \frac{V_3^2}{2 c_p T_3} \tag{17}$$

Combining Equation 17 with the continuity equation and the equation of state and rearranging,

$$\frac{T_1}{T_3}\left(\frac{T_{03}}{T_1}\right) = 1 + G^2\left(\frac{R}{2c_p}\right)\left(\frac{RT_1}{P_3^2}\right)\left(\frac{T_3}{T_1}\right)\left(\frac{P_1^2}{P_1^2}\right)$$

$$\Psi = \frac{G[RT_1]^{1/2}}{P_1} = \left[\frac{2c_p}{R}\right]^{1/2}\left(\frac{P_1}{P_3}\right)^{-1}\left\{\frac{T_1}{T_3}\left[\left(\frac{T_1}{T_3}\right)\left(\frac{T_{03}}{T_1}\right) - 1\right]\right\}^{1/2} \tag{18}$$

If the friction coefficient is known, Equations 16 and 18 can be solved simultaneously to determine Ψ and T_1/T_3. Once these nondimensional variables are acquired, the gas flow and the temperature at station 3 of the concrete slab are easily calculated.

The success of the correlation developed by Green and Duwez (1951) for sintered metals suggests that the friction coefficient be set equal to the sum of a viscous and an inertial term,

$$\bar{C}_f = \frac{C_1''}{N_{Re}} + C_2 = \frac{C_1'}{G} + C_2$$

Cross-sectional dimensions and viscosity terms of the Reynolds number N_{re} are lumped into the coefficient C_1'. C_1' and C_2 have the units mass flux/length and 1/length, respectively. Both are determined experimentally. The test procedure and the calculation of the wall friction coefficients are described in Appendix B.

The flow parameter derived in this manner describes flow through the total cross section of the concrete specimen rather than through a single passage. To account for this difference, a third constant is added to Equation 16. Noting that,

$$G_{total} = G\left(\frac{A}{A_{total}}\right) * \text{Number of passages}$$

defining

$$C_3 \equiv \left(\frac{A}{A_{total}}\right) * \text{Number of passages}$$

and redefining the flow parameter ψ,

$$\psi \equiv \frac{G_{total}[R T_1]^{1/2}}{P_1}$$

Equation 16 becomes:

$$\psi = \frac{G_{total}[R T_1]^{1/2}}{P_1} = \frac{C_3\left[C_6 - C_7\left(\frac{P_1}{P_3}\right)^{-2}\left(\frac{T_1}{T_3}\right)^{2}\right]^{1/2}}{\left\{\left(\frac{2c_p - R}{c_p}\right)\ln\left[\left(\frac{P_1}{P_3}\right)\left(\frac{T_1}{T_3}\right)^{-1}\right] + \left(\frac{C_1}{G_{total}} + C_2\right)L\right\}^{1/2}} \quad (19)$$

By lumping C_3 into C_1', to obtain C_1, G_{total}, rather than G, is used to calculate the friction coefficient.

Equation 18 is similarly modified,

$$\psi = \frac{G_{total}[R T_1]^{1/2}}{P_1} = C_3\left[\frac{2c_p}{R}\right]^{1/2}\left(\frac{P_1}{P_3}\right)^{-1}\left\{\frac{T_1}{T_3}\left[\frac{T_1}{T_3}\left(\frac{T_{03}}{T_1}\right) - 1\right]\right\}^{1/2} \quad (18a)$$

Equations 18a and 19 together will be used as a constitutive momentum relationship, analogous to the way Darcy's law is used.

Qualitative Validation of Flow Equation

Entrance losses were neglected in the derivation of Equation 19 (i.e., the pressure drop between station 1 and station 2 was assumed very small compared to the drop between station 2 and station 3). Reexamine Figure 10. In the absence of heat transfer, this is the only difference between Equation 19 and the momentum equation describing Fanno flow. Therefore, for large friction coefficients and under adiabatic conditions, Equation 19 should approach Fanno flow. The comparison is made in Figure 11(a) using one-dimensional compressible flow tables (Zucrow and Hoffman, 1976) as the Fanno flow "equation." The pressure ratio, $\frac{P_1}{P_3}$, required to choke the flow is used as the dependent variable as the coefficient C_2 is increased. The difference between the two equations reduces to fractions of a percent long before friction coefficients reach values common in concrete.

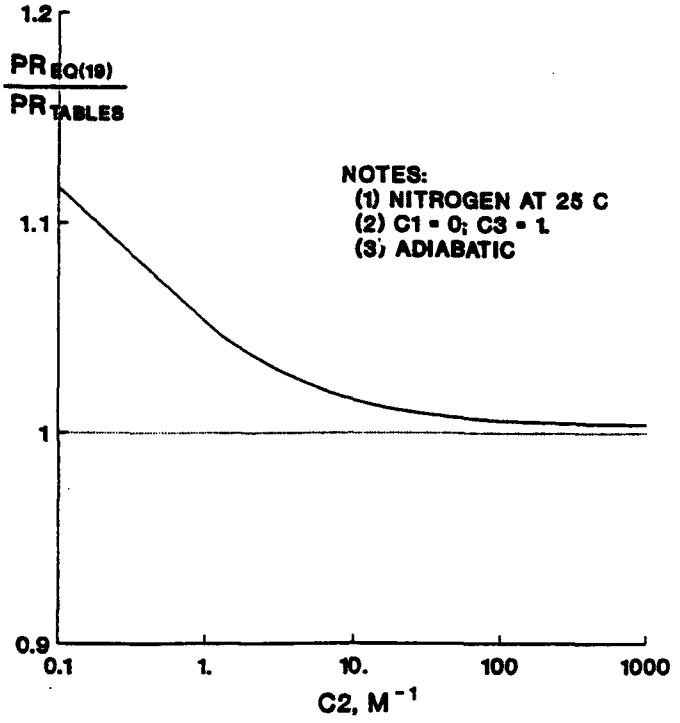

11(a) Varying friction.

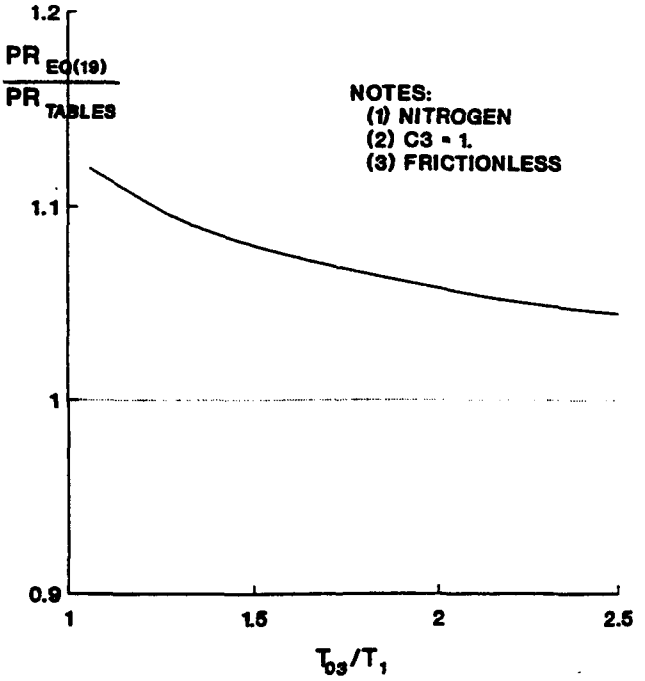

11(b) Varying heating.

Figure 11
Pressure ratio required to choke flow, comparing Equation 19 with compressible flow tables.

Similarly, when friction is absent, Equation 19 should describe Rayleigh flow. Here, any error is the result of approximations inherent in the method used to evaluate the integrals in Equation 10. The comparison is made in Figure 11(b). Errors range from 5 to 10 percent over the heating rates (temperature ratios) experienced by airfield pavements.

Fanno flow through porous iron, as predicted by Equation 19, is shown in Figure 12. The inertial friction coefficient is used as a parameter. The relationships between flow resistance, flow rate, and choking, characteristic of compressible flows, are apparent in this figure.

Heating a compressible flow decreases mass flow rate and increases the pressure ratio required to choke the flow, analogous to increasing friction. The ability of Equation 19 to correctly predict the effects of heating is shown in Figure 13. (For illustrative purposes, the choking pressure ratio was increased by maintaining a small flow resistance.)

With restrictions, Equation 19 reduces to the Forchheimer equation for an ideal gas. Combining the constants together as α and β, the Forchheimer equation can be written (Geertsma, 1974):

$$-\frac{P_1^2 - P_3^2}{L} = \alpha R T_1 G + \beta R T_1 G^2$$

Rearranging,

$$\frac{G[R T_1]^{1/2}}{P_1} = \frac{\left[1 - \left(\frac{P_1}{P_3}\right)^{-2}\right]^{1/2}}{\left[\left(\frac{\alpha}{G} + \beta\right) L\right]^{1/2}}$$

or

$$\frac{G[R T_1]^{1/2}}{P_1} = \frac{C_3\left[1 - \left(\frac{P_1}{P_3}\right)^{-2}\right]^{1/2}}{\left[\left(\frac{\alpha'}{G} + \beta'\right) L\right]^{1/2}}$$

which approximates Equation 19 for adiabatic conditions when the flow rates are low, $T_1 \approx T_3 \approx T_{03}$, and the log term in the denominator, very small compared to the flow resistance of concrete, is neglected.

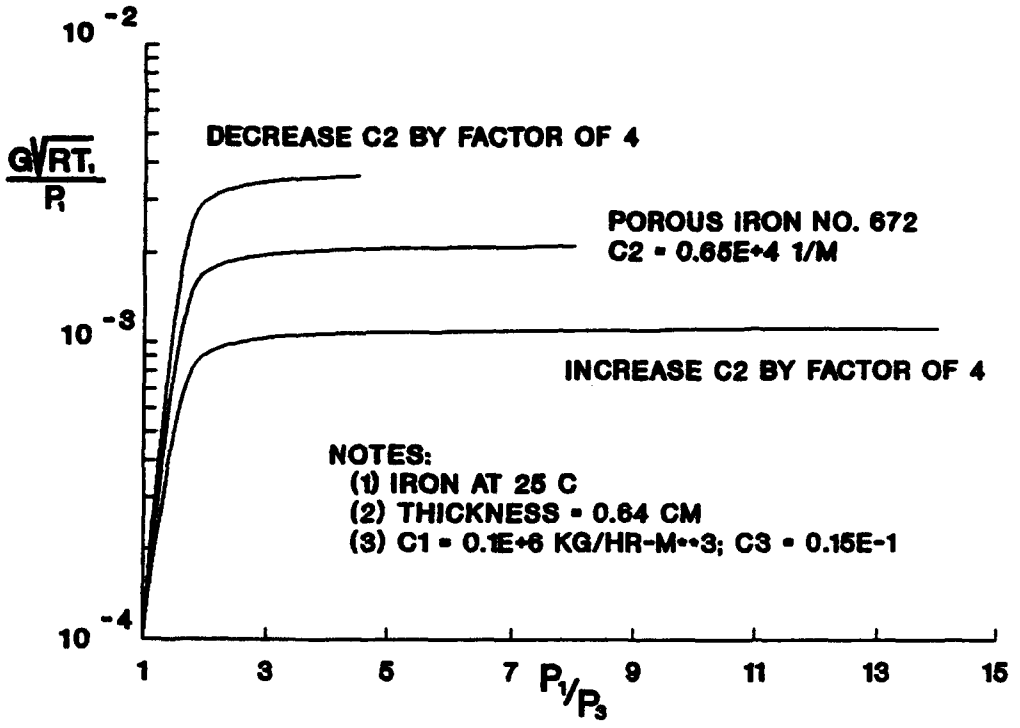

Figure 12
Effect of friction on the flow of nitrogen through porous iron.

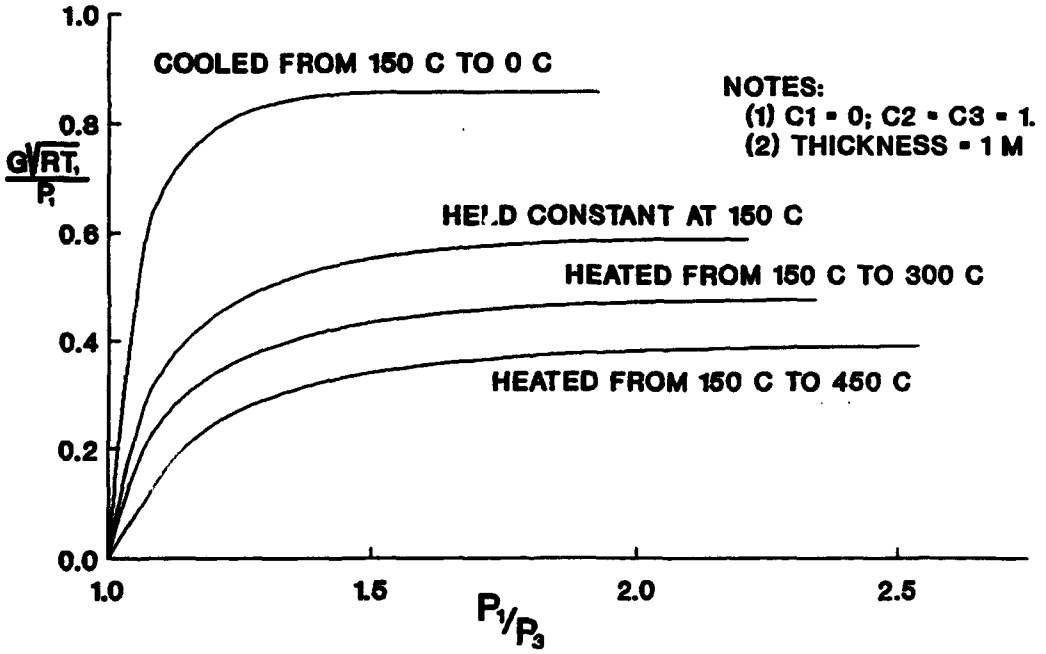

Figure 13
Effect of heating on the flow of nitrogen through a low resistance medium.

MEASURED FLOW CHARACTERISTICS

There is very little high resistance porous media flow data available that is complete enough to use to develop a flow parameter. The Air Force Civil Engineering Support Agency, also studying the airfield deterioration problems, has contracted Professor M.C. McVay, of the University of Florida, to determine the permeability of different mixes of concrete. Flow parameters developed from McVay's data are being used in this work. Appendix B describes these flow tests and the preparation of the concrete.

Flow rates through porous metals and through sandstone were published in the 1950s. The work was well done, and examination of flow parameters developed from these data contributes to a validation of Equation 19. The porous metal data are particularly valuable since pressure ratios were increased high enough to choke the flow.

Concrete

Parameters describing the flow of nitrogen (air) through three mixes of concrete are compared in Figure 14. Friction coefficients were set to make Equation 19 match the flow data of McVay and Rish (1993). Maximum test pressure ratios are nowhere near high enough to choke the flow. The total number of flow passages was assumed to be unaffected by the aggregate. The aggregate acts as an obstacle, increasing the effective length of the passageways. The area coefficient C_3 is independent of the aggregate; the flow resistances C_1 and C_2 vary with the aggregate.

The extremely high resistance to flow through concrete is obvious. This will become even more apparent by comparing concrete flow parameters with flow parameters of porous metals and sandstone that are discussed in the next section. Also obvious is the effect that aggregate has on flow through concrete. There are two orders of magnitude difference between flow parameters of mortar and of concrete made with the impervious Calara limestone.

Figure 15 compares flow parameters of steam at 225°C and nitrogen at 25°C through the same mortar. The resistance coefficients for both gases are identical. This is extremely important. The coefficients of Equation 19 depend only upon the porous medium; they are independent of the fluid. When heated by a jet exhaust, a mixture of steam and air is being forced through the pores of the concrete airfield pavement. If C_1 and C_2 were dependent upon the composition of the gas, they would be changing with both time and depth into the concrete. A model based on Equation 19 would become very clumsy.

Other Porous Media

The most extensive measurements of flows through high resistance porous media are still the data of Green and Duwez (1951), measuring the flow of nitrogen through unheated porous metals. These data are plotted as flow parameter versus pressure ratio in Figures 16(a) and (b). The gas flow through these 0.6-cm specimens chokes at very moderate pressure ratios. If these were runway material, gases would have to be treated as "compressible."

Noted on these figures are the coefficients C_1, C_2 and C_3 used to fit Equation 19 to this data. Several observations are pertinent. The difference in flow characteristics through "iron no. 672" and through "iron no. 641" appears attributable to a change in flow resistance (i.e., through a single passageway); more nitrogen is flowing through iron no. 672, but this metal chokes at a lower pressure ratio. The friction coefficients for iron no. 641 are more than an

order of magnitude greater. The restricting flow area, proportional to the coefficient C_3, is roughly the same for the two metals.

The difference in nitrogen flow through "stainless steel no. 1" and through iron no. 641 appears attributable to differences in both the flow resistance and the number of flow passages. The iron chokes at a much lower pressure ratio, implying a lower flow resistance. At high pressure ratios, however, flow through both metals is about the same. There must be more flow passages through the stainless steel.

Characteristics describing the flow of air and nitrogen through a higher resistance porous media, sandstone, are shown in Figure 17(a). The coefficients were set to match the flow data of Cornell (1952). Experimental pressure ratios were not increased high enough to choke the flow. Even though the flow equation fits the data extremely well, there is not enough information to uniquely determine the coefficients C_1, C_2, and C_3. This is discussed in the comments below.

Figure 17(b) shows flow parameters of different gases through brown dolomite. The resistance coefficients were set to match the air and nitrogen flow data. Using these same coefficients, flow parameters for methane and helium are plotted and compared with data. Although the resulting "fit" is not as good as shown above for nitrogen and steam flowing through concrete, considering the huge differences in properties of these gases, the flow parameters are certainly encouraging.

Comments

All the flow tests cited were conducted under adiabatic conditions. A complete validation of Equation 19 requires some flow measurements of heated gases.

The exit static temperature, T_3, was not measured on any of the flow tests described above, and this variable probably cannot be accurately measured. Therefore, there are two equations, Equations 16 and 17, to solve for the four unknowns C_1, C_2, C_3, and T_1/T_3. The resistance coefficients C_1 and C_2 are dominant at low and high flow rates, respectively, and can be determined independently of each other. If test pressure ratios are increased high enough to choke the flow, as was done for the porous metals, the exit static temperature is known from the relationship (Shapiro, 1953):

$$\frac{T_3}{T_{03}} = \frac{2}{\gamma + 1}$$

where γ is the ratio of specific heats. Since T_1 and T_{03} are boundary conditions, C_2 and C_3, and then C_1, can be determined uniquely. If the test flows were not choked, a unique solution is not possible. Coefficients that accurately predict mass flows can be determined, however, and this is often sufficient for modeling.

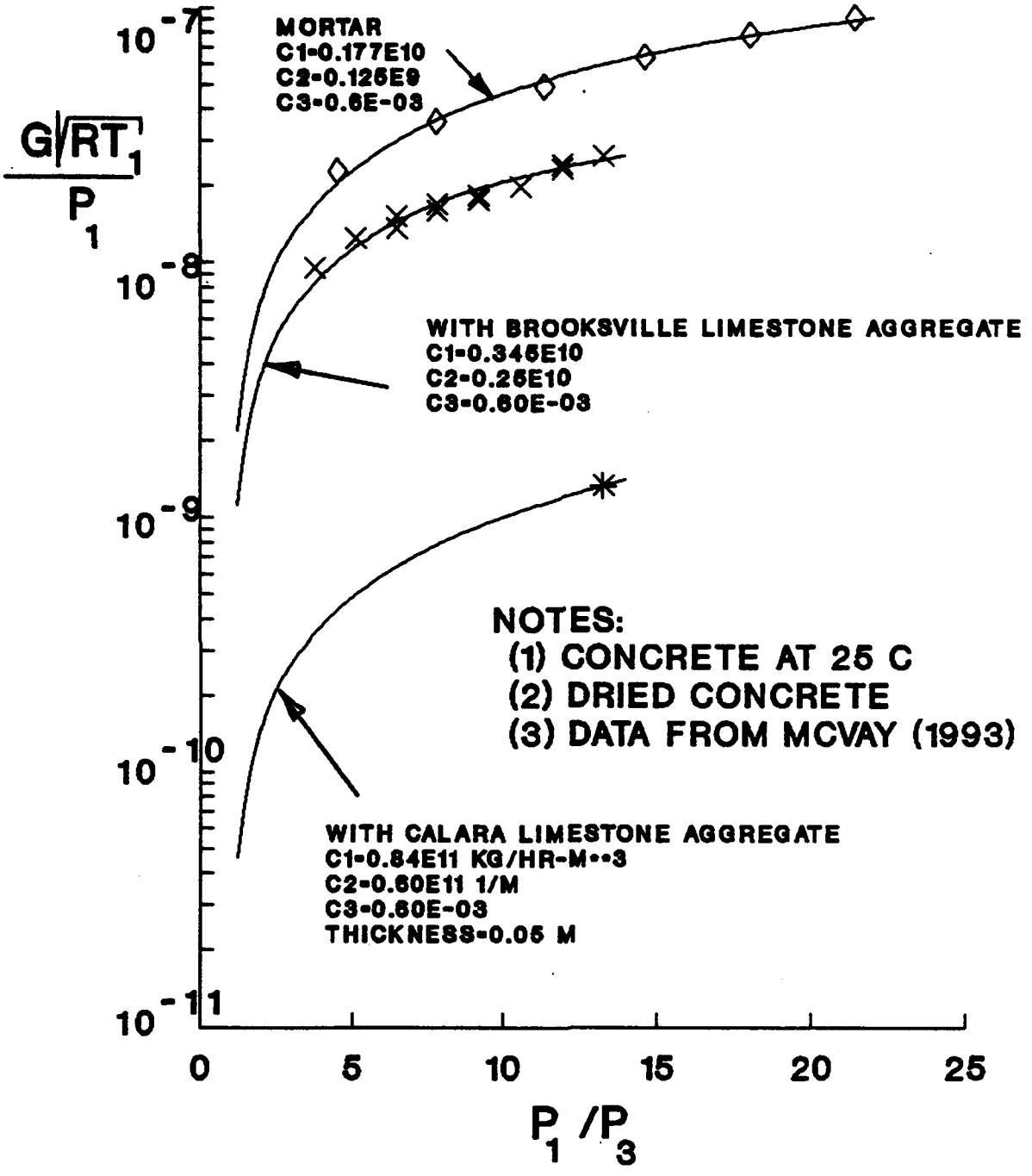

Figure 14
Nitrogen flow through portland cement concrete.

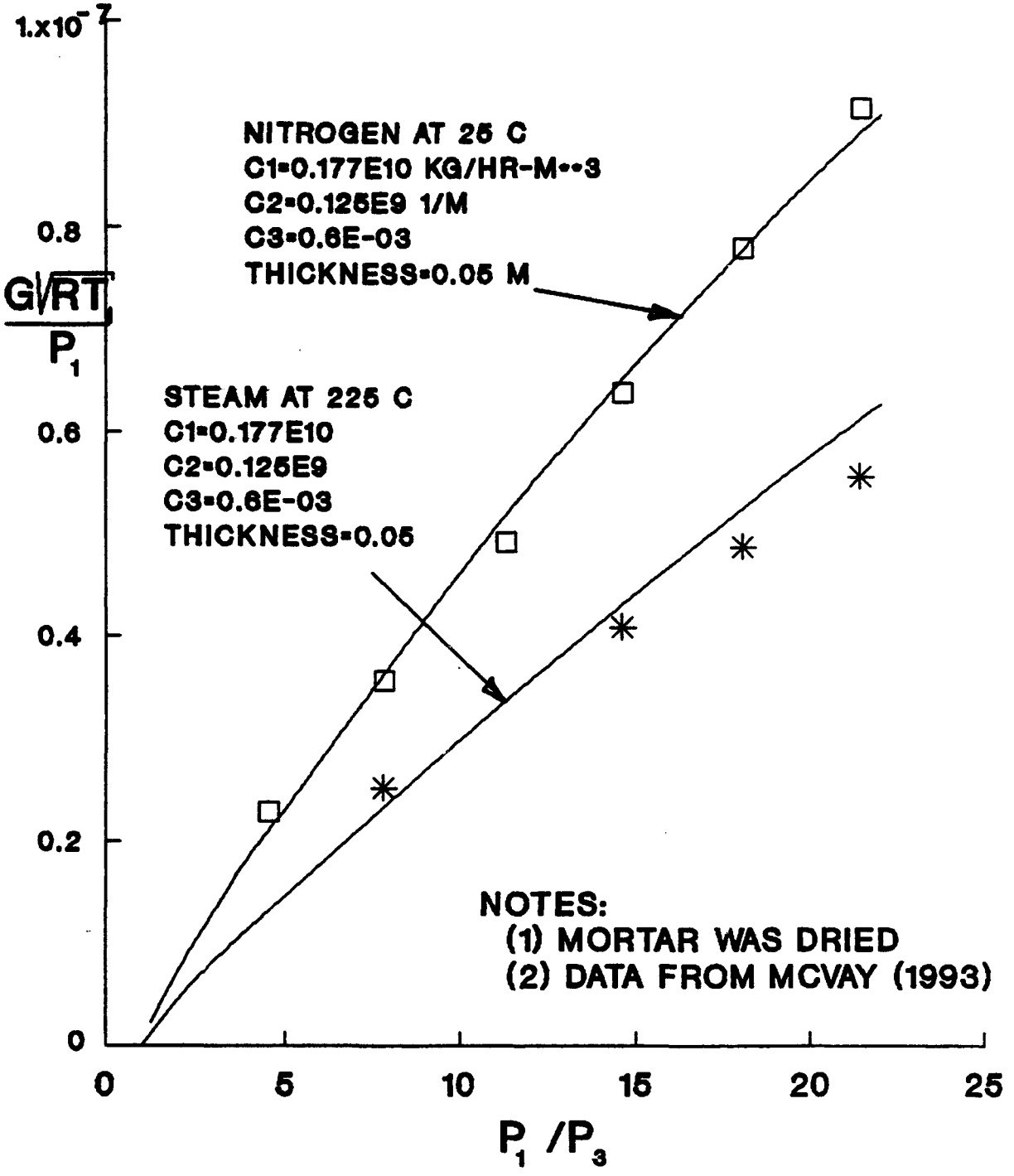

Figure 15
Gas flow through mortar.

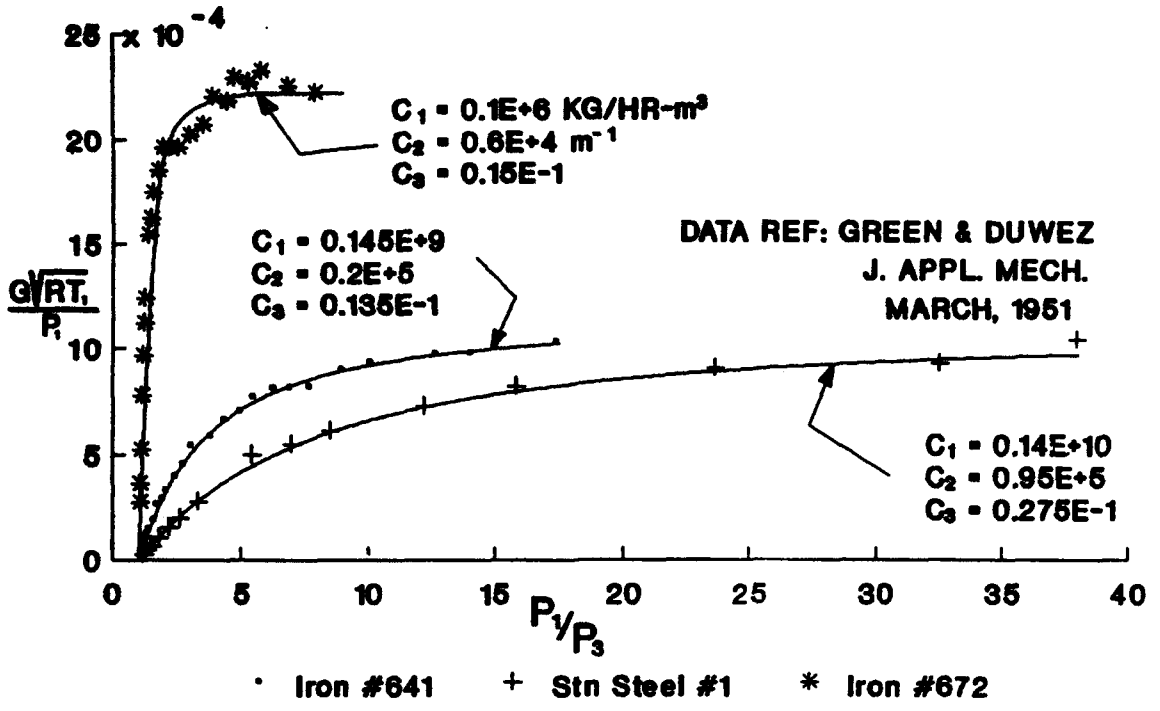

Figure 16(a)
Flow of nitrogen through porous metals.

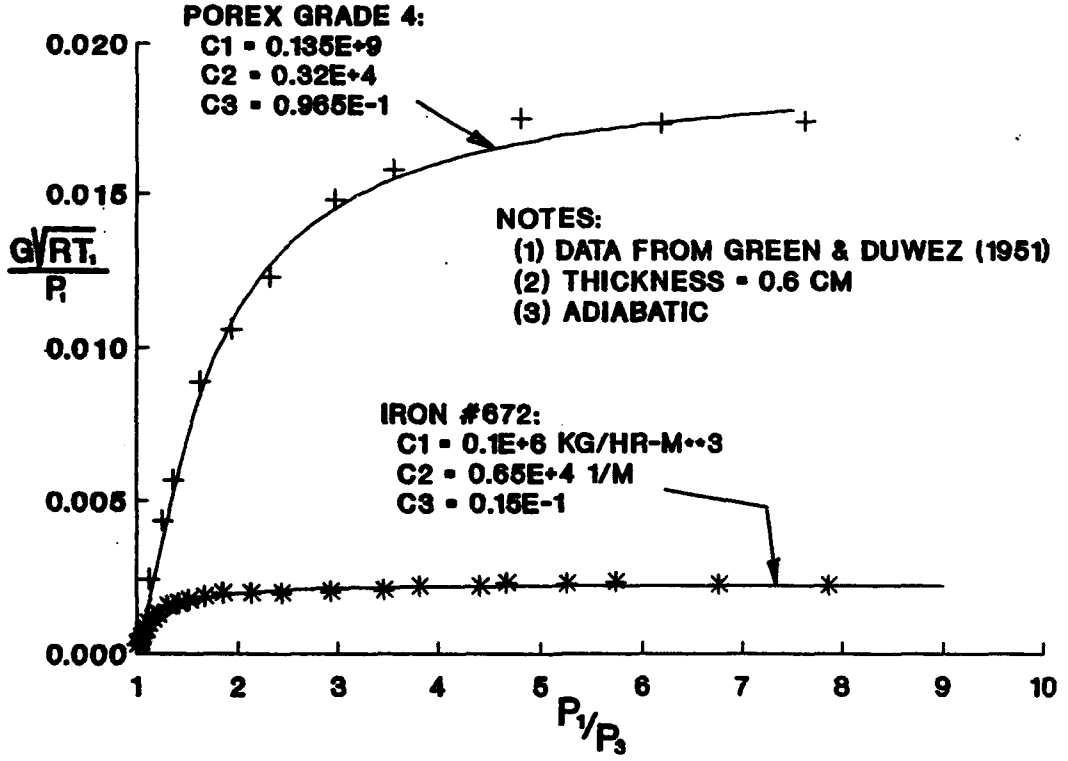

Figure 16(b)
Flow of nitrogen through porous metals.

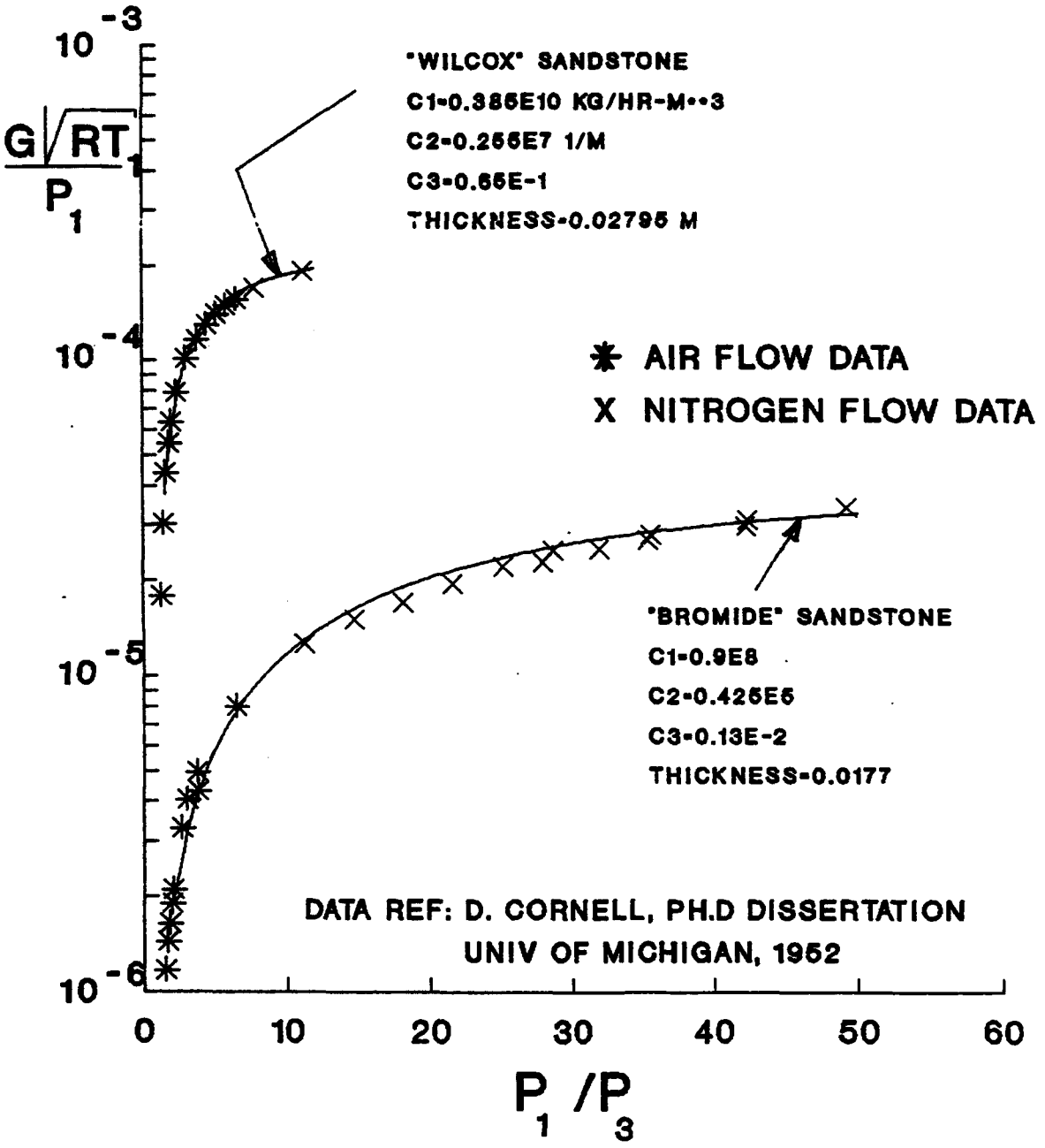

Figure 17(a)
Flow of nitrogen and air through sandstone.

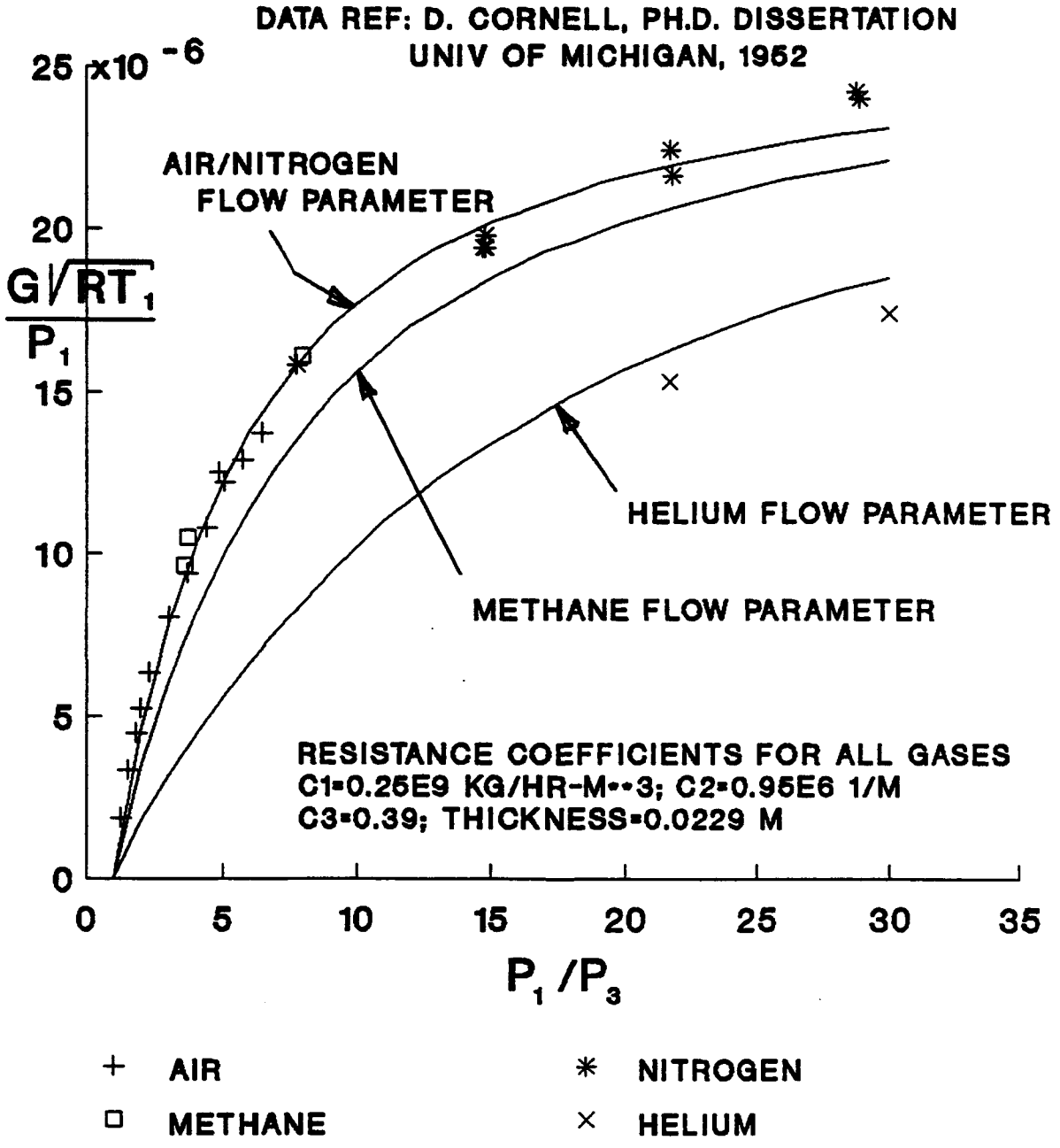

Figure 17(b)
Flow of different gases through brown dolomite.

EFFECTIVE FLOW AREA

The flow parameters were developed from gas flow data that were acquired using dry concrete as the medium. In order to accurately predict pore pressures, the additional flow resistance provided by liquid water in the pores must be accounted for. This is analogous to adding a relative permeability to Darcy's law.

For this study, the effect of liquid water will be included as a change in the concrete flow parameter via a change in effective cross-sectional area of the flow passages. Data sufficient to determine these effective areas are not yet complete. In the meantime, relative permeabilities will be used. There are many such functions published in the soil science and petroleum literature. The function most apropos to this work is the relative permeability, k_r, developed by Verma et al. (1985) for the concurrent flow of steam and water through an unconsolidated porous medium (Verma et al., 1985; Doughty and Pruess, 1990),

$$k_r = 1.259 - 1.7615S + 0.5089S^2$$

S is the pore saturation, the volume fraction of liquid water in the pores. This function is applied to the cross-sectional area in Equation 19 through the coefficient C_3,

$$C_3 = \frac{A}{A_{total}} * \text{Passages} * (1.259 - 1.7615S + 0.5089S^2)$$

MATHEMATICAL SIMULATION OF AIRFIELD PAVEMENT

Now consider the slab as a homogeneous continuum, a cement/aggregate solid matrix interspersed with pores filled with air and/or water. Some of these pores connect to form passages through the slab.

Make the following assumptions:

1. Energy and mass transport are one-dimensional.

2. Air is an ideal gas; mixtures of air and water vapor are ideal.

3. Local thermal equilibrium exists; the temperature of the fluids is the same as the temperature of the surrounding solid.

4. Movement of liquid water is negligible.

5. Phase equilibrium exists inside each pore; if there is liquid water in the pore, the water vapor pressure is its saturation pressure.

6. There is no dehydration; the physical properties of the concrete remain constant.

7. Capillary forces are negligible.

Homogeneity and the first two listed assumptions were discussed during development of the flow equation. The assumption of thermal equilibrium is based upon the huge passage wall to cross-section area ratios occurring in porous media. Thus, as suggested by Sahota and Pagni (1979), "the response time for local heat transfer between the fluid and the solid is several orders of magnitude smaller than the times of interest." Sahota and Pagni also offer arguments for neglecting movement of liquid water. They emphasize the very great resistance to the flow of liquids through porous media compared to the resistance to gases. They also point out that "the liquid, particularly at low moisture content, is present in the pendular state, that is, the liquid in different pores is not interconnected." McVay and Rish (1993) measured mass flow rates of nitrogen and liquid water through samples of concrete, finding that the gas flows were about 300 times greater. Arguments supporting the assumption of phase equilibrium are more tacit. The high pressure flow of air and water vapor through the pores will tend to break up the liquid water, forming large vapor-liquid interfacial areas, and, in addition, transporting both phases toward/away from these interfaces.

It is stipulated that there is no dehydration. These analyses are valid only when the chemical and physical structure of the concrete does not vary.

Governing Equations

Figure 10 illustrates the problem. The unknown variables are:

G_{air} = Mass flow rate of air per unit cross-sectional area of the concrete slab.

G_{vapor} = Mass flow rate of water vapor per unit cross-sectional area of the slab.

G_{total} = Total flow rate of air plus water vapor.

M_{air} = Mass of the air in the slab.

M_{vapor} = Mass of the water vapor in the slab.

M_{water} = Mass of the liquid water in the slab.

P_{air} = Pressure of air in the pores.

P_{gas} = Pressure of the air-water vapor mixture in pores.

P_{vapor} = Pressure of water vapor in the pores.

P_{water} = Pressure of liquid water in the pores.

Q_{fg} = Energy of vaporization/condensation.

T = Slab temperature, also the stagnation temperature of the gases.

V_{gas} = Volume of air plus water vapor in the slab.

V_{water} = Volume of liquid water.

v_{vapor} = Specific volume of water vapor.

v_{water} = Specific volume of liquid water.

These variables are to be determined in terms of both time, t, and location, x.

Applying conservation of energy to the slab,

$$\frac{\partial(\rho c T)}{\partial t} + \frac{\partial(G_{total} c_p T)}{\partial x} = \frac{\partial}{\partial x}\left(k \frac{\partial T}{\partial x}\right) + Q_{fg} \tag{20}$$

The heat capacity, ρc, and the thermal conductivity, k, are mass averages of the concrete and liquid water. The specific heat of the gas mixture, c_p, is the molar average of the air and water vapor.

$$Q_{fg} = \frac{h_{fg}}{V_{total}} \frac{\partial M_{water}}{\partial t} \tag{21}$$

The heat of vaporization of water, h_{fg}, is assumed constant. V_{total} is the total volume of the slab.

Conserving the mass of the air and the water,

$$\frac{1}{V_{total}} \frac{\partial M_{air}}{\partial t} + \frac{\partial G_{air}}{\partial x} = 0 \tag{22}$$

$$\frac{1}{V_{total}} \frac{\partial}{\partial t} (M_{vapor} + M_{water}) + \frac{\partial G_{vapor}}{\partial x} = 0 \tag{23}$$

Air is assumed to be an ideal gas,

$$P_{air} V_{gas} = M_{air} R_{air} T \tag{24}$$

where R_{air} is the gas constant for air.

Equations of state of the compressed water and saturated and superheated water vapor were acquired from the steam tables of Keenan and Keyes (1936) using provided fits of the data,

$$P_{vapor} = f_2(T) \tag{25}$$

$$v_{vapor} = f_3(T) \tag{26}$$

$$v_{water} = f_4(T, P_{water}) \tag{27}$$

Using the definition of specific volume,

$$v_{vapor} M_{vapor} = V_{gas} \tag{28}$$

$$v_{water} M_{water} = V_{water} \tag{29}$$

The air-water vapor mixture is considered a mixture of ideal gases.

$$G_{air} = \left(\frac{P_{air}}{P_{gas}}\right) G_{gas} \tag{30}$$

$$G_{vapor} = \left(\frac{P_{vapor}}{P_{gas}}\right) G_{gas} \tag{31}$$

$$P_{air} + P_{vapor} = P_{gas} \tag{32}$$

The pores are always filled with either water or gas or both,

$$V_{gas} + V_{water} = eV_{total} \tag{33}$$

where ϵ is the porosity of the concrete.

The final equation required is a relationship between the gas and liquid water pressures inside the pores. This pressure difference is a function of the interfacial tension between the two phases and the size and shape of the pores. The presence of air further complicates such a relationship. For this work, capillarity is assumed negligible,

$$P_{gas} = P_{water} \tag{34}$$

The error introduced by neglecting capillarity is difficult to appraise. Defay and Prigogine (1966) estimated the effect of curvature on the difference in pressure inside and outside water vapor bubbles at 18°C. When the bubble has a radius of 10^{-3} mm, the difference is about 1.4 atmospheres; when the bubble has a radius of only 10^{-5} mm, the difference is about 140 atmospheres. Concrete pore radii range roughly between 10^{-5} and 10^{-3} mm. In the larger capillary pores, therefore, surface tension forces are small. Capillarity should have only a minor effect on mass flow rates through a segment of concrete. In the smaller pores, capillarity will be significant. This will tend to "skew" pore pressures through the interior of the concrete segment and will affect saturation of smaller pores.

Initial and Boundary Conditions

The concrete is initially at the ambient temperature T_∞. When the jet is started, the surface temperature of the pavement, T_{surf}, is steadily increased,

$$T = T_\infty \qquad @\ 0 \le X \le L,\ t \le 0$$

$$T = T_{surf}(t) \qquad @\ X = 0,\ t > 0$$

$$T = T_\infty \qquad @\ X = L,\ t > 0$$

The effects of the jet do not penetrate the concrete beyond a depth of L.

The initial saturation of the pores, S_∞, is stipulated. The liquid and vapor phases are in equilibrium. The water vapor pressure is the saturated vapor pressure at T_∞. Air occupies the same volume as the water vapor. The initial pore pressure is equal to the ambient pressure, P_∞.

$$M_{water} = \frac{e S_w V_{total}}{v_{water}} \qquad @\ 0 \le x \le L,\ t \le 0$$

$$M_{vapor} = \frac{e\,(1 - S_w)\,V_{total}}{v_{vapor}} \qquad @\ 0 \le x \le L,\ t \le 0$$

$$M_{air} = \frac{(P_a - P_{vapor})\,e\,(1 - S_w)\,V_{total}}{R_{air} T_a} \qquad @\ 0 \le x \le L,\ t \le 0.$$

A constant cement porosity, e, of 0.25 is assumed for this work.

Computational Procedures

Equations 18 through 34 are solved simultaneously for the 16 variables listed above and the temperature T_3. Finite differences are used to approximate Equations 20, 22, and 23. Single step iteration, with an option to apply relaxation, is employed. Details of the computational procedures and a listing of the computer code, called POREFLOW, are included in Appendix A.

THEORETICAL RESULTS

The flow parameter for mortar, shown in Figure 15, was used in these analyses. The scaling occurs in the cement. Furthermore, there is little aggregate at or close to the surface where the maximum pressures are occurring. Neglecting the flow resistance of the aggregate, at worst, results in higher predicted flow rates and lower predicted pore pressures.

APU Heated Pavements

The effect of moisture on F/A-18 APU heated concrete pavements was examined theoretically using POREFLOW. Pavement surface temperatures measured by Houck et al. (1992) were used as a boundary condition. These temperatures are shown in Figures 18(a) and (b) along with the curve fit that was added to the code.

An important initial condition is the saturation of the cement. The greater the initial saturation, the greater the thermal expansion of the water and the greater the probability of high pore pressures. Complete saturation is unlikely; some residual air is expected to always remain in most pores. This value has never been determined for concrete, however. Osoba et al. (1951), studying the flow characteristics of oil and natural gas through rock, measured a gas residual of about 10 percent. Verma et al. (1985), in a laboratory study of the flow of steam and water through 100-μm glass beads, measured a steam residual of also about 10 percent. The possibility of phase changes makes these measurements very rough.

Figure 19 was developed to examine the effect of the initial saturation on pore pressures when the concrete is heated by the exhaust of an F/A-18 APU. Pore pressure just below the pavement surface is the dependent variable. The key point shown by this figure is that an initial

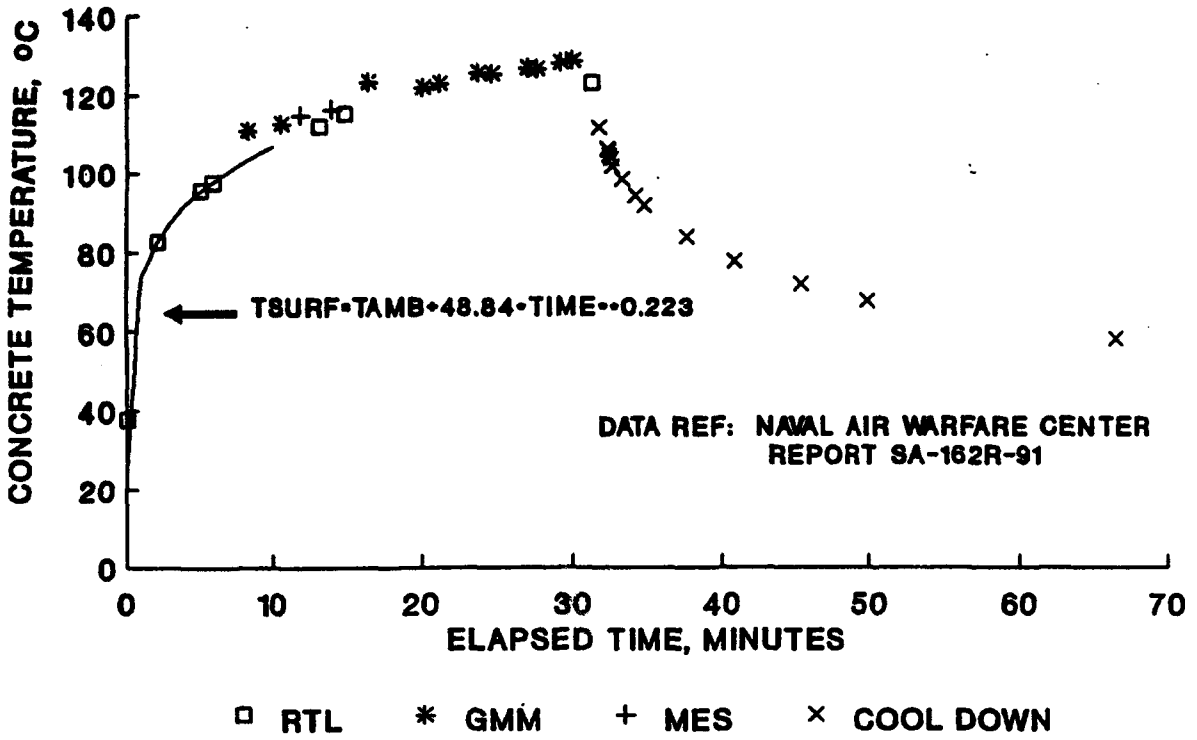

Figure 18(a)
Surface temperatures of concrete heated by an impinging F/A-18 APU.

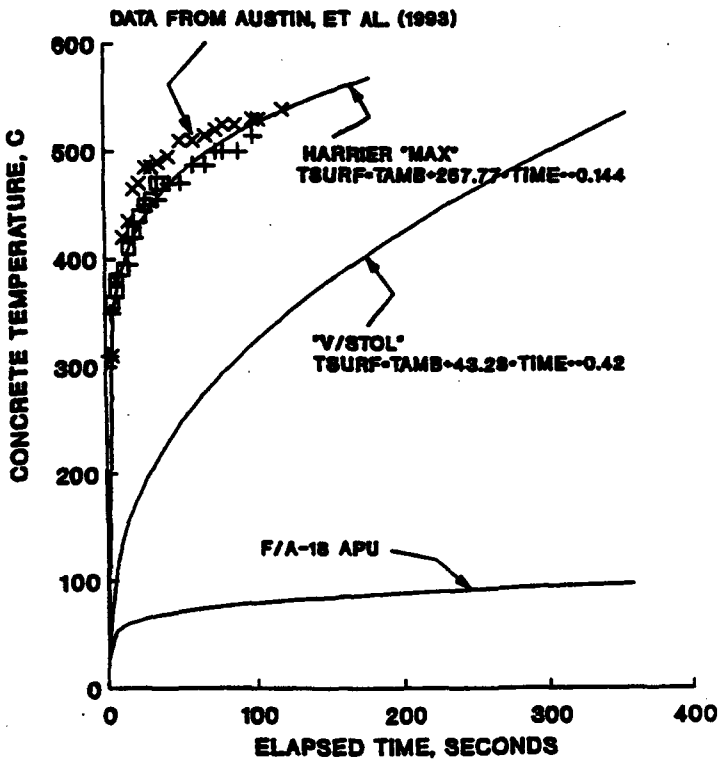

Figure 18(b)
Surface temperatures of concrete heated by an impinging VSTOL jet.

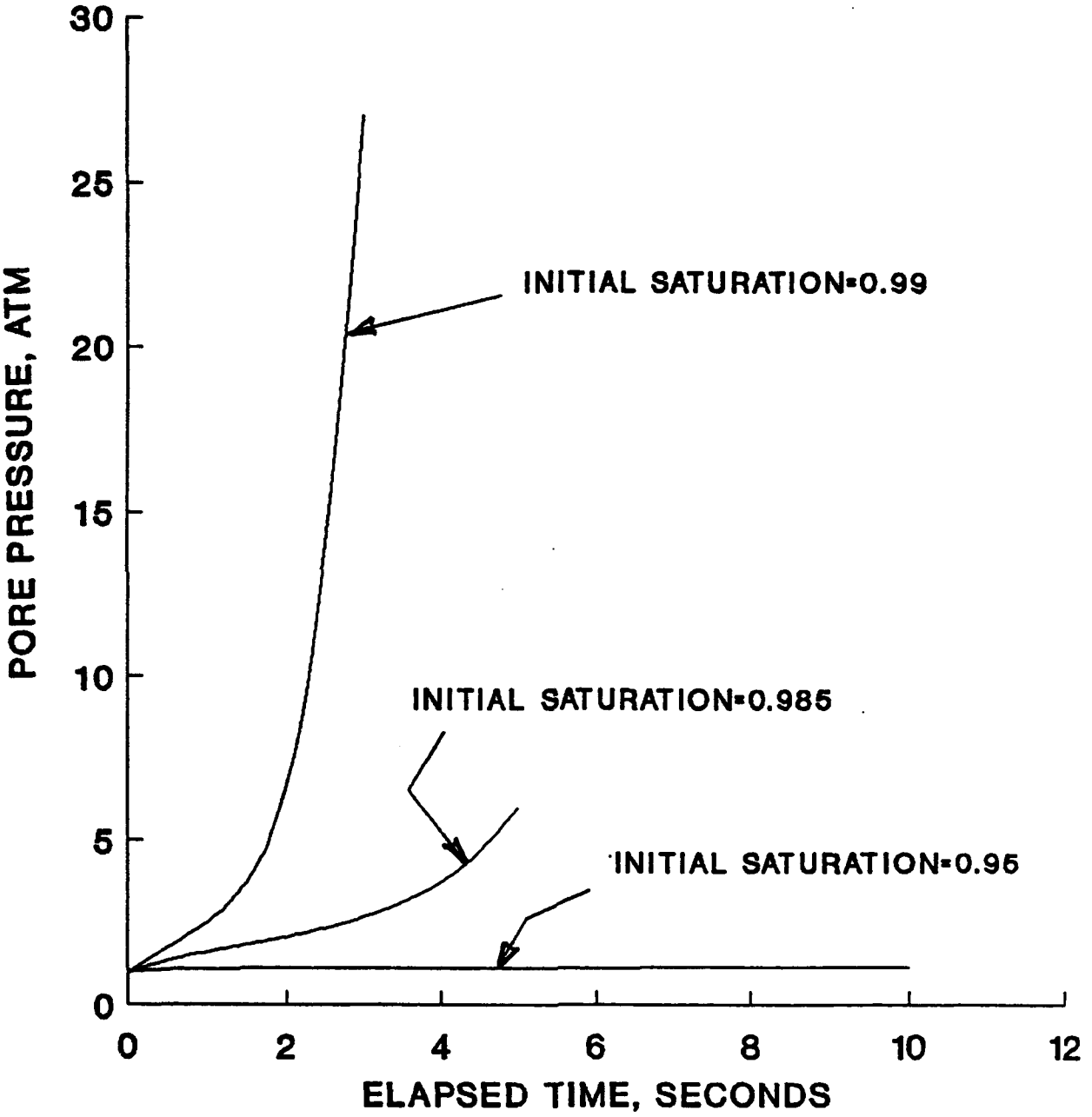

Figure 19
Concrete pore pressures at a depth of 0.1 mm when pavement heated by exhaust of F/A-18 APU.

saturation less than 95 percent has little influence on pore pressures. For the F/A-18 APU study, the initial saturation was set at 90 percent, i.e., assuming a maximum residual air of 10 percent.

Results of the POREFLOW simulation are summarized in Figures 20(a) through 20(c). The first 120 seconds following APU startup were simulated. This is the period during which concrete temperatures would be increasing most rapidly (see Figure 18(a)).

Figure 20(a) shows predicted pore pressure profiles down through the cement plotted after different intervals. Pore pressures were set initially at one atmosphere. The pavement surface pressure remains at one atmosphere. Pore pressures are increasing with time, but at a decreasing rate. After 120 seconds, the maximum APU induced pore pressure is only about 2 atmospheres. After the first 30 seconds, the maximum pressure gradient, which occurs at the surface, barely changes. The depth of the maximum pressure is slowly increasing with time.

As explained previously, the pore pressure is the sum of the water vapor pressure and the pressure of any air in the pores. Vapor pressure is a function of pore temperature, which is increasing slowly and at a decreasing rate at all depths, as shown by Figure 20(b). The air pressure is a function of the mass and volume of the air in the pores as well as the temperature. Near the pavement surface, air is being forced out of the pores faster than the air volume is decreased by the expansion of the liquid water, i.e., by the increase in saturation. This phenomenon is illustrated in Figure 20(c). The pore air pressure is actually decreasing near the surface. The increase in vapor pressure and decrease in air pressure cancel each other, and the pore pressure barely changes. Away from the surface, both the vapor pressure and air pressure are slowly increasing with time.

VSTOL Heated Pavements

To estimate potential runway damage when the cement is heated more rapidly, a pavement surface temperature versus time boundary condition was formulated to simulate temperatures that would be induced by the exhaust of a VSTOL taking off or landing. These surface temperatures are shown in Figure 18(b). The curve labeled Harrier "max" was extrapolated from laboratory data (Austin et al., 1993) in which the heating was almost a step function. The concrete was shielded until the test engine powered up to Harrier "conditions," and then the shield was mechanically yanked off. Pavement temperatures beneath an actual VSTOL exhaust would increase more slowly as the engine was started up before takeoff or the aircraft approached for a landing. With this in mind, the heating rate was arbitrarily decreased. The curve labeled "VSTOL" was used as a boundary condition and POREFLOW again was used to predict the influence of moisture on airfield pavement.

Figures 21(a) through 21(f) were developed assuming an initial saturation of 0.9. Except for the higher pavement surface temperature, initial and boundary conditions are identical to those used to study the effects of the APU exhaust. The results are strikingly different. Pore pressures at the surface (Figure 21(a)) increase very quickly to values high enough to cause the concrete to fail. This is primarily due to an increase in pore air pressure. Pore temperatures are now increasing rapidly (Figure 21(b)), and thermal expansion of the liquid water is filling up the pores (Figure 21(c)). This phenomenon is analogous to moving up from state "B1" on Figure 7. Unlike the APU heated concrete, the pore air does not have time to escape (Figure 21(d)), and is compressed by the expanding water. The pressure of water vapor in the pores, although increasing, contributes little to the total pore pressure that fails the concrete (Figure 21(e)).

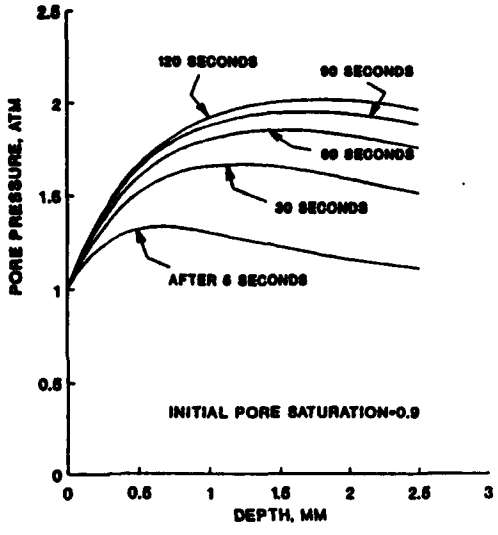

Figure 20(a)
Predicted pore pressure through concrete pavements heated by an F/A-18 APU.

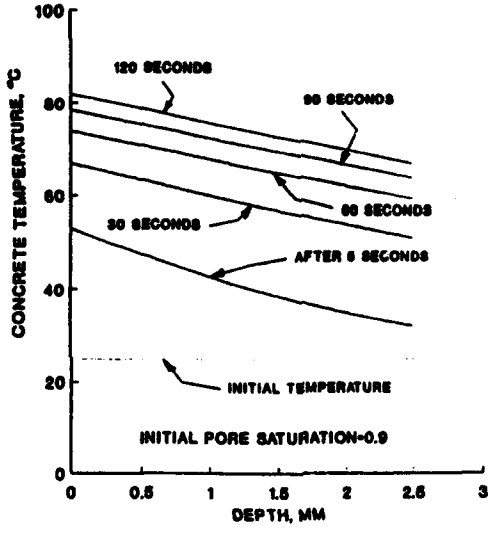

Figure 20(b)
Predicted temperature profiles through concrete pavements heated by an F/A-18 APU exhaust.

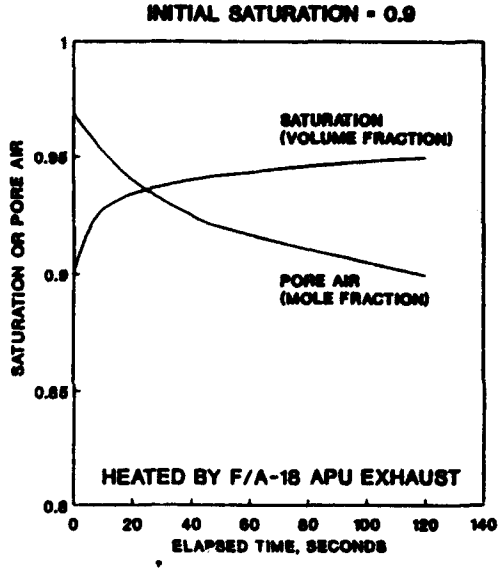

Figure 20(c)
Change in concrete pore air and saturation at a depth of 0.1 mm.

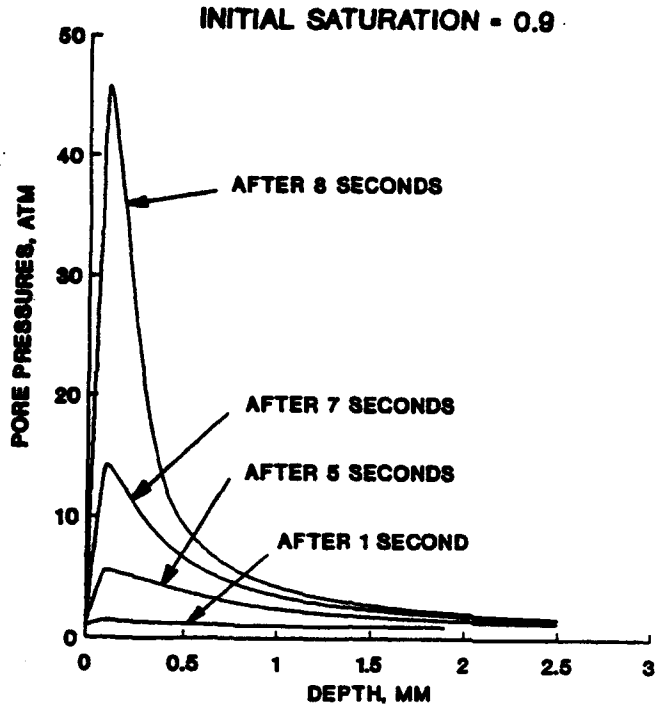

Figure 21(a)
Predicted pore pressures through concrete pavements heated by VSTOL exhaust.

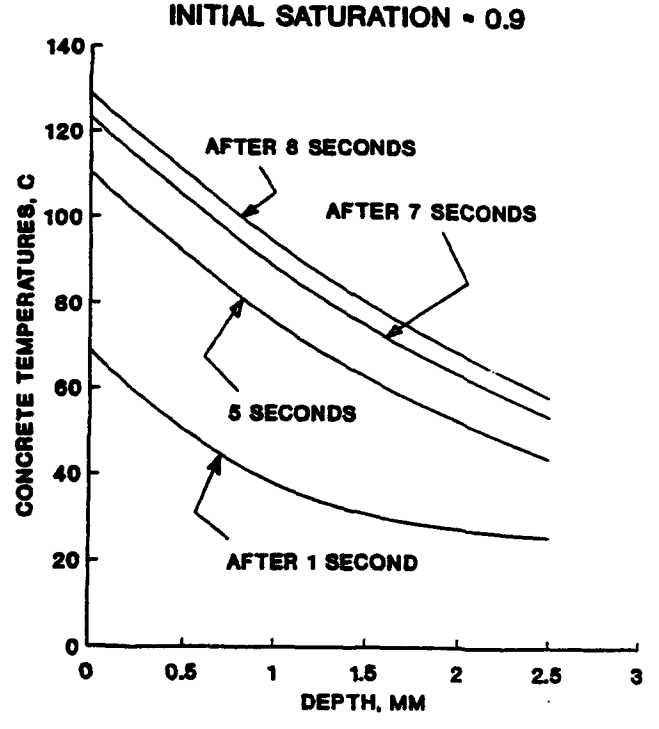

Figure 21(b)
Predicted temperature profiles through concrete pavements heated by VSTOL exhaust.

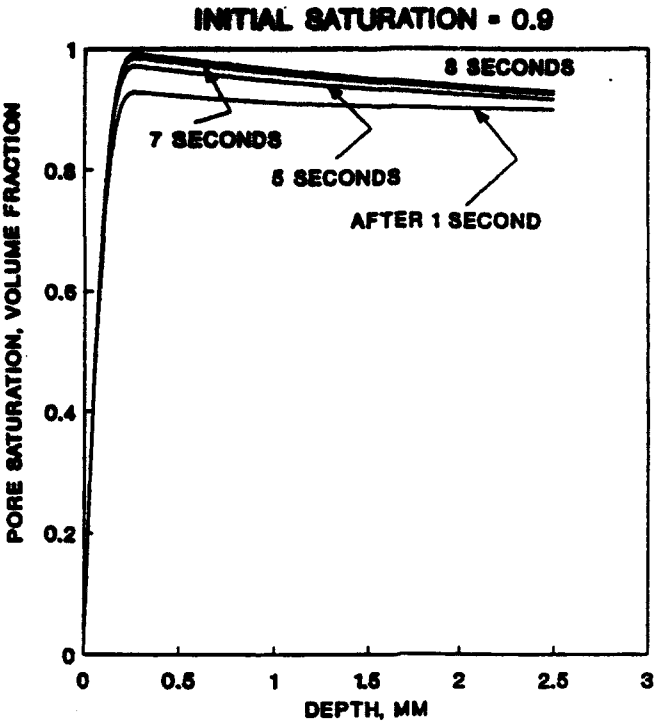

Figure 21(c)
Predicted saturation through concrete pavements heated by VSTOL exhaust.

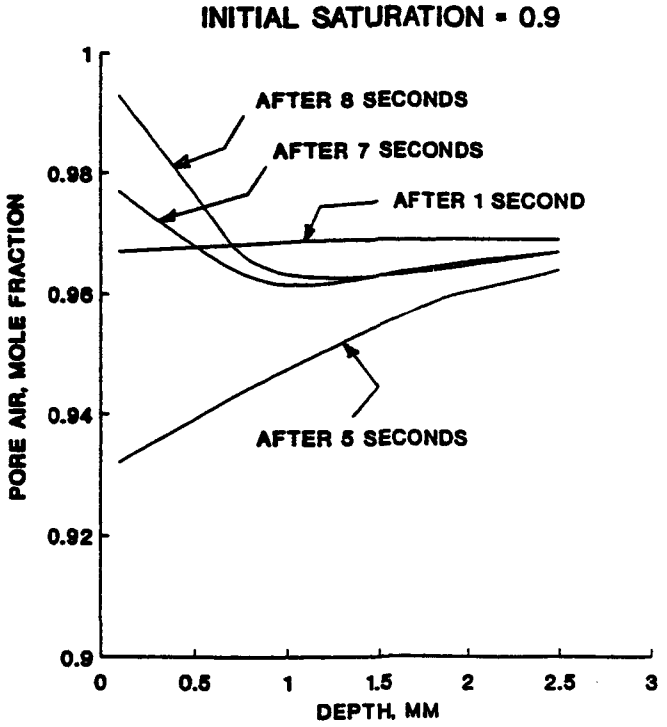

Figure 21(d)
Predicted air in pores of concrete pavements heated by VSTOL exhaust.

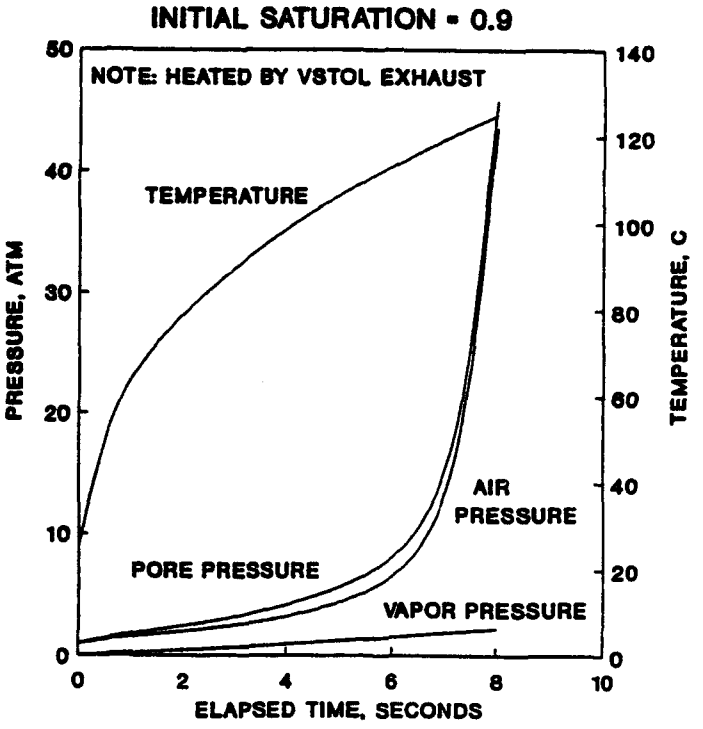

Figure 21(e)
Change in concrete pressure and temperature at a depth of 0.1 mm.

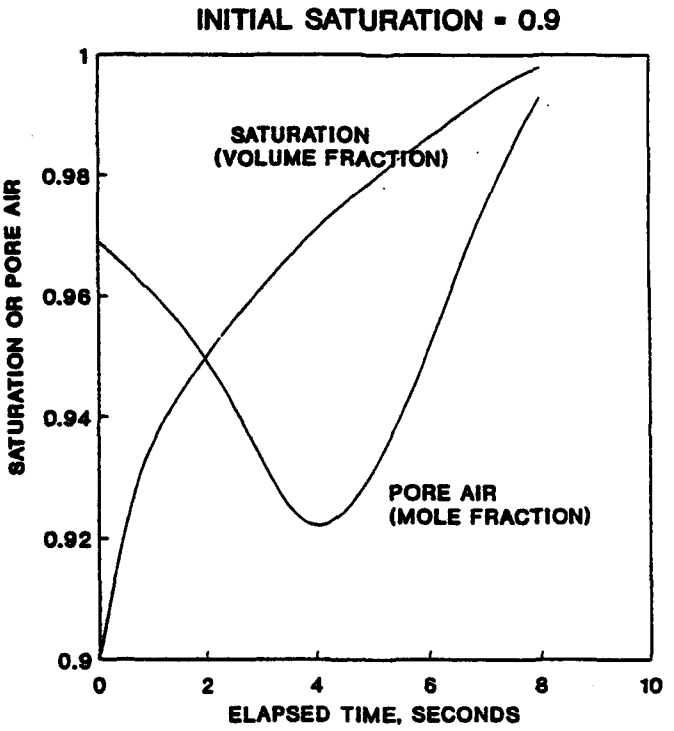

Figure 21(f)
Change in concrete pore air and saturation at a depth of 0.1 mm.

Figures 22(a) through 22(f) were developed assuming a VSTOL exhaust and an initial saturation of 0.7. Again, pore pressures at the surface increase to values high enough to cause the concrete to fail (Figure 22(a)). Pore temperatures are increasing at roughly the same rate (Figure 22(b)), and again the expanding water is filling up the pores (Figure 22(c)). This time, there is more air space to fill, and the air has time to escape (Figure 22(d)). This phenomena is analogous to the phenomena occurring in the APU heated pavement discussed above. Temperatures are much higher, however, and vapor pressures become significant (Figure 22(e)). The pavement would probably fail due to the pressure of the water vapor in the pores before the liquid water filled up the pore and was compressed.

The phenomena of moisture induced high pore pressures is perhaps better understood after comparing Figures 21(e) and 22(e) and comparing Figures 21(f) and 22(f).

Figures 23(a) through 23(d) were developed assuming a VSTOL exhaust and an initial saturation of 0.2. Pore pressures reach about the same levels they do when the pores are more saturated (Figure 23(a)), but it takes twice as long. Maximum pressures do not occur at the surface. Pressure gradients are not as severe as when the pores are more saturated. The rate of increase in pore temperatures is slightly higher due to the decrease in heat capacity caused by the decrease in the mass of water (Figure 23(b)).

These differences are all attributable to the low initial saturation. Vapor flowing out of the pores is sufficient to start draining the pores of the little liquid water that was initially present. This draining begins at the surface and progresses into the concrete as shown in Figure 23(c). Most of the air also leaves the pores near the surface. Maximum pressures now occur in the hottest pores that still have some liquid water and air in them. Pore pressures in the "dry" pores are induced primarily by superheated steam and perhaps a small amount of air passing through.

Figure 23(d) plots these phenomena together in a pore near the surface. After about 20 seconds, most of the air has been forced out of these pores. At this time, there is a decrease in the rate of increase of pore pressure. After about 42 seconds, the pore has been drained; there is not enough water left in the pores to support a liquid phase. This time there is an even sharper decrease in the rate at which pore pressures are increasing. After the pore is "dry," further increases in pressure are the result of further superheating the steam.

EXPERIMENTAL RESULTS

To substantiate the predictions of the model, small blocks of airfield pavement concrete were heated by a small burner at rates corresponding to an F/A-18 APU and then a VSTOL environment. Heating rates were determined by monitoring the surface temperature of the samples. The burner was set at whatever rate was necessary to duplicate the increases in surface temperatures shown in Figures 18(a) through 18(b).

Only the surface temperature was measured. Microscope photographs of the surfaces were taken at various stages of the heating. For each test, two concrete specimens were heated at the same rate. One of the specimens was "completely" saturated; the other was dried to remove all evaporable water. The dried specimens were used to identify failure modes not caused by pore water.

Preparation of the samples and details of the test procedures are discussed in Appendix C.

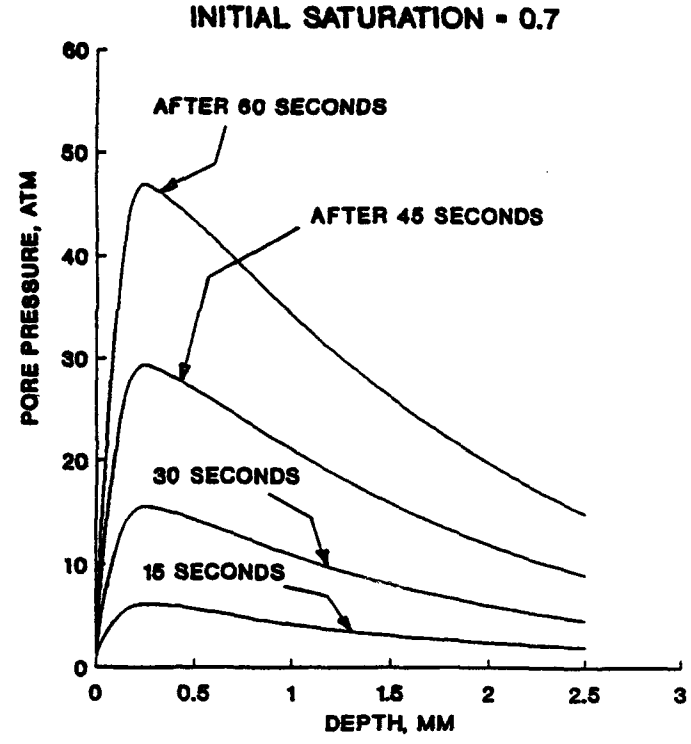

Figure 22(a)
Predicted pore pressures through concrete pavements heated by VSTOL exhaust.

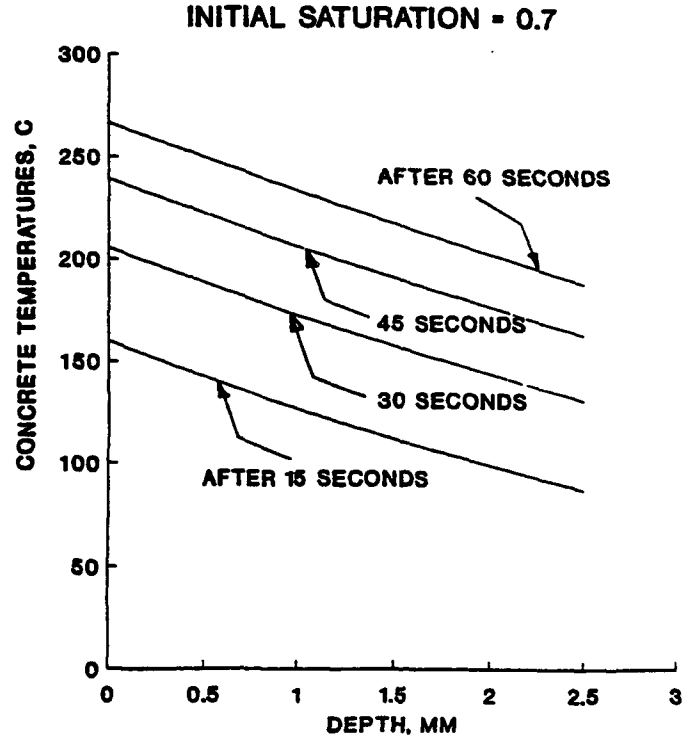

Figure 22(b)
Predicted temperature profiles through concrete pavements heated by VSTOL exhaust.

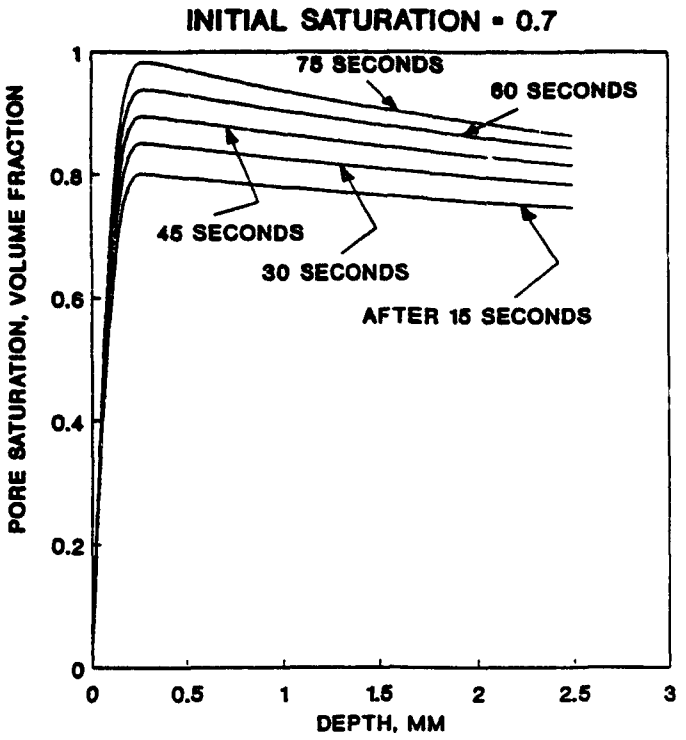

Figure 22(c)
Predicted saturation through concrete pavements heated by VSTOL exhaust.

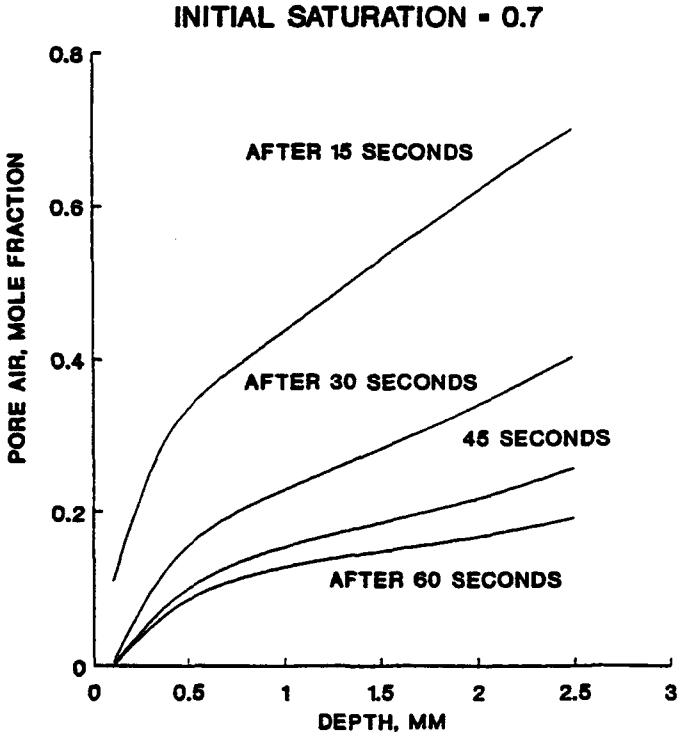

Figure 22(d)
Predicted air in pores of concrete pavements heated by VSTOL exhaust.

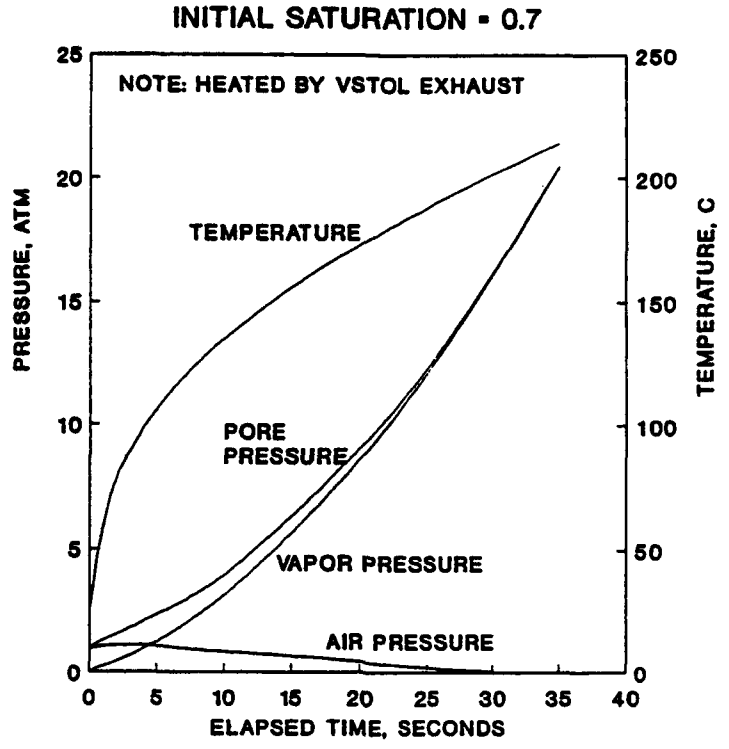

Figure 22(e)
Change in concrete pressure and temperature at a depth of 0.1 mm.

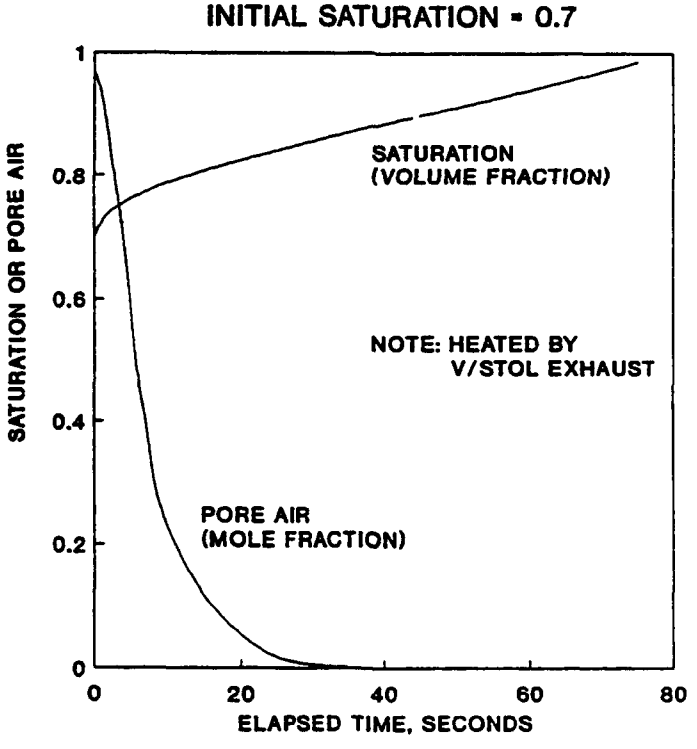

Figure 22(f)
Change in concrete pore air and saturation at a depth of 0.1 mm.

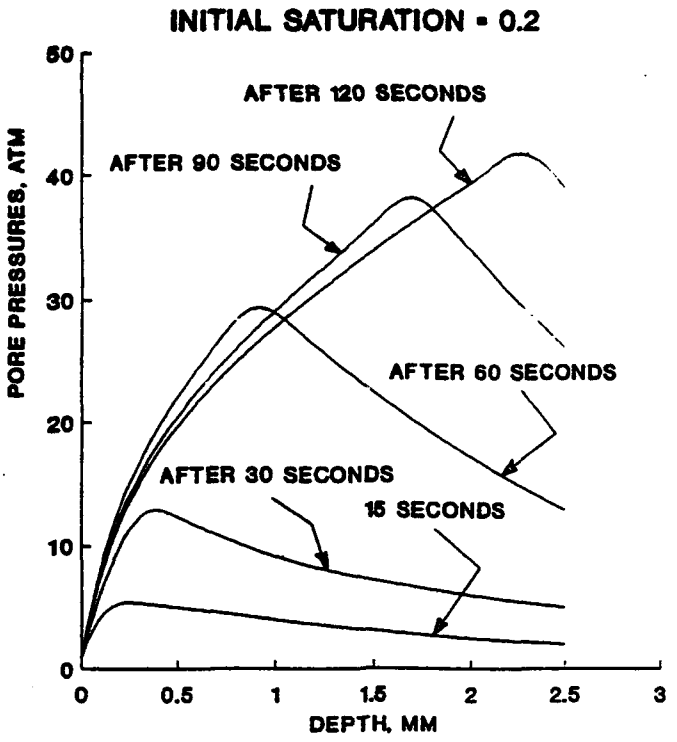

Figure 23(a)
Predicted pore pressures through concrete pavements heated by VSTOL exhaust.

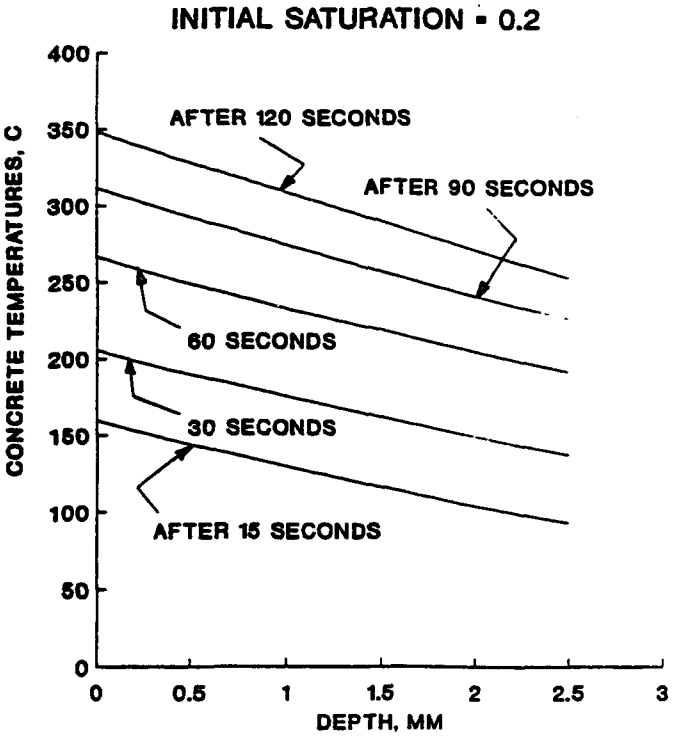

Figure 23(b)
Predicted temperature profiles through concrete pavements heated by a VSTOL exhaust.

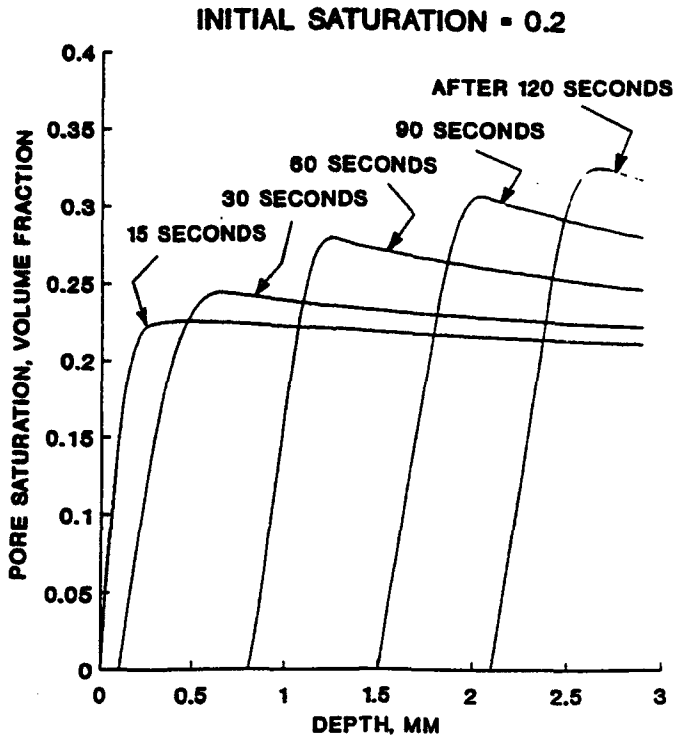

Figure 23(c)
Predicted saturation through concrete pavements heated by VSTOL exhaust.

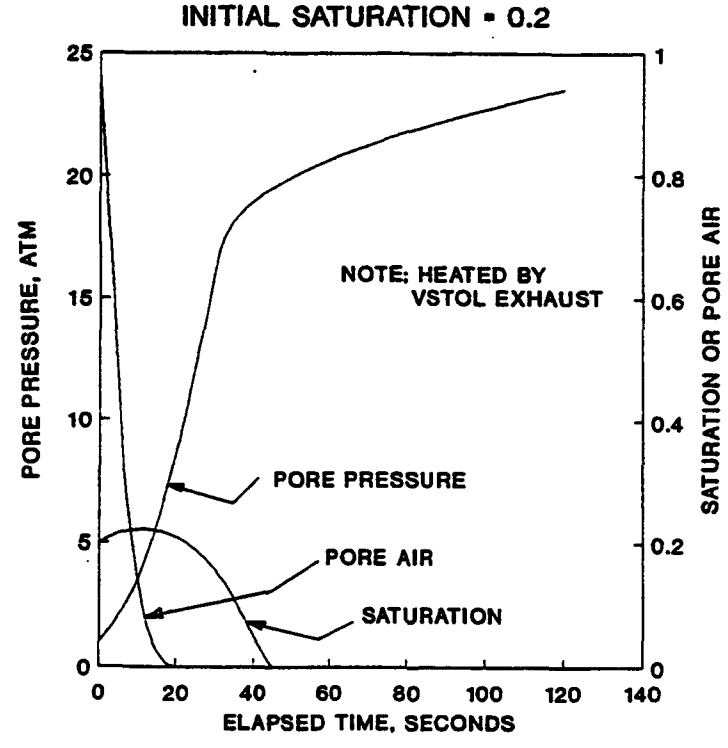

Figure 23(d)
Change in pore pressure and pore air at a depth of 0.1 mm.

None of the specimens heated at the APU rate showed any indication of scaling or any other type of surface damage other than an occasional crack. A layer of translucent crystals formed on the surface of the saturated specimens, as shown in Figure 24, which could cover pore size damage.

Three of the six saturated specimens heated at the VSTOL rate failed. In two cases, the failure mode was an explosive spall rather than a gradual scaling. Only the cement failed. No damage to the aggregate was apparent on either spall. Figure 25 is a 4X photograph showing the crater of a spall type material failure of cement between and around several pieces of aggregate. Figure 26 is a 25X photograph showing the edge and floor of this crater. Note that the cement is torn off the aggregate beneath the surface. This particular specimen failed when the surface temperature reached 230°C. The other spall occurred at about 300°C. In the third failure, the cement was not torn completely away but formed a fissure as shown in Figure 27. This figure is a 15X photograph. Steam could be observed leaving the concrete through this opening.

Cracks also formed in the specimens heated at the VSTOL rate. This damage occurred in both the saturated and dried specimens and can be presumed to be caused by the uneven expansion of the cement and aggregate. The cracks formed through the cement and along the interface with the aggregate (Figure 28). Cracks also formed in small oases among the crystallized surfaces.

COMMENTS

This research was based upon the hypothesis that the concrete failure was the result of thermally expanding pore water filling up the pore volume and then being compressed. A major corollary of this work is that pore pressures can exceed the tensile strength of concrete via three mechanisms:

1. High saturated water pressures.

2. Water expanding against the air in the pores.

3. Water expanding against the solid walls of the pores after all air has been forced out.

The failure mode, and whether failure occurs, was found to be dependent upon the initial pore saturation and the heating rate, i.e., type of engine. Although not included as a parameter in this work, it is presumed that the type of cement and the mix characteristics, since both influence flow resistance, also influence mode of failure.

Perhaps the specimens used in the experiments should have been made of mortar rather than concrete. The model assumes mortar. Non-moisture related failure modes such as expansion cracks would have been eliminated.

The apparent scaling of airfield pavements by the F/A-18 APU was the catalyst for this research. The work was expanded to include potential pavement problems generated by VSTOL aircraft during takeoff and landing. No changes in the model were made for the VSTOL study. For example, dehydration of the cement was not included. At VSTOL temperatures, dehydration reactions would change the evaporable water in the pores of the cement and probably change the resistance to flow through the cement.

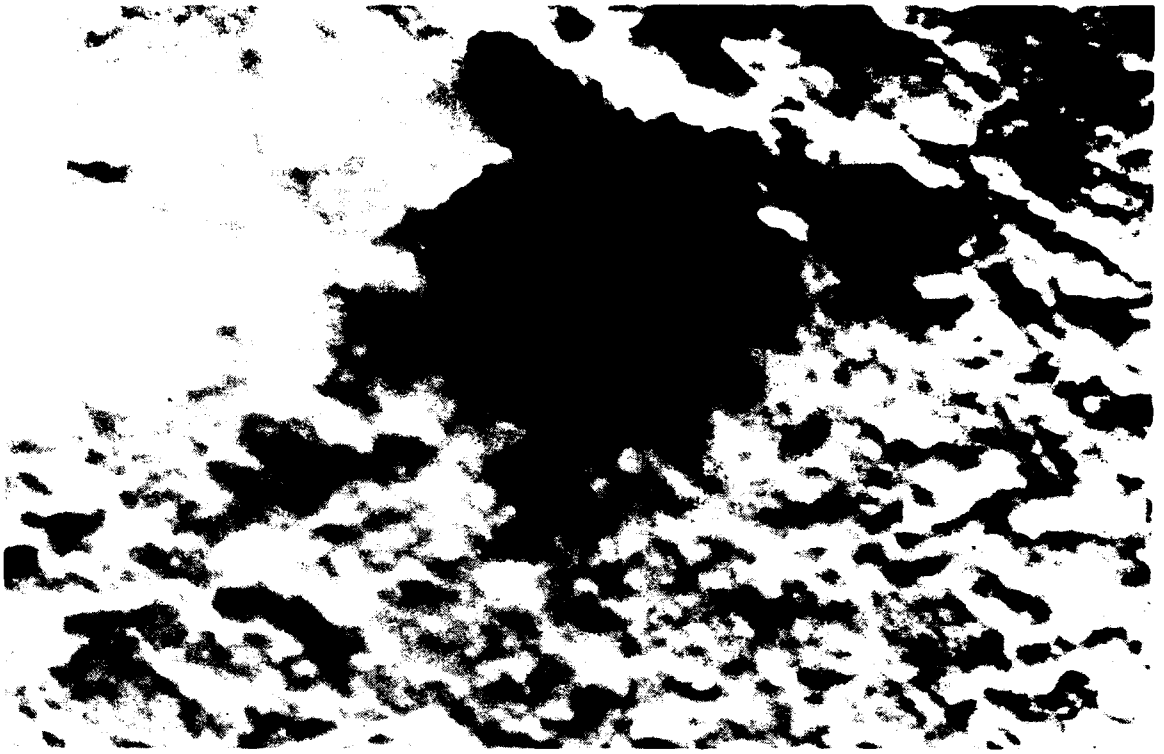

Figure 24
25X photograph of saturated concrete subjected to
six cycles of a simulated F/A-18 APU exhaust.

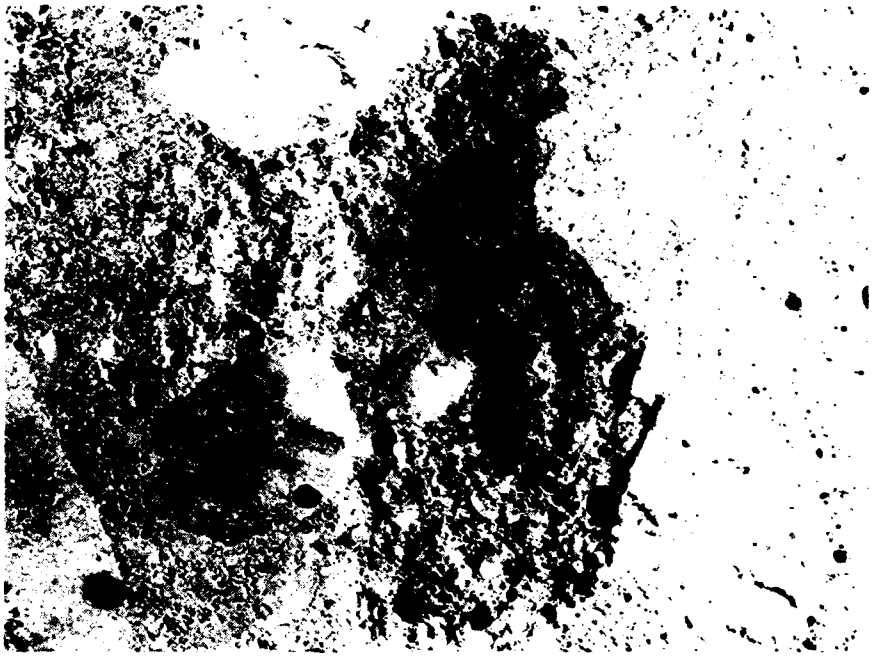

Figure 25
Crater formed by explosive spall of saturated concrete
heated at a rate equivalent to a VSTOL taking off.

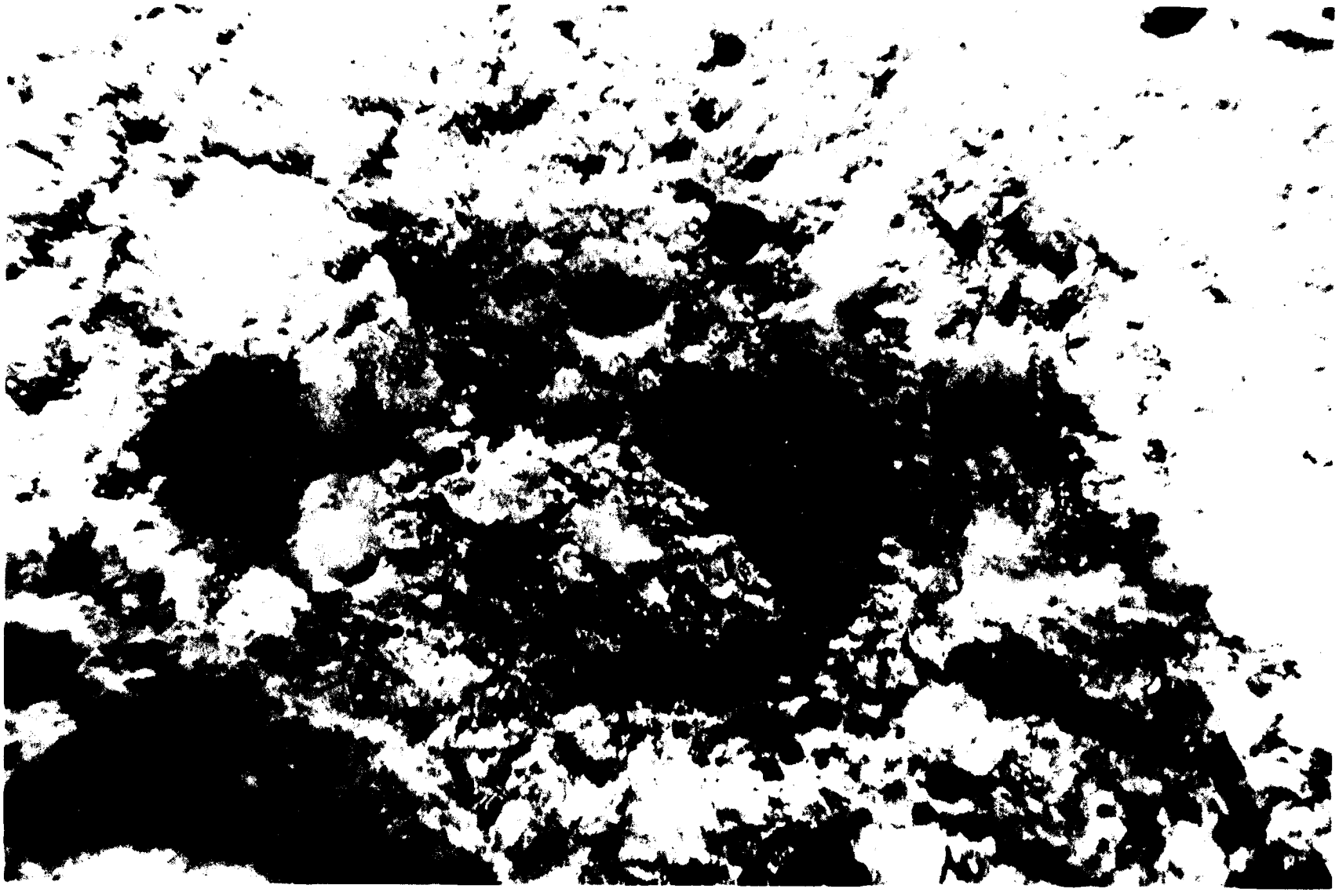

Figure 26
25X photograph of the edge and floor of the crater.

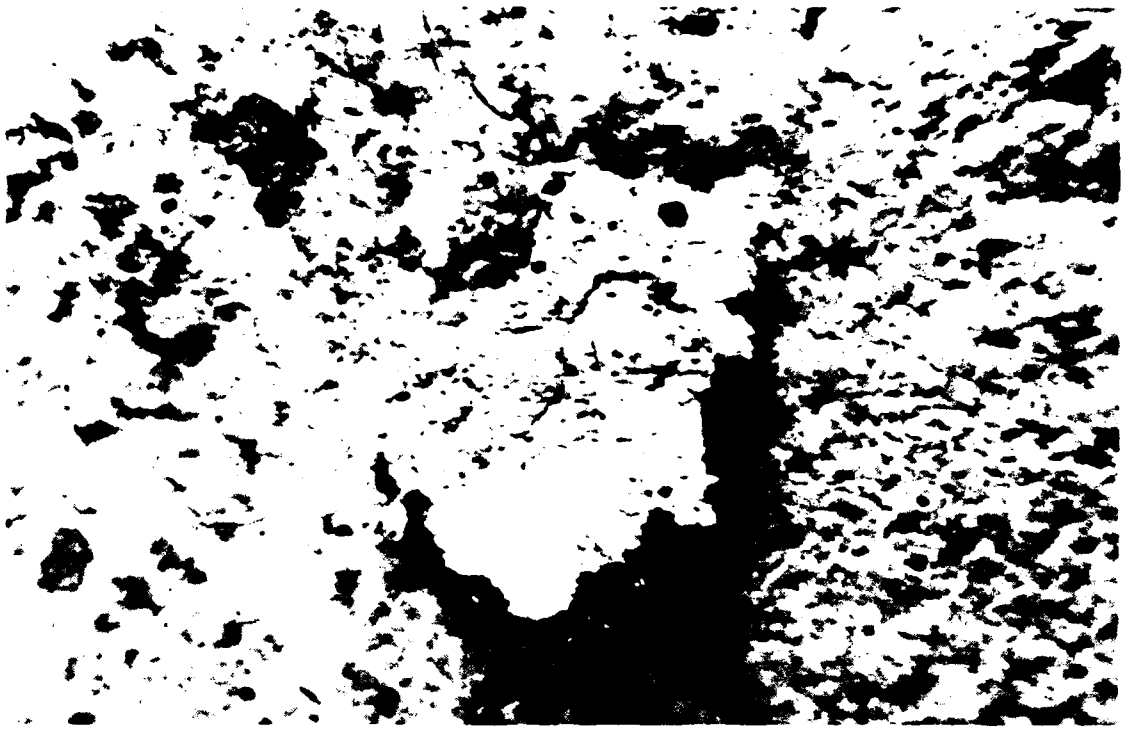

Figure 27
Fissure formed in saturated concrete heated at a rate equivalent to an impinging VSTOL aircraft jet.

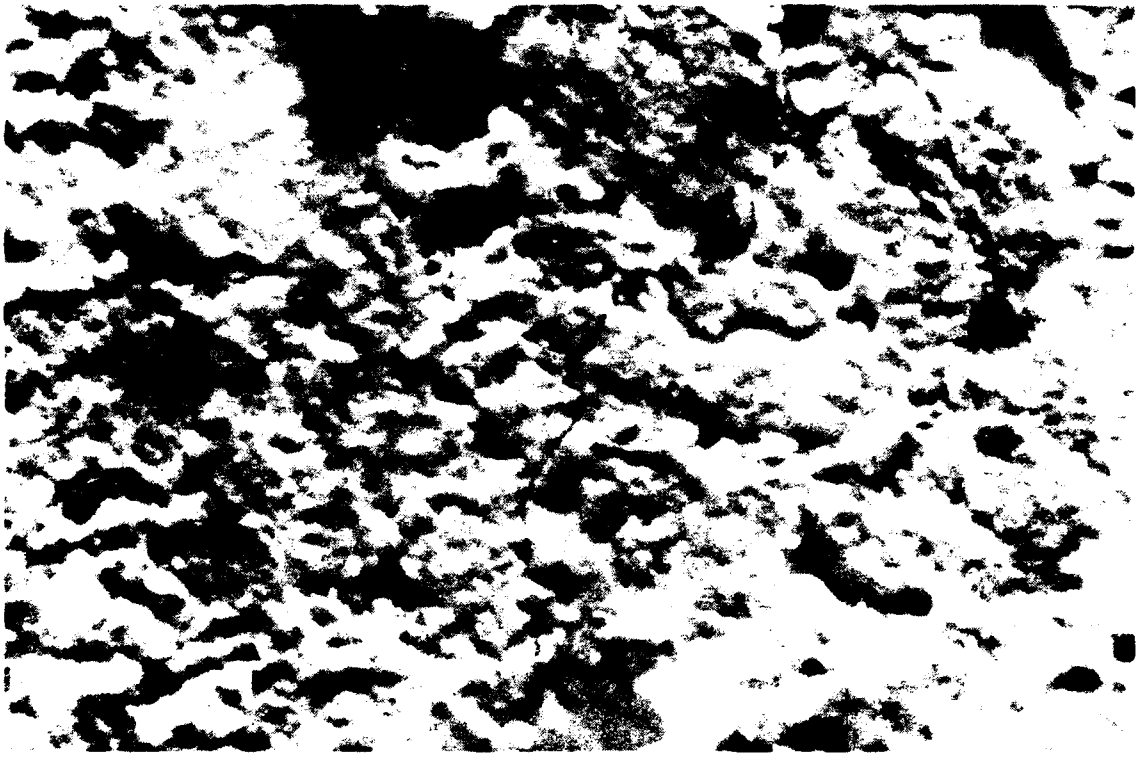

Figure 28
Surface of dried concrete heated at a rate equivalent to a VSTOL taking off or landing.

Pore size damage was anticipated but never observed. Experimentally induced failures were in the form of an explosive spall, or cracks, rather than gradual scaling. Perhaps airfield pavements are rarely completely saturated.

CONCLUSIONS

Moisture in the pores of the cement is unlikely to be the primary cause of material failure in airfield pavements heated by the F/A-18 APU. The pavement surface reaches a maximum temperature of only about 130°C. The saturated vapor pressure at this temperature is less than three atmospheres. Heating is relatively slow. Even if the pores have been nearly saturated, the water will escape before any damage can be done.

Moisture is a probable cause of pavement failure, however, when the cement is being heated by the exhaust of a VSTOL, such as the AV-8B Harrier, during takeoff and landing. For an initial pore saturation of 90 percent or greater, extremely high pore pressures result from air being compressed by the thermal expansion of liquid water. Maximum pressures occur near the surface of the concrete, and very large pressure gradients are induced. Failure would occur very rapidly.

Concrete temperatures beneath a VSTOL exceed 500°C. The water vapor pressure corresponding to a temperature of only 250°C would be sufficient to induce a tensile failure in portland cement concrete. For moderate or even low pore saturation, high pore pressures can still occur, resulting from the high vapor pressures of pore water. Failure will take longer. Pressure gradients are usually less severe.

REFERENCES

Ahmed, N. and D.K. Sunada (1969). "Nonlinear flow in porous media," Journal of the Hydraulics Division, Proceedings of the American Society of Civil Engineers, vol 95, no. HY6, 1969, pp 1847-1857.

Auskern, A. and W. Horn (1973). "Capillary porosity in hardened cement paste," Journal of Testing and Evaluation, vol 1, no. 1, 1973, pp 74-79.

Austin, S.A., P.J. Robins, and M.R. Richards (1993). "Jet-blast resistant concrete for Harrier aircraft pavements," submitted as a candidate for publication in the Journal of the Institute of Structural Engineers, 1993.

Bazant, Z.P. and W. Thonguthal (1978). "Pore pressure and drying of concrete at high temperature," Journal of the Engineering Mechanics Division, Proceedings of the American Society of Civil Engineers, vol 104, no. EM5, 1978, pp 1059-1079.

Bazant, Z.P. and W. Thonguthal (1979). "Pore pressure in heated concrete walls: theoretical prediction," Magazine of Concrete Research, vol 32, no. 107, 1979, pp 67-76.

Bazant, Z.P. (1982). Normal and refractory concretes for LMFBR applications; Volume 1: Review of literature on high temperature behavior of portland cement and refractory concretes, Electric Power Research Institute, Technical Report EPRP-2437. Palo Alto, CA, 1982.

Bear, J. (1972). Dynamics of fluids in porous media. New York, NY, Elsevier, 1972.

Bier, T.A., S. Wise, and P. Chang (1991). A mechanistic study of failure of concrete subjected to cyclic thermal loads. Naval Civil Engineering Laboratory, Contract Report CR 91.008. CEMCOM Research Associates, Inc., Lanham, MD, 1991.

Brooks, R.H. and A.T. Corey (1964). Hydraulic properties of porous media, Hydrology paper no. 3, Colorado State University. Fort Collins, CO, 1964.

Chekhovsky, J.V., L.E. Berlin, and M.I. Brusser (1973). "Investigation into cement concrete porous structure and its relationship with technological factors and physical properties of concrete," Proceedings of the International Symposium RILEM/UPAC, ed. by S. Modry, Prague, 18-21 Sep 1973, pp B-51 to B-69.

Collepardi, M. (1973). "Pore structure of hydrated tricalcium silicate," Proceedings of the International Symposium RILEM/UPAC, ed. by S. Modry, Prague, 18-21 Sep 1973, pp B-25 to B-49.

Conte, S.D. and C. de Boor (1972). Elementary numerical analysis, 2nd ed. New York, NY, McGraw-Hill, 1972, pp 284-290.

Copeland, L.E. and J.C. Hayes (1953). "Determination of non-evaporable water in hardened portland cement paste," ASTM Bulletin No. 194, 1953, pp 70-74.

Cornell, D. (1952). Flow of gases through consolidated porous media, Ph.D. dissertation, University of Michigan. Ann Arbor, MI, 1952.

Cornell, D. and D.L. Katz (1953). "Flow of gases through consolidated porous media," Industrial and Engineering Chemistry, vol 45, no. 10, 1953, pp 2145-2152.

Dass, W.C. (1990). Applied Research Associates, Inc. Letter Report: ASTOVL slab tests. Air Force Engineering and Services Center, Tyndall AFB, FL, 31 Oct 1990.

Defay, R. and I. Prigogine (1966). Surface tension and adsorption, 1st ed. London, U.K., Longmans-Green and Co., Ltd., Chapter XV, 1966.

Diamond, S. (1973). "Pore structure of hardened cement paste as influenced by hydration temperature," Proceedings of the International Symposium RILEM/UPAC, ed. by S. Modry, Prague, 18-21 Sep 1973, pp B-73 to B-88.

Double, D.D. and A. Hellawell (1977). "The solidification of cement," Scientific American, vol 237, no.1, 1977, pp 82-90.

Doughty, C. and K. Pruess (1990). "A similarity solution for two phase fluid and heat flow near high-level nuclear waste packages emplaced in porous media," International Journal of Heat and Mass Transfer, vol 33, no. 6, 1990, pp 1205-1222.

Dullien, F.A.L. (1979). Porous media fluid transport and pore structure, 1st ed. New York, NY, Academic Press, 1979, pp 143-145.

England, G.L. and A.D. Ross (1970). "Shrinkage, moisture, and pore pressure in heated concrete," in Concrete for Nuclear Reactors, American Concrete Institute Special Publication No. 34, Detroit, MI, 1970, pp 883-907.

England, G.L. and T.J. Sharp (1971). "Migration of moisture and pore pressures in heated concrete," Proceedings of the First International Conference on Structural Mechanics in Reactor Technology, Paper no. H2/4, Berlin, Germany, 1971.

Fagerlund, G. (1982). "On the capillarity of concrete," Nordic Concrete Research Publication No. 1, The Nordic Concrete Federation. Oslo, Norway, 1982, pp 6.1-6.20.

Fancher, G.H. and J.A. Lewis (1933). "Flow of simple fluids through porous materials," Industrial and Engineering Chemistry, vol 25, no. 10, 1933, pp 1139-1147.

Fatt, I. and W.A. Klikoff (1959). "Effect of fractional wettability on multiphase flow through porous media," AIME Technical Note No. 2043, AIME Transactions, vol 216, 1959, pp 426-432.

Firoozabadi, A. and D.L. Katz (1979). "An analysis of high velocity gas flow through porous media," Journal of Petroleum Technology, 1979, pp 211-216.

Geertsma, J. (1974). "Estimating the coefficient of inertial resistance in fluid flow through porous media," Society of Petroleum Engineers Journal, 1974, pp 445-450.

Green, L. and P. Duwez (1951). "Fluid flow through porous metals," Journal of Applied Mechanics, vol 18, 1951, pp 39-45.

Hassanizadeh, S.M. and W.G. Gray (1987). "High velocity flow in porous media," Transport in Porous Media, vol 2, 1987, pp 521-531.

Haynes, H.H. and R.D. Rail (1986). Handbook for design of undersea, pressure resistant concrete structures, Naval Civil Engineering Laboratory, Technical Note N-1760. Port Hueneme, CA, 1986.

Harmathy, T.Z. and J.E. Berndt (1966). "Hydrated portland cement and lightweight concrete at elevated temperatures," Journal of the American Concrete Institute, vol 63, no. 1, 1966, pp 93-111.

Houck, M.L. (1990). F-18 auxiliary power unit exhaust gas footprint evaluation test, U.S. Naval Air Propulsion Center, Technical Report LR-90-18. Trenton, NJ, 1990.

Houck, S.W., D.N. Gordge, and C.A. Hadfield (1992). Evaluation of an F/A-18 auxiliary power unit modified nozzle, Naval Air Warfare Center, Report SA-162R-91. Patuxent River, MD, 1992.

Huang, C.L.D. and G.N. Ahmed (1991). "Influence of slab thickness on responses of concrete walls under fire," Numerical Heat Transfer, Part A, vol 119, 1991, pp 43-64.

Jung, M. (1973). "The porosity of hydrated cement as a function of temperature in the range 20 to 1400 C and its influence on refractory concrete characteristics," Proceedings of the International Symposium RILEM/UPAC, ed. by S. Modry, Prague, 18-21 Sep 1973, pp B-89 to B-107.

Keenan, J.H. and F.G. Keyes (1936). Thermodynamic properties of steam, 1st ed. New York, NY, John Wiley, 1936, pp 11-24.

Lankard, D.R., D.L. Birkimer, F. Fondriest, and M.J. Snyder (1971). "Effects of moisture content on the structural properties of portland cement concrete exposed to temperatures up to 500 F," in Temperature and Concrete, American Concrete Institute publication SP-25. Detroit, MI, 1971, pp 59-102.

McVay, M.C., L.D. Smithson, and C.W. Manzione (1993). "Chemical damage to airfield concrete aprons from heat and oils," to be published in the Proceedings of the American Concrete Institute, Materials Journal, 1993.

McVay, M.C. and J.W. Rish (1993). "Flow of nitrogen and superheated steam through cement mortar," submitted for publication to the Journal of Thermophysics and Heat Transfer, 1993.

Muskat, M. (1937). The flow of homogeneous fluids through porous media, 1st ed. New York, NY, McGraw-Hill, 1937.

Neville, A.M. (1973). Properties of concrete, 2nd ed. New York, NY, Pitman Publishing, 1973, pp 23-36.

Noman, R. and J.S. Archer (1988). "High velocity flow in liquid saturated porous media and its visualization," Journal of Canadian Petroleum Technology, vol 27, no. 3, 1988, pp 64-69.

Ortega, J.M. and W.C. Rheinboldt (1970). Iterative solution of nonlinear equations in several variables, 1st ed. New York, NY, Academic Press, 1970, pp 219-220.

Osoba, J.S., J.G. Richardson, J.K. Kerver, J.A. Hafford, and P.M. Blair (1951). "Laboratory measurements of relative permeability," Petroleum Transactions, American Institute of Mining and Metallurgical Engineers, vol 192, 1951, pp 47-56.

Powers, T.C. (1949). "The nonevaporable water content of hardened portland-cement paste--Its significance for concrete research and its method of determination," American Society of Testing and Materials Bulletin No. 158, Philadelphia, PA, 1949, pp 68-76.

Sahota, M.S. and P.J. Pagni (1979). "Heat and mass transfer in porous media subject to fires," International Journal of Heat and Mass Transfer, vol 22, no. 7, 1979, pp 1069-1081.

Scheidegger, A.E. (1974). The physics of flow through porous media, 3rd ed. Toronto, Canada, University of Toronto Press, 1974, pp 152-170.

Shapiro, A.H. (1953). The dynamics and thermodynamics of compressible fluid flow, Volume I, 1st ed. New York, NY, Ronald Press, 1953, Chapter 4.

Temeng, K.O. (1988). Effects of high pressure gradients on the flow of real gases through porous media, Ph.D. dissertation, Stanford University. Stanford, CA, 1988.

Tomita, H. (1960). Effects of jet engine exhaust on Virginia Diabase Concrete pavement, Naval Civil Engineering Laboratory, Technical Report R-89. Port Hueneme, CA, 1960.

van Genuchten, M.Th. (1980). "A closed form equation for predicting the hydraulic conductivity of unsaturated soils," Soil Science Society of America Journal, vol 44, 1980, pp 892-898.

Verbeck, G. (1966). "Pore structure," in Special Publication No. 169-A: Significance of tests and properties of concrete making materials, American Society of Testing and Materials, Philadelphia, PA, 1966, pp 211-219.

Verma, A.K., K. Pruess, C.F. Tsang, and P.A. Witherspoon (1985). "A study of two-phase concurrent flow of steam and water in an unconsolidated porous medium," Proceedings of the 23rd ASME/AIChE National Heat Transfer Conference, HTD Volume 46: Heat Transfer in Porous Media and Particulate Flows, American Society of Mechanical Engineers, Denver, CO, 1985, pp 135-143.

Winslow, D.N. and S. Diamond (1970). "A mercury porosimetry study of the evolution of porosity in portland cement," Journal of Materials, vol 5, no.3, 1970, pp 564-585.

Wright, D.E. (1968). "Nonlinear flow through granular media," Journal of the Hydraulics Division, Proceedings of the American Society of Civil Engineers, vol 94, no. HY 4, 1968, pp 851-872.

Zucrow, M.L. and J.D. Hoffman (1976). Gas Dynamics, Volume I, 1st ed. New York, NY, John Wiley, Appendix C, 1976.

Appendix A

COMPUTATIONAL PROCEDURES

This appendix discusses the method used to evaluate the integrals in Equation 10 in the main text of this report and the numerical techniques used to solve the governing equations. A sample calculation and a listing of the FORTRAN program developed to make these calculations are also included.

INTEGRATION SCHEME

Rewriting Equation 10,

$$f_1 = \frac{2}{c_p T_1}\left[\int_2^3 \rho Q d\rho + \int_2^3 \rho^2 dQ\right] \qquad \text{(A-1)}$$

Integrating the first integral by parts,

$$\int_2^3 \rho Q d\rho = \frac{Q\rho^2}{2}\Big|_2^3 - \frac{1}{2}\int_2^3 \rho^2 dQ$$

$$\int_2^3 \rho Q d\rho = \frac{\bar{Q}\rho_3^2}{2} - \frac{1}{2}\int_2^3 \rho^2 dQ$$

and using the result to eliminate this integral from Equation A-1,

$$f_1 = \frac{2}{c_p T_1}\left[\frac{\bar{Q}\rho_3^2}{2} + \frac{1}{2}\int_2^3 \rho^2 dQ\right]$$

The remaining integral is evaluated numerically, employing a trapezoidal approximation (Conte and de Boor, 1972),

$$\int_2^3 \rho^2 dQ = \frac{\bar{Q}}{2}\left(\rho_2^2 - \rho_3^2\right) + \bar{Q}\rho_3^2$$

$$\int_2^3 \rho^2 dQ = \frac{\bar{Q}}{2}\left(\rho_2^2 + \rho_3^2\right)$$

and

$$f_1 = \frac{2\bar{Q}}{c_p T_1}\left(\frac{1}{4}\rho_2^2 + \frac{3}{4}\rho_3^2\right) \qquad \text{(A-1a)}$$

Comparing Equation A-1a with Equation 10a,

$$C_4 = \frac{1}{4}$$

$$C_5 = \frac{3}{4}$$

These values of the constants C_4 and C_5 are assumed throughout this work.

SOLUTION OF GOVERNING EQUATIONS

The partial differential Equations 20, 22, and 23 are approximated using finite differences. Equations 18 through 34 are then solved simultaneously for the unknown variables. Although slab temperature was found to be a weak function of gas flow rate through the concrete, a more universal model was desired, and the convective term in the energy equation was retained. This term makes the problem nonlinear and necessitates an iterative solution. Several iterative techniques were tried, but only the simplest, single step iteration (Ortega and Rheinboldt, 1970) would converge over the entire range of boundary conditions required for the concrete analyses.

COMPUTER PROGRAM "POREFLOW"

The system of equations is programmed in FORTRAN 77, and the problems are run on an IBM compatible 486 PC. Run times in hours are typical.

The solution is complicated by the great disparity in the magnitudes of the variables and in their convergence rates. Successive relaxation is applied to all variables. Gas pressures require considerable underrelaxation. Convergence of each of the governing equations is monitored separately. When convergence is achieved, the equation is deleted from the iteration loop. A variable time step is used but with limited success; rates of change of the different variables reach their maximums at different times.

Running the Program

The input is all contained in the first few lines of POREFLOW: the type of concrete, geometry, initial and boundary conditions. Time steps are also input. Convergence tolerance and the relaxation coefficients are parameters. The coefficients C_1, C_2, and C_3 of Equation 19 are an input.

Sample Problem

Predicted results of heating highly saturated concrete have already been discussed in some detail. The equations governing POREFLOW are also valid when the pores are dry or only partially saturated. Such a problem makes a good example to illustrate the output of the program.

Figure A-1 shows concrete surface temperatures used as a boundary condition. The heating and cooling have been accelerated; heating lasts 10 seconds, and the concrete surface is cooled back down to ambient in another 20 seconds. Therefore, the results are only qualitative. All pores initially contain 10 percent liquid water. Brooksville limestone aggregate is assumed, mixed at a water/cement ratio of 0.38. Figure A-2 shows predicted temperature profiles through the concrete during the heating/cooling cycle.

Concrete pore pressures calculated to occur during the heating cycle are shown in Figure A-3(a). The maximum pressure occurs at the surface and just after the jet initially strikes the concrete. This would be expected. Pore pressure is the sum of the saturated vapor pressure, increasing exponentially with temperature and thus maximum at the surface, and the air pressure. Air pressure increases with temperature and also with decrease in volume as the liquid water expands in the pore, both maximum at the surface.

After a short period of time, much of the water and air contained in the surface pores is forced out the top. There is not enough water left in these pores to sustain a liquid phase, and the vapor pressure drops below saturation. Air pressure decreases. The peak pore pressure now occurs deeper into the concrete where there is still liquid water and air. This is happening faster than the interior temperature is increasing, therefore, the peak pressure is decreasing with time.

The movement of water and air are shown in Figures A-4(a) and A-5(a), respectively. Note that both fluids are being forced away from the maximum pressure, out the top or deeper into the interior of the concrete. The increase in peak saturation, shown in Figure A-4(a) after 5 and 10 seconds, is caused by an increase in water volume rather than an increase in the total mass of liquid water.

Pore pressures calculated to occur during the cooling of the concrete are shown in Figure A-3(b). Of particular interest is the suction generated in the pores as the gases cool. Pressure ratios are low, and the gas density is decreasing faster than the mass can be increased by flow from adjacent pores. Although Figure A-4(b) does not show it very well, fluids are being sucked in from the surface and up from the interior of the concrete.

The program listing below includes the input used to generate Figures A-1 through A-5. Table A-1 is a typical output for this sample problem.

FORTRAN LISTING

```
C  U.S. NAVAL CIVIL ENGINEERING LABORATORY PROGRAM "POREFLOW"
C  TO CALCULATE THE PRESSURES IN THE PORES OF A HEATED CONCRETE
C  SLAB...INDUCED BY THE EXPANSION, VAPORIZATION AND MIGRATION OF
C  INTERNAL FREE MOISTURE AND THE MIGRATION OF AIR... MODERATE
C  TEMPERATURES ARE ASSUMED, I.E., TEMPS ARE LOW ENOUGH THAT NO
C  CHEMICAL/DEHYDRATION REACTIONS OCCUR; THEREFORE, PORE FREE
C  WATER ARRIVES/LEAVES THE CONCRETE ONLY THRU THE PORES, AND THE
C  FLOW RESISTANCE IS CONSTANT.
C  PROGRAM DEVELOPED BY:  DR. C.A. KODRES
C                  NAVAL CIVIL ENGINEERING LABORATORY
C                  PORT HUENEME, CALIFORNIA 93043-5003
C                  (805) 982-1656
C  DATE OF THIS VERSION: 01/08/93
      DIMENSION T(50),PV(50),PAIR(50),PWATER(50),PGAS(50),GVAPOR(51)
     1,GAIR(51),GGAS(51),VGAS(50),VWATER(50),CP(50),RGAS(50),X(50)
     2,QFG(50),OLDT(50),OLDAIR(50),OLDVAP(50),OLDH2O(50),S(50)
     3,VOLH2O(50),DEVMAX(10),DEVSAV(10)
      REAL MWV,MWAIR,MCRIT,MFRAC(50),MOLES1,MOLES2,NPRT
      CHARACTER*80 AGGR
      DOUBLE PRECISION VGAS,VWATER,MVAPOR(50),MAIR(50),MWATER(50)
      COMMON/PROPS/RGAS,CP
      COMMON/FLOW/GGAS,TAMB,TSURF,PAMB,S
      COMMON/TEST/PRATIO,TRATIO,FPARA,DX
      COMMON/GASFLOW/C1,C2,C3
      PARAMETER(NODES=50)
      PARAMETER(MWV=18.016,MWAIR=28.967)
      PARAMETER(UNITS1=1.E03,UNITS2=101.35E03,UNITS3=3600.)
      PARAMETER(ITER=50,TOL=1.E-06,TOLG=1.E-03,TINY=1.E-08)
      PARAMETER(RELAXT=1.0,RELAXP=0.1,RELAXM=0.01,RELAXG=1.0)
      PARAMETER(CPAIR=1004.6,RAIR=287.1)
      PARAMETER(CPV=1863.6,RVAPOR=461.6,HFG=2.28E06)
      DATA COND1,COND2,RHOC1,RHOC2/1.73,0.66,1.88E06,4.023E06/
         OPEN(6,FILE='\RUNWAYS\POREFLOW.OUT',STATUS='NEW')
C
C  INPUT THE DESCRIPTION OF THE CONCRETE: AGGREGATE, WATER TO
     CEMENT MIX
C  RATIO AND AGE IN MONTHS
      AGGR='BROOKSVILLE AGGREGATE WITH 20% FLY ASH'
      WC=0.38
      AGE=6.
C  INPUT THE THICKNESS (CM) AND POROSITY (FRACTION) OF THE SLAB
      X0=1.
      EPSI=0.25
C  INPUT THE INITIAL TEMPERATURE (DEGC), GAS PRESSURE (ATM), AND
C  INITIAL SATURATION (FRACTION) OF THE SLAB
      TAMB=25.
      PAMB=1.
```

```
      SAMB=0.1
C  INPUT THE MOMENTUM CONSTANTS OF THE SLAB; C1 IS IN KG/HR-M**3,
C  C2 IS IN 1/M, AND C3 IS DIMENSIONLESS
      C1=0.345E10
      C2=0.25E10
      C3=0.60E-03
C  INPUT THE TIME TO STOP THE ANALYSES (SECONDS) AND THE TIME INTERVAL
C  TO PRINT THE RESULTS
      TSTOP=120.1
      TPRINT=2.
C
C  PRINT THE INITIAL CONDITIONS
      WRITE(6,4) AGGR,WC,AGE
      WRITE(6,6) XO,EPSI
      WRITE(6,7) TAMB,PAMB,SAMB
C  SET TIME STEPS AND PROGRAM INDICATORS
      DELMIN=0.01
      DELMAX=5.76
      DELTAU=DELMIN
      TAU=DELMIN
C  HEAT THE SURFACE AS WITH VSTOL EXHAUST
      TSURF=TAMB+43.28*TAU**0.42
      PRTIND=DELMIN
      NPRT=1.
      ICONVG=0
      ICONVT=0
C  DIVIDE THE SLAB INTO "CELLS" FOR NUMERICAL CALCULATIONS
      DELX=XO/NODES
      X(1)=0.5*DELX
      DO 5 I=2,NODES
      X(I)=X(I-1)+DELX
    5 CONTINUE
      DELX=0.01*DELX
      XO=0.01*XO
C  CALCULATE VOLUME OF CONCRETE SLAB (M**3)
      V=XO
      DELV=V/NODES
C  CALCULATE THE INITIAL MASS (KG) OF WATER, WATER VAPOR, AND
C  AIR IN THE SLAB; INITIALIZE THE NECESSARY VARIABLES
      TAMB=TAMB+273.16
      THOT=TSURF
      TSURF=TSURF+273.16
      VAMB=SPVOL(TSURF,PAMB)
      CALL VAPOR(TAMB,PVAMB,SPVOLV)
C  MASSES ARE CONTINUUM VALUES; I.E., MASSES (KG) OF FLUID CONTAINED
C  IN A ONE SQUARE METER BY DELX VOLUME
      EQ1=EPSI*(1.-SAMB)*DELV/SPVOLV*UNITS1
      EQ2=EPSI*SAMB*DELV/SPVOL(TAMB,PAMB)*UNITS1
      EQ3=(PAMB-PVAMB)*EPSI*(1.-SAMB)*DELV/RAIR/TAMB*UNITS2
      EQ4=DELV*EPSI*(1.-SAMB)
      EQ5=DELV*EPSI*SAMB
      DO 10 I=1,NODES
      T(I)=TAMB
      OLDT(I)=T(I)
```

```
      PWATER(I)=PAMB
      VGAS(I)=EQ4
      MVAPOR(I)=EQ1
      OLDVAP(I)=MVAPOR(I)
      MWATER(I)=EQ2
      OLDH2O(I)=MWATER(I)
      MAIR(I)=EQ3
      OLDAIR(I)=MAIR(I)
      PV(I)=PVAMB
      VWATER(I)=EQ5
      PGAS(I)=PAMB
      PAIR(I)=PAMB
   10 CONTINUE
      DO 15 I=1,NODES+1
      GGAS(I)=0.
      GVAPOR(I)=0.
   15 CONTINUE
C  COMBINE CONSTANTS TO SIMPLIFY ANALYSES
      CONST4=DELTAU*DELV/DELX/UNITS3
      CONST5=HFG/DELV/DELTAU
      CONST8=EPSI*DELV
C  AN ITERATIVE TECHNIQUE IS EMPLOYED TO SOLVE THE GOVERNING
C  EQUATIONS...SINGLE STEP ITERATION IS USED WITH AN OPTION
C  TO APPLY LINEAR RELAXATION AS DESIRED
   20 DO 100 K=1,ITER
      DO 25 I=1,10
      DEVMAX(I)=0.
   25 CONTINUE
      DO 30 I=1,NODES
C  USE KG-MOLE FRACTIONS TO ESTIMATE PROPERTIES OF AIR-VAPOR MIXTURE
      MOLES1=MAIR(I)/MWAIR
      MOLES2=MVAPOR(I)/MWV
      CP(I)=(MOLES1*CPAIR+MOLES2*CPV)/(MOLES1+MOLES2)
      RGAS(I)=(MOLES1*RAIR+MOLES2*RVAPOR)/(MOLES1+MOLES2)
      MFRAC(I)=MOLES1/(MOLES1+MOLES2)
C  CALCULATE THE PRESSURE AND SPECIFIC VOLUME OF VAPOR IN THE
C  PORES WHEN LIQUID WATER IS PRESENT
      SAVE=PV(I)
      IF (ICONVT.GT.2) GO TO 26
      CALL VAPOR(T(I),PV(I),SPVOLV)
C  MASS OF WATER IN PORE IF COMPLETELY FILLED WITH VAPOR PHASE
C  AT SATURATION, I.E., VAPOR AT T(I) AND PV(I)
      MCRIT=CONST8/SPVOLV*UNITS1
   26 SAVE1=VWATER(I)
      SAVE2=MVAPOR(I)
      SAVE3=VGAS(I)
      SAVE4=MWATER(I)
      IF (MVAPOR(I)+MWATER(I).LT.MCRIT) THEN
C  PORE FILLED WITH SUPERHEATED STEAM
      VWATER(I)=0.
      S(I)=0.
      MVAPOR(I)=OLDVAP(I)+OLDH2O(I)-CONST4*(GVAPOR(I+1)-GVAPOR(I))
      VGAS(I)=DELV*EPSI
      SPVOLV=VGAS(I)/MVAPOR(I)*UNITS1
```

```
      PV(I)=PSTEAM(T(I),SPVOLV)
      PV(I)=SAVE+RELAXP*(PV(I)-SAVE)
      DEV=ABS(PV(I)-SAVE)/SAVE
      IF (DEV.GT.DEVMAX(1)) DEVMAX(1)=DEV
      MWATER(I)=0.
      ELSE
C  PORE FILLED WITH WATER AND SATURATED STEAM
      VOLH2O(I)=SPVOL(T(I),PWATER(I))
      VWATER(I)=MWATER(I)*VOLH2O(I)/UNITS1
      S(I)=VWATER(I)/CONST8
      VGAS(I)=CONST8-VWATER(I)
      MVAPOR(I)=VGAS(I)/SPVOLV*UNITS1
      MWATER(I)=OLDVAP(I)-MVAPOR(I)+OLDH2O(I)-CONST4*(GVAPOR(I+1)
     1-GVAPOR(I))
      ENDIF
      VWATER(I)=SAVE1+RELAXM*(VWATER(I)-SAVE1)
      DEV=ABS(VWATER(I)-SAVE1)/(SAVE1+TINY)
      IF (DEV.GT.DEVMAX(2)) DEVMAX(2)=DEV
      MVAPOR(I)=SAVE2+RELAXM*(MVAPOR(I)-SAVE2)
      DEV=ABS(MVAPOR(I)-SAVE2)/(SAVE2+TINY)
      IF (DEV.GT.DEVMAX(3)) DEVMAX(3)=DEV
      VGAS(I)=SAVE3+RELAXM*(VGAS(I)-SAVE3)
      DEV=ABS(VGAS(I)-SAVE3)/(SAVE3+TINY)
      IF (DEV.GT.DEVMAX(4)) DEVMAX(4)=DEV
      MWATER(I)=SAVE4+RELAXM*(MWATER(I)-SAVE4)
      DEV=ABS(MWATER(I)-SAVE4)/(SAVE4+TINY)
      IF (DEV.GT.DEVMAX(5)) DEVMAX(5)=DEV
C  CALCULATE GAS AND WATER PRESSURES (ATM)
      SAVE=PAIR(I)
      PAIR(I)=MAIR(I)*RAIR*T(I)/VGAS(I)/UNITS2
      PAIR(I)=SAVE+RELAXP*(PAIR(I)-SAVE)
      DEV=ABS(PAIR(I)-SAVE)/(SAVE+TINY)
      IF (DEV.GT.DEVMAX(6)) DEVMAX(6)=DEV
      PGAS(I)=PV(I)+PAIR(I)
      PWATER(I)=PGAS(I)
C  HEAT OF VAPORIZATION (W/M**3)
      QFG(I)=CONST5*(MWATER(I)-OLDH2O(I))
   30 CONTINUE
C  CALCULATE THE GAS FLOWS (KG/SEC-M**2) THROUGHOUT THE SLAB
      IF (ICONVG.GT.2) THEN
      DEVMAX(7)=DEVSAV(7)
      DEVMAX(8)=DEVSAV(8)
      GO TO 45
      ENDIF
      CALL FLOWPARA(PGAS,T,DELX,NODES)
      DO 40 I=2,NODES
      SAVE1=GVAPOR(I)
      SAVE2=GAIR(I)
      II=I-1
      IF (GGAS(I).LT.0.) II=I
      GVAPOR(I)=PV(II)/PGAS(II)*GGAS(I)
      GAIR(I)=PAIR(II)/PGAS(II)*GGAS(I)
      GVAPOR(I)=SAVE1+RELAXG*(GVAPOR(I)-SAVE1)
      DEV=ABS(GVAPOR(I)-SAVE1)/(SAVE1+TINY)
```

```
      IF (DEV.GT.DEVMAX(7)) THEN
      DEVMAX(7)=DEV
      DEVSAV(7)=DEVMAX(7)
      ENDIF
      GAIR(I)=SAVE2+RELAXG*(GAIR(I)-SAVE2)
      DEV=ABS(GAIR(I)-SAVE2)/(SAVE2+TINY)
      IF (DEV.GT.DEVMAX(8)) THEN
      DEVMAX(8)=DEV
      DEVSAV(8)=DEVMAX(8)
      ENDIF
   40 CONTINUE
      SAVE=GVAPOR(1)
      GVAPOR(1)=PV(1)/PGAS(1)*GGAS(1)
      GVAPOR(1)=SAVE+RELAXG*(GVAPOR(1)-SAVE)
      DEV=ABS(GVAPOR(1)-SAVE)/(SAVE+TINY)
      IF (DEV.GT.DEVMAX(7)) THEN
      DEVMAX(7)=DEV
      DEVSAV(7)=DEVMAX(7)
      ENDIF
      SAVE=GAIR(1)
      GAIR(1)=PAIR(1)/PGAS(1)*GGAS(1)
      GAIR(1)=SAVE+RELAXG*(GAIR(1)-SAVE)
      DEV=ABS(GAIR(1)-SAVE)/(SAVE+TINY)
      IF (DEV.GT.DEVMAX(8)) THEN
      DEVMAX(8)=DEV
      DEVSAV(8)=DEVMAX(8)
      ENDIF
      SAVE=GVAPOR(NODES+1)
           GVAPOR(NODES+1)=PAIR(NODES)/PGAS(NODES)*GGAS(NODES+1)
      GVAPOR(NODES+1)=SAVE+RELAXG*(GVAPOR(NODES+1)-SAVE)
      DEV=ABS(GVAPOR(NODES+1)-SAVE)/(SAVE+TINY)
      IF (DEV.GT.DEVMAX(7)) THEN
      DEVMAX(7)=DEV
      DEVSAV(7)=DEVMAX(7)
      ENDIF
      SAVE=GAIR(NODES+1)
      GAIR(NODES+1)=PAIR(NODES)/PGAS(NODES)*GGAS(NODES+1)
      GAIR(NODES+1)=SAVE+RELAXG*(GAIR(NODES+1)-SAVE)
      DEV=ABS(GAIR(NODES+1)-SAVE)/(SAVE+TINY)
      IF (DEV.GT.DEVMAX(8)) THEN
      DEVMAX(8)=DEV
      DEVSAV(8)=DEVMAX(8)
      ENDIF
      IF ((DEVMAX(7).LE.TOLG).AND.(DEVMAX(8).LE.TOLG)) ICONVG=5
   45 CONTINUE
C  CALCULATE MASS (KG) OF AIR IN THE PORES
      DO 50 I=1,NODES
      IF (MFRAC(I).LT.0.001) GO TO 50
      SAVE=MAIR(I)
      MAIR(I)=OLDAIR(I)-CONST4*(GAIR(I+1)-GAIR(I))
      MAIR(I)=SAVE+RELAXM*(MAIR(I)-SAVE)
      DEV=ABS(MAIR(I)-SAVE)/(SAVE+TINY)
      IF (DEV.GT.DEVMAX(9)) DEVMAX(9)=DEV
   50 CONTINUE
```

```
C  FINALLY, CALCULATE THE TEMPERATURE PROFILE (DEGK) THROUGH THE SLAB
C  AS A FUNCTION OF TIME
      IF (ICONVT.GT.2) THEN
      DEVMAX(10)=DEVSAV(10)
      GO TO 90
      ENDIF
      DO 60 I=2,NODES-1
C  HEAT THE CONCRETE AND LIQUID WATER, THE HEAT CAPACITY OF THE GASES
C  IS ASSUMED NEGLIGIBLE
      RHOCP=RHOC1*(1.-EPSI)+RHOC2*S(I)*EPSI
      CONST1=DELTAU/DELX/RHOCP/UNITS3
C  CONDUCTIVITY IS A CONCRETE-WATER EFFECTIVE VALUE, HEAT TRANSFER
C  THROUGH THE GASES IS NEGLECTED
      COND=COND1*(1.-EPSI)+COND2*EPSI*S(I)
      CONST2=DELTAU*COND/RHOCP/DELX**2
      CONST3=DELTAU/RHOCP
      SAVE=T(I)
C  GOVERNING EQS BASED ON DIRECTION OF FLOWS
      IF ((GGAS(I+1).LE.0.).AND.(GGAS(I).LE.0.)) THEN
      T(I)=(OLDT(I)-CP(I+1)*CONST1*T(I+1)*GGAS(I+1)+CONST2*(T(I+1)
     1+T(I-1))+CONST3*QFG(I))/(1.-CP(I)*CONST1*GGAS(I)+2.*CONST2)
      ELSEIF ((GGAS(I+1).LE.0.).AND.(GGAS(I).GT.0.)) THEN
      T(I)=(OLDT(I)-CP(I+1)*CONST1*T(I+1)*GGAS(I+1)+CP(I-1)*CONST1
     1*T(I-1)*GGAS(I)+CONST2*(T(I+1)+T(I-1))+CONST3*QFG(I))
     2/(1.+2.*CONST2)
      ELSEIF ((GGAS(I+1).GT.0.).AND.(GGAS(I).LE.0.)) THEN
      T(I)=(OLDT(I)+CONST2*(T(I+1)+T(I-1))+CONST3*QFG(I))/(1.-CP(I)
     1*CONST1*GGAS(I)+CP(I)*CONST1*GGAS(I+1)+2.*CONST2)
      ELSEIF ((GGAS(I+1).GT.0.).AND.(GGAS(I).GT.0.)) THEN
      T(I)=(OLDT(I)+CP(I-1)*CONST1*T(I-1)*GGAS(I)+CONST2*(T(I+1)
     1+T(I-1))+CONST3*QFG(I))/(1.+CP(I)*CONST1*GGAS(I+1)+2.*CONST2)
      ENDIF
      T(I)=SAVE+RELAXT*(T(I)-SAVE)
      DEV=ABS(T(I)-SAVE)/SAVE
      IF (DEV.GT.DEVMAX(10)) THEN
      DEVMAX(10)=DEV
      DEVSAV(10)=DEVMAX(10)
      ENDIF
   60 CONTINUE
C  THE TEMPERATURE BOUNDARY CONDI[illegible] AT THE HOT SURFACE
      RHOCP=RHOC1*(1.-EPSI)+RHOC[illegible]*EPSI
      COND=COND1*(1.-EPSI)+COND2[illegible]I*S(1)
      CONST1=DELTAU/DELX/RHOCP/UNITS3
      CONST2=DELTAU*COND/RHOCP/DELX**2
      CONST6=2.*CONST2
      CONST7=CONST2+CONST6
      SAVE=T(1)
      IF (GGAS(2).LE.0.) THEN
      T(1)=(OLDT(1)-CP(2)*CONST1*T(2)*GGAS(2)+CONST2*T(2)+CONST6
     1*TSURF+CONST3*QFG(1))/(1.-CP(1)*CONST1*GGAS(1)+CONST7)
      ELSE
      T(1)=(OLDT(1)+CONST2*T(2)+CONST6*TSURF+CONST3*QFG(1))/(1.+CP(1)
     1*CONST1*(GGAS(2)-GGAS(1))+CONST7)
      ENDIF
```

```
      T(1)=SAVE+RELAXT*(T(1)-SAVE)
      DEV=ABS(T(1)-SAVE)/SAVE
      IF (DEV.GT.DEVMAX(10)) THEN
      DEVMAX(10)=DEV
      DEVSAV(10)=DEVMAX(10)
      ENDIF
C  THE TEMPERATURE BOUNDARY CONDITION AT THE BOTTOM OF THE SLAB
      RHOCP=RHOC1*(1.-EPSI)+RHOC2*S(NODES)*EPSI
      COND=COND1*(1.-EPSI)+COND2*EPSI*S(NODES)
      CONST1=DELTAU/DELX/RHOCP/UNITS3
      CONST2=DELTAU*COND/RHOCP/DELX**2
      CONST6=2.*CONST2
      CONST7=CONST2+CONST6
      SAVE=T(NODES)
      IF (GGAS(NODES).LE.0.) THEN
      T(NODES)=(OLDT(NODES)+CONST6*TAMB+CONST2*T(NODES-1)+CONST3
     1*QFG(NODES))/(1.-CP(NODES)*CONST1*GGAS(NODES)+CP(NODES)*CONST1
     2*GGAS(NODES+1)+CONST7)
      ELSE
      T(NODES)=(OLDT(NODES)+CP(NODES-1)*CONST1*T(NODES-1)*GGAS(NODES)
     1+CONST6*TAMB+CONST2*T(NODES-1)+CONST3*QFG(NODES))/(1.+CP(NODES)
     2*CONST1*GGAS(NODES+1)+CONST7)
      ENDIF
      T(NODES)=SAVE+RELAXT*(T(NODES)-SAVE)
      DEV=ABS(T(NODES)-SAVE)/SAVE
      IF (DEV.GT.DEVMAX(10)) THEN
      DEVMAX(10)=DEV
      DEVSAV(10)=DEVMAX(10)
      ENDIF
      IF (DEVMAX(10).LE.TOL) ICONVT=5
   90 CONTINUE
      IF ((ICONVG.GT.2).AND.(ICONVT.GT.2)) GO TO 105
  100 CONTINUE
C       WRITE(6,1)
C       WRITE(6,11) TOL,ITER
C       WRITE(6,1)
C  CHECK TO SEE IF TIME TO PRINT RESULTS
  105 IF (PRTIND.LT.TPRINT) GO TO 140
      THOT=TSURF-273.16
      VAMB=SPVOL(TSURF,PAMB)
      WRITE(6,8) TAU,THOT,GGAS(1),VAMB
      DO 130 I=1,15
      T(I)=T(I)-273.16
      GNET=GGAS(I)-GGAS(I+1)
      PPORE=AMAX1(PGAS(I),PWATER(I))
      IF (S(I).GT.0.999) S(I)=1.
      WRITE(6,9) X(I),T(I),PPORE,S(I),GNET,MFRAC(I),PV(I),VOLH2O(I)
     1,MWATER(I)
      T(I)=T(I)+273.16
  130 CONTINUE
      DO 135 I=1,10
      DEVMAX(I)=100.*DEVMAX(I)
  135 CONTINUE
      WRITE(6,2) K
```

```
      WRITE(6,3) DEVMAX(10),DEVMAX(1),DEVMAX(6),DEVMAX(5),DEVMAX(7)
     1,DEVMAX(8),DEVMAX(2),DEVMAX(3),DEVMAX(9),DEVMAX(4)
      NPRT=NPRT+1.
C  CHECK TO SEE IF TIME TO STOP
  140 IF (TAU.GE.TSTOP) GO TO 200
C  CONTINUE THE ANALYSES
      TAU=TAU+DELTAU
C  HEAT SURFACE AT SAME RATE AS VSTOL EXHAUST
      TSURF=TAMB+43.28*TAU**0.42
C  OPTION TO CHANGE TIME STEP AS RUN PROGRESSES
      DELTAU=DELMIN+TAU/TSTOP*(DELMAX-DELMIN)
      IF (DELTAU.GT.0.05) DELTAU=0.05
      PRTIND=TAU/NPRT
      DO 150 I=1,NODES
      OLDT(I)=T(I)
      OLDVAP(I)=MVAPOR(I)
      OLDH2O(I)=MWATER(I)
      OLDAIR(I)=MAIR(I)
  150 CONTINUE
      ICONVG=0
      ICONVT=0
      GO TO 20
  200 STOP
    1 FORMAT(1H ,5X,'**********************************************************
     1********')
    2 FORMAT(1H ,/6X,'PERCENT CHANGE, PER ITERATION, IN CALC VALUE AFTER
     1 ',I3,' ITERATIONS')
    3 FORMAT(1H ,5X,'TEMP   = ',E10.3,4X,'PV     = ',E10.3,4X,'PAIR   =
     1',E10.3,/6X,'MWATER = ',E10.3,4X,'GVAPOR = ',E10.3,4X,'GAIR   = ',
     2E10.3,/6X,'VWATER = ',E10.3,4X,'MVAPOR = ',E10.3,4X,'MAIR   = ',E1
     30.3,/6X,'VGAS   = ',E10.3//)
    4 FORMAT(1H ,5X,'MOISTURE MIGRATION THROUGH A HEATED CONCRETE SLAB'
     1/11X,'PORTLAND CEMENT',/11X,A60,/11X,'W/C RATIO = ',F4.2,/11X,'AGE
     2 = ',F3.0,' MONTHS')
    6 FORMAT(1H ,10X,'SLAB THICKNESS = ',E10.4,' CM',/11X,'POROSITY = '
     1,F4.2/)
    7 FORMAT(1H ,5X,'AMBIENT (INITIAL) CONDITIONS:',/11X,'TEMPERATURE =
     1 ',F4.0,' DEGC',/11X,'PRESSURE = ',F4.2,' ATM',/11X,'PORE SATURATI
     2ON = ',F5.3/)
    8 FORMAT(1H ,/6X,'MOISTURE THROUGHOUT THE SLAB AFTER ',F6.1,' SECOND
     1S',//6X,'DEPTH',5X,'TEMPERATURE',5X,'PORE PRESS',3X,'SATURATION',7
     2X,'NET FLOW',8X,'PORE AIR ',6X,'VAPOR PRESS',4X,'WATER VOL',4X,'WA
     3TER MASS',/7X,'(CM)',8X,'(DEGC)',9X,'(ATM)',6X,'(FRACTION)',5X,'(K
     4G/HR-M**2)',5X,'(MOLE FRAC)',7X,'(ATM)',7X,'(CM**3/GM)',7X,'(KG)'/
     56X,'0.',11X,F6.2,10X,'1.',11X,'0.',10X,E11.4,9X,'0.',14X,'0.',11X,
     6F5.3,7X,'0.')
    9 FORMAT(1H ,5X,F5.3,8X,F6.2,8X,F6.2,9X,F5.3,7X,E11.4,9X,F5.3,8X,
     1F8.3,8X,F5.3,6X,E11.4)
   11 FORMAT(1H ,5X,'DID NOT CONVERGE TO WITHIN ',E8.1,' AFTER ',I4,' IT
     1ERATIONS'/)
      END
C
C  PROGRAM "VAPOR" TO CALCULATE THE VAPOR PRESSURE AND SPECIFIC
C  VOLUME OF WATER VAPOR...THE FORMULAE ARE CURVE FITS ACQUIRED
```

```
C  FROM THE STEAM TABLES...REF: "THERMODYNAMIC PROPERTIES OF STEAM,"
C  J.H. KEENAN AND F.G. KEYES, JOHN WILEY & SONS, NEW YORK, 1936
       SUBROUTINE VAPOR(T,P,V)
       PARAMETER(TC=647.27,PC=218.167)
       DATA A,B,C,D,E,A1,B1,C1,D1/3.346313,4.14113D-02,7.515484D-09
      1,1.3794481D-02,6.56444D-11,3.2437814,5.86826D-03,1.1702379D-08
      2,2.1878462D-03/
C  TEMPERATURE IS IN DEGREES KELVIN, PRESSURE IN ATMOSPHERES, AND
C  SPECIFIC VOLUME IN CUBIC CENTIMETERS PER GRAM
       X=TC-T
       IF (T.GT.373.) THEN
       F1=X/T*(A+B*X+C*X**3+E*X**4)/(1.+D*X)
       ELSE
       F1=X/T*(A1+B1*X+C1*X**3)/(1.+D1*X)
       ENDIF
       P=PC/10.**F1
       TAU=1./T
C  FOR TEMPS LESS THAN APPROX 450. DEGK, G3 IS NEGLIGIBLE
C       G3=3.635D-04-6.768D64*TAU**24
       G2=0.21828-1.2697D5*TAU**2
       G1=82.546*TAU-1.6246D5*TAU**2
       B0=1.89-2641.62*TAU*10.**(80870.*TAU**2)
       CONST1=0.
C      CONST1=B0**13*TAU**12*P**12*G3
       B2=B0+B0**2*G1*TAU*P+B0**4*G2*TAU**3*P**3-CONST1
       V=4.55504*T/P+B2
       RETURN
       END
C
C  PROGRAM "PSTEAM" TO CALCULATE THE PRESSURE OF SUPERHEATED STEAM
C  IN ATMOSPHERES...FORMULAE FROM THE STEAM TABLES ARE USED...
C  REF: KEENAN AND KEYES
       FUNCTION PSTEAM(TDEGK,SPVOL)
       DIMENSION F(2),WVSL(2),WVSM(2)
       REAL JH2O(2,2)
       PARAMETER(ITER=100,TOL=1.E-04)
C  TEMPERATURE IS IN DEGREES KELVIN; SPECIFIC VOLUME IN CM**3/GM
       TAU=1./TDEGK
C  FOR TEMPS BELOW APPROX 450 DEGK, G3 IS NEGLIGIBLE
C       G3=3.635D-04-6.768D64*TAU**24
       G2=0.21828-1.2697D5*TAU**2
       G1=82.546*TAU-1.6246D5*TAU**2
       B0=1.89-2641.62*TAU*10.**(80870.*TAU**2)
C  THE TERM "G3" AND ITS DERIVATIVE IS NEGLIGIBLE FOR TEMPERATURES
C  BELOW ABOUT 450 DEGK
C      CONST1=B0**13*TAU**12*PSTEAM**12*G3
C      DC1DP=12.*B0**13*G3*TAU**12*PSTEAM**11
       CONST1=0.
       DC1DP=0.
C  SOLVE FOR UNKNOWNS PSTEAM AND THE CONSTANT B2...USE NEWTON-RAPHSON
C  ITERATION...FIRST, ESTIMATE THE TWO VARIABLES
       PSTEAM=1.1
       B2=-5.
       DEVMAX=B2
```

```
C  BEGIN THE ITERATION
       DO 20 K=1,ITER
       DSAVE=DEVMAX
       DEVMAX=0.
C  UPDATE THE FUNCTIONS
       F(1)=B0+B0**2*G1*TAU*PSTEAM+B0**4*G2*TAU**3*PSTEAM**3-CONST1-B2
       F(2)=4.55504*TDEGK/(SPVOL-B2)-PSTEAM
C  CALCULATE THE JACOBIAN OF THESE FUNCTIONS WITH RESPECT
C  TO THE UNKNOWNS
       JH2O(1,1)=B0**2*G1*TAU+3.*B0**4*G2*TAU**3*PSTEAM**2-DC1DP
       JH2O(1,2)=-1.
       JH2O(2,1)=-1.
       JH2O(2,2)=4.55504*TDEGK/(SPVOL-B2)**2
C  INVERT THE JACOBIAN
       CALL MINV(JH2O,2,D,WVSL,WVSM)
C  THEN IMPROVE ON THE VARIABLE ESTIMATES
       SAVE1=PSTEAM
       SAVE2=B2
       DO 5 I=1,2
       PSTEAM=PSTEAM-JH2O(1,I)*F(I)
       B2=B2-JH2O(2,I)*F(I)
    5  CONTINUE
       DEV=ABS((SAVE1-PSTEAM)/SAVE1)
       IF (DEV.GT.DEVMAX) DEVMAX=DEV
       DEV=ABS((SAVE2-B2)/SAVE2)
       IF (DEV.GT.DEVMAX) DEVMAX=DEV
C  CHECK TO SEE IF ITERATION IS CONVERGING
       IF (K.LE.5) GO TO 10
       IF (DEVMAX.LE.DSAVE) GO TO 10
       WRITE(6,2)
       WRITE(6,1) K
       WRITE(6,2)
       GO TO 30
C  CHECK TO SEE IF ITERATION CONVERGED TO WITHIN TOLERANCE
   10  IF (DEVMAX.LE.TOL) GO TO 30
   20  CONTINUE
       WRITE(6,2)
       ERROR=TOL*100.
       WRITE(6,3) ERROR,ITER
       WRITE(6,2)
   30  CONTINUE
       RETURN
    1  FORMAT(1H ,5X,'SUPERHEATED STEAM PRESSURE CALCS DIVERGE AFTER '
      1,I3,' ITERATIONS'/)
    2  FORMAT(1H ,5X,'**************************************************
      1********'/)
    3  FORMAT(1H ,5X,'STEAM PRESSURE CALCS DID NOT CONVERGE TO WITHIN ',E
      110.4,' PERCENT AFTER',I4,' ITERATIONS'/)
       END
C
C  PROGRAM "SPVOL" TO CALCULATE THE SPECIFIC VOLUME OF COMPRESSED
C  LIQUID WATER IN CUBIC CENTIMETERS PER GRAM...FORMULA FROM THE
C  STEAM TABLES IS USED...REF: KEENAN AND KEYES
       FUNCTION SPVOL(TDEGK,P)
```

```
      T=TDEGK-273.16
      Z=374.1-T
      Y=385.-T
            SPVOL=3.086-0.899017*Z**0.147166-0.4/Y**1.6*(P-218.5)
      RETURN
      END
C
C  PROGRAM "FLOWPARA" TO DETERMINE THE COMPRESSIBLE FLOW PARAMETER
C  OF A HIGH PRESSURE GAS OF KNOWN PROPERTIES FLOWING, AGAINST FRICTION,
C  THROUGH A CONCRETE SLAB...THE OPTION FOR HEAT TRANSFER IS PROVIDED...
C  THE FOLLOWING ASSUMPTIONS ARE MADE:
C        (1)  ONE-DIMENSIONAL
C        (2)  IDEAL GAS
C        (3)  NO MECHANICAL WORK
C        (4)  CONSTANT PROPERTIES
C        (5)  STEADY FLOW
C        (6)  GAS TEMPERATURE EQUAL TO TEMP OF SURROUNDING SOLID
      SUBROUTINE FLOWPARA(PGAS,TGAS,DELX,NN)
      DIMENSION P(52),T(52),PGAS(50),TGAS(50),S(50)
      REAL MDOT(51),L
      COMMON/PROPS/R(50),SPHT(50)
      COMMON/FLOW/MDOT,TAMB,TSURF,PAMB,S
      COMMON/TEST/PRATIO,TRATIO,FPARA,DX
      COMMON/GASFLOW/C1,C2,C3
      PARAMETER(ITER=100,TOL=1.E-04,RELAX=1.0)
      PARAMETER(UNITS1=3.6E08,TINY=1.E-03)
      PARAMETER(CPAIR=1004.6,RAIR=287.1)
      DATA C4,C5/0.25,0.75/
C  DETERMINE WHICH DIRECTION THE FLOW IS GOING
C  TEMPERATURES IN DEGK...PRESSURES IN ATM...FLOWS IN KG/HR-M**2
      DO 5 I=2,NN+1
      P(I)=PGAS(I-1)
      T(I)=TGAS(I-1)
    5 CONTINUE
      P(1)=PAMB
      T(1)=TSURF
      P(NN+2)=PAMB-TINY
      T(NN+2)=TAMB
      DO 30 I=1,NN+1
      L=DELX
      IF ((I.EQ.1).OR.(I.EQ.NN+1)) L=0.5*DELX
      IF (P(I+1).GT.P(I)) THEN
      II=I+1
      JJ=I
C  NEGATIVE FLOWS ARE IN THE DIRECTION OF THE HOT SURFACE
      DIR=-1.
      IJ=I
      IF (IJ.GT.NN) IJ=NN
      ELSE
      II=I
      JJ=I+1
      DIR=1.
      IJ=I-1
      IF (IJ.LT.1) IJ=1
```

```
      ENDIF
C  FLOW CROSS SECTION
C  USE CORRELATION OF VERMA, ET AL., 23RD ASME NATIONAL HT CONF,
C  HTD VOL 46, PP 135-143, 1985.
      AREA=1.259-1.7615*S(IJ)+0.5089*S(IJ)**2
      P1=P(II)
      P3=P(JJ)
      PDIFF=ABS(P1-P3)
      IF (PDIFF.LE.TINY) THEN
      MDOT(I)=0.
      GO TO 30
      ENDIF
      T1=T(II)
      T03=T(JJ)
      P1P3=P1/P3
C  CHECK FOR FLOW ENTERING THE SLAB...AN ERROR
      IF ((II.LE.1).OR.(II.GE.NN+2)) THEN
      CP=CPAIR
      RGAS=RAIR
      GO TO 8
      ENDIF
      RGAS=R(II-1)
      CP=SPHT(II-1)
    8 C6=1.-2.*C4*(T03/T1-1.)
      C7=1.+2.*C5*(T03/T1-1.)
C  CHECK IF ENOUGH PRESSURE TO INITIATE FLOW
      TRSHLD=C6-C7*(T1/T03/P1P3)**2
      IF (TRSHLD.LE.TINY) THEN
      MDOT(I)=0.
      GO TO 30
      ENDIF
C  COMBINE CONSTANTS TO SIMPLIFY CALCULATIONS
      CONST1=T03/T1
      CONST2=2.*CONST1
      CONST3=2.*CP/RGAS
      CONST4=4.*CONST1/C3**2/CONST3
      CONST5=(2.*CP-RGAS)/CP
      CONST6=SQRT(RGAS*T1)/P1/AREA/UNITS1
C  SOLVE FOR THE UNKNOWNS PSI, T1T3 AND CF...FIRST MAKE AN INITIAL
C  ESTIMATE OF THE UNKNOWNS
      T1T3=1.
      PSI=C3**2
      MDOT(I)=PSI/CONST6
      CF=C1/MDOT(I)+C2
C  AN ITERATIVE TECHNIQUE IS EMPLOYED TO SOLVE THE GOVERNING
C  EQUATIONS...SINGLE STEP ITERATION WITH AN OPTION TO APPLY
C  LINEAR RELAXATION AS DESIRED
      DEVMAX=1.
      DO 20 K=1,ITER
      DSAVE=DEVMAX
      DEVMAX=0.
      SAVE=T1T3
      T1T3=(1.+SQRT(1.+CONST4*PSI**2*P1P3**2))/CONST2
      T1T3=RELAX*(T1T3-SAVE)+SAVE
```

```
      DEV=ABS(T1T3-SAVE)/SAVE
      IF (DEV.GT.DEVMAX) DEVMAX=DEV
      SAVE=PSI
      PSI=C3*SQRT(C6-C7*(T1T3/P1P3)**2)/SQRT(CONST5*ALOG(P1P3/T1T3)
     1+CF*L)
      PSI=RELAX*(PSI-SAVE)+SAVE
      DEV=ABS(PSI-SAVE)/SAVE
      IF (DEV.GT.DEVMAX) DEVMAX=DEV
      SAVE=CF
      MDOT(I)=PSI/CONST6
      CF=C1/MDOT(I)+C2
      CF=RELAX*(CF-SAVE)+SAVE
      DEV=ABS(CF-SAVE)/SAVE
      IF (DEV.GT.DEVMAX) DEVMAX=DEV
C  CHECK TO SEE IF ITERATION IS CONVERGING
      IF (K.LE.3) GO TO 15
      IF (DEVMAX.LT.DSAVE) GO TO 15
      WRITE(6,1)
      WRITE(6,3) K
      WRITE(6,1)
      STOP
C  CHECK TO SEE IF ITERATION HAS CONVERGED TO WITHIN TOLERANCE
   15 IF (DEVMAX.LE.TOL) GO TO 25
   20 CONTINUE
      ERROR=100.*TOL
      WRITE(6,4) ERROR,ITER
   25 CONTINUE
      MDOT(I)=DIR*MDOT(I)
      IF (I.EQ.1) THEN
      PRATIO=P1P3
      TRATIO=T1T3
      FPARA=PSI
      DX=L
      ENDIF
   30 CONTINUE
      RETURN
    1 FORMAT(1H ,5X,'**************************************************
     1********')
    3 FORMAT(1H ,5X,'CALCULATIONS DIVERGING AFTER ',I3,' ITERATIONS')
    4 FORMAT(1H ,5X,'CALCULATIONS DID NOT CONVERGE TO WITHIN ',E8.2,' PE
     1RCENT AFTER ',I3,' ITERATIONS')
      END
C
C  PROGRAM 'MINV' TO INVERT A GENERAL MATRIX
      SUBROUTINE MINV(A,N,D,L,M)
      DIMENSION A(4),L(2),M(2)
C  SEARCH FOR THE LARGEST ELEMENT
      D=1.0
      NK=-N
      DO 80 K=1,N
      NK=NK+N
      L(K)=K
      M(K)=K
      KK=NK+K
```

```
      BIGA=A(KK)
      DO 20 J=K,N
      IZ=N*(J-1)
      DO 20 I=K,N
      IJ=IZ+I
      IF (ABS(BIGA)-ABS(A(IJ))) 15,20,20
   15 BIGA=A(IJ)
      L(K)=I
      M(K)=J
   20 CONTINUE
C  INTERCHANGE ROWS
      J=L(K)
      IF (J-K) 35,35,25
   25 KI=K-N
      DO 30 I=1,N
      KI=KI+N
      HOLD=-A(KI)
      JI=KI-K+J
      A(KI)=A(JI)
   30 A(JI)=HOLD
C  INTERCHANGE COLUMNS
   35 I=M(K)
      IF (I-K) 45,45,38
   38 JP=N*(I-1)
      DO 40 J=1,N
      JK=NK+J
      JI=JP+J
      HOLD=-A(JK)
      A(JK)=A(JI)
   40 A(JI)=HOLD
C  DIVIDE COLUMN BY MINUS PIVOT
   45 IF (BIGA) 48,46,48
   46 D=0.0
      RETURN
   48 DO 55 I=1,N
      IF (I-K) 50,55,50
   50 IK=NK+I
      A(IK)=A(IK)/(-BIGA)
   55 CONTINUE
C  REDUCE MATRIX
      DO 65 I=1,N
      IK=NK+I
      HOLD=A(IK)
      IJ=I-N
      DO 65 J=1,N
      IJ=IJ+N
      IF (I-K) 60,65,60
   60 IF (J-K) 62,65,62
   62 KJ=IJ-I+K
      A(IJ)=HOLD*A(KJ)+A(IJ)
   65 CONTINUE
C  DIVIDE ROW BY PIVOT
      KJ=K-N
      DO 75 J=1,N
```

```
      KJ=KJ+N
      IF (J-K) 70,75,70
   70 A(KJ)=A(KJ)/BIGA
   75 CONTINUE
C  PRODUCT OF PIVOTS
      D=D*BIGA
C  REPLACE PIVOT BY RECIPROCAL
      A(KK)=1.0/BIGA
   80 CONTINUE
C  FINAL ROW AND COLUMN INTERCHANGE
      K=N
  100 K=(K-1)
      IF (K) 150,150,105
  105 I=L(K)
      IF (I-K) 120,120,108
  108 JQ=N*(K-1)
      JR=N*(I-1)
      DO 110 J=1,N
      JK=JQ+J
      HOLD=A(JK)
      JI=JR+J
      A(JK)=-A(JI)
  110 A(JI)=HOLD
  120 J=M(K)
      IF (J-K) 100,100,125
  125 KI=K-N
      DO 130 I=1,N
      KI=KI+N
      HOLD=A(KI)
      JI=KI-K+J
      A(KI)=-A(JI)
  130 A(JI)=HOLD
      GO TO 100
  150 RETURN
      END
```

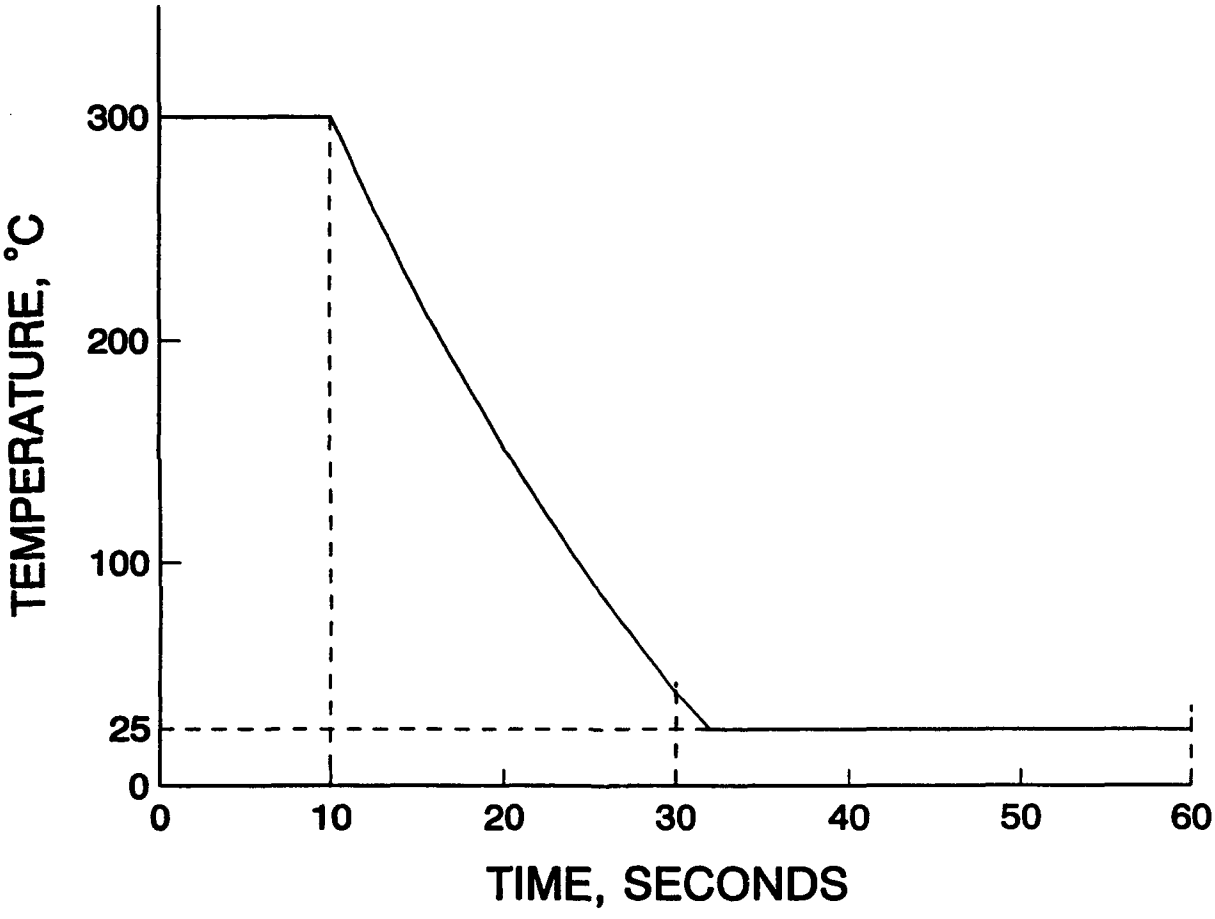

Figure A-1
Concrete surface temperature.

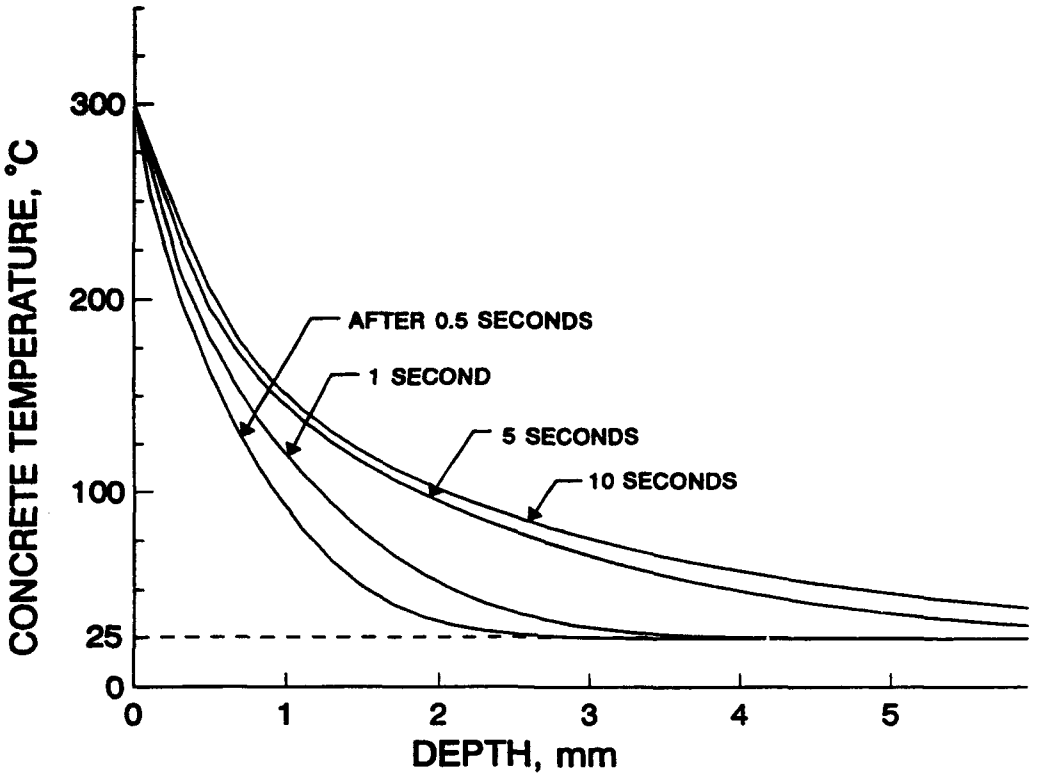

Figure A-2(a)
Concrete temperature profiles during heating (porosity = 0.25, initial saturation = 0.1).

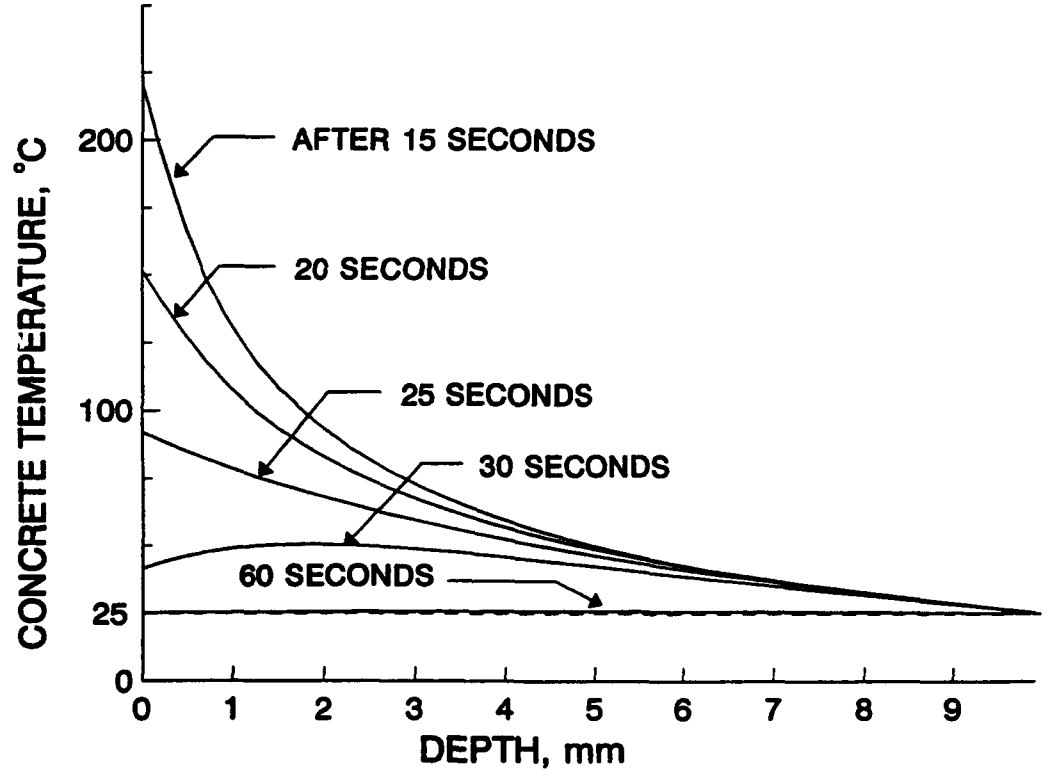

Figure A-2(b)
Concrete temperature profiles during cooling.

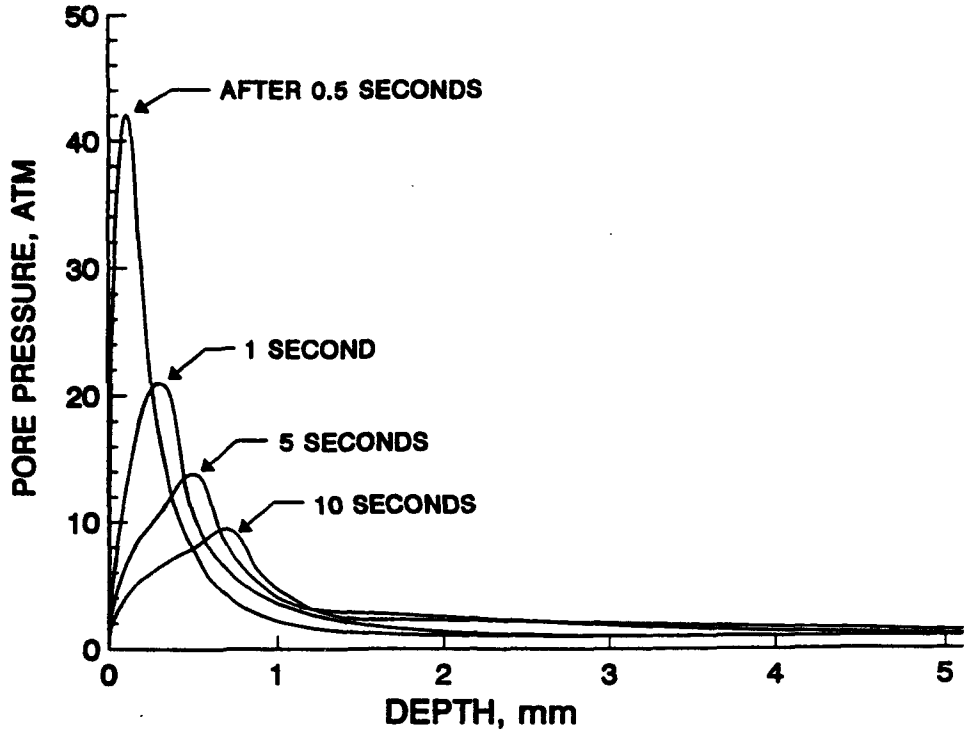

Figure A-3(a)
Concrete pore pressure profiles during heating
(Brooksville aggregate with 20 percent flyash, w/c = 0.38, initial saturation = 0.1).

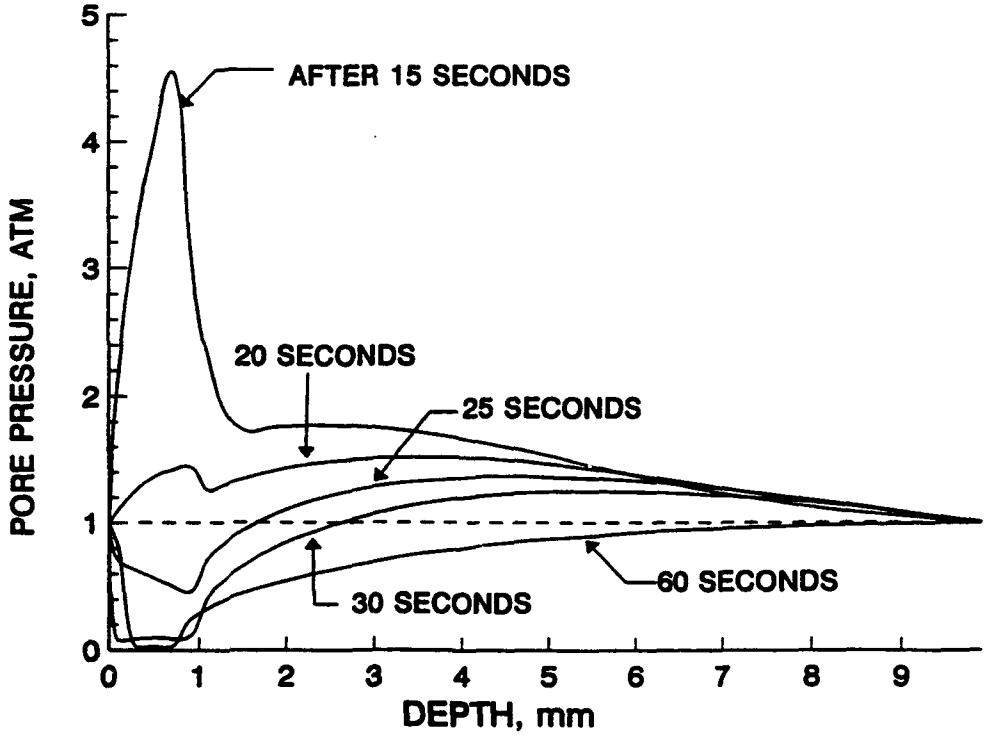

Figure A-3(b)
Concrete pore pressure profiles during cooling.

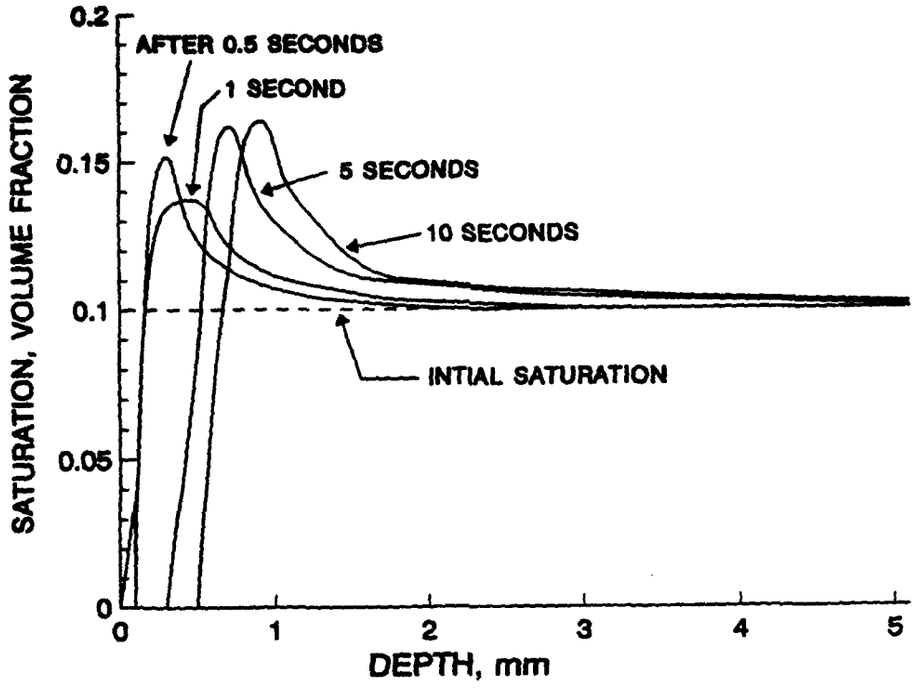

Figure A-4(a)
Concrete saturation profile during heating.
(Saturation defined as the fraction of pore volume filled with liquid water.)

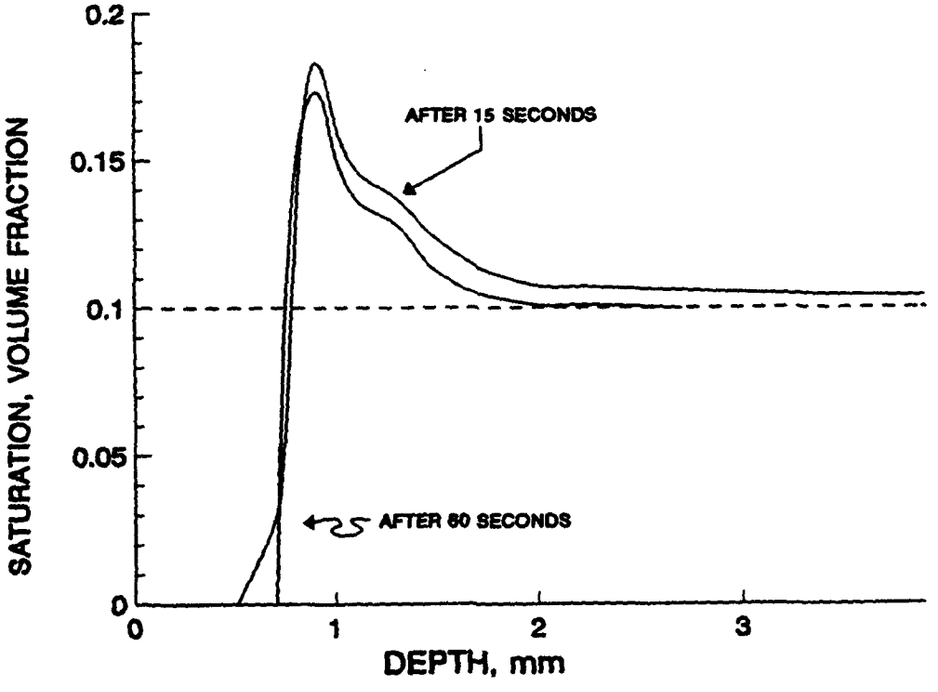

Figure A-4(b)
Concrete saturation profile during cooling.

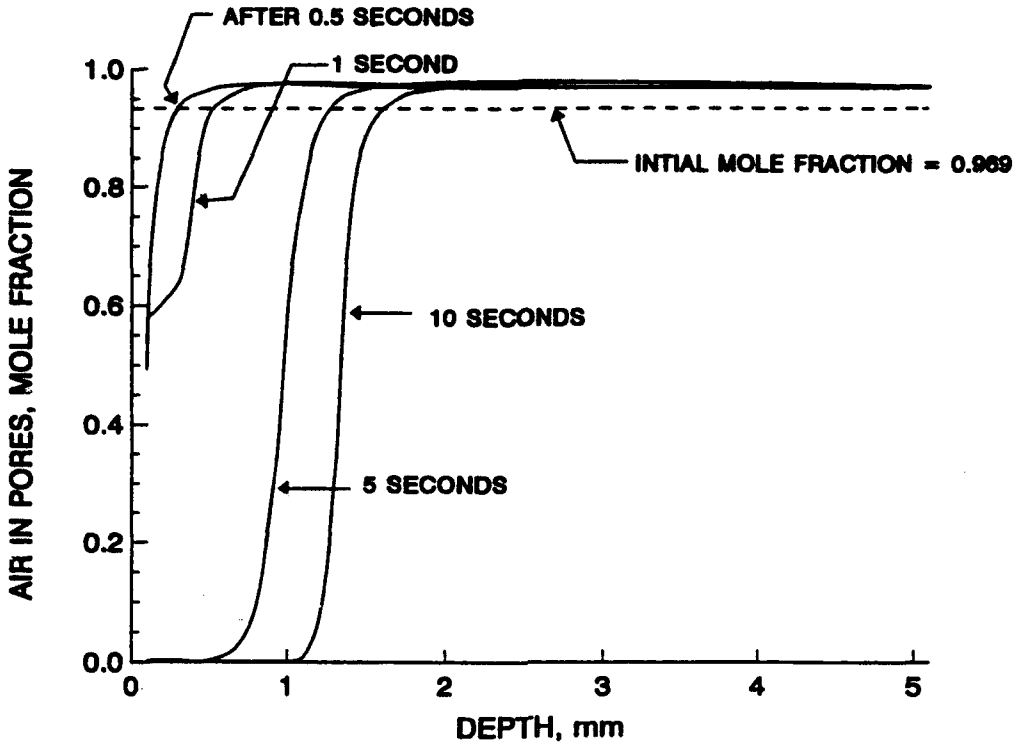

Figure A-5(a)
Amount of air in concrete pores during heating (mole fraction in air-water vapor mixture).

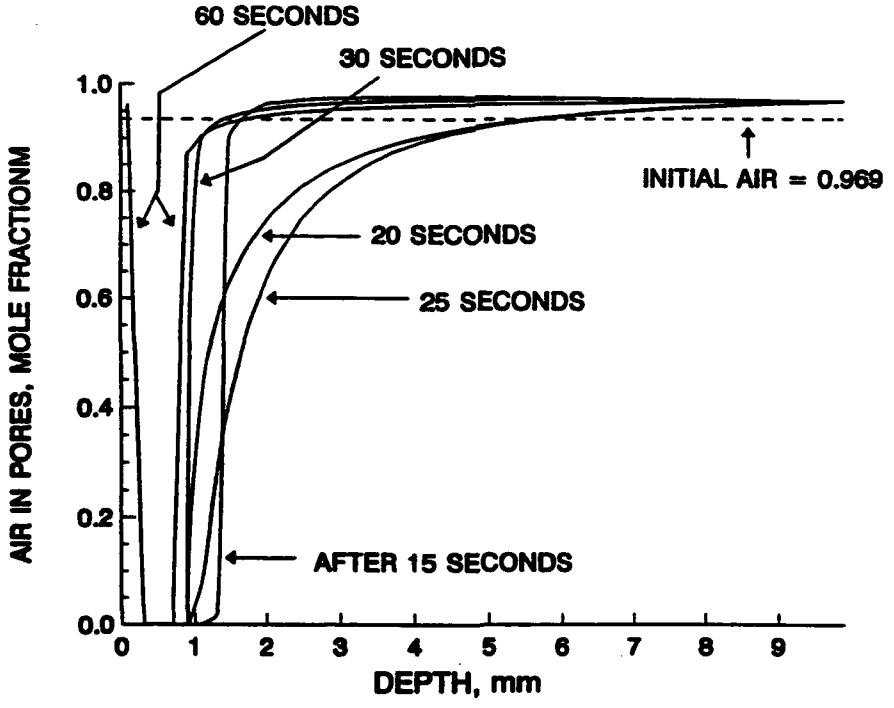

Figure A-5(b)
Amount of air in concrete pores during cooling.

Table A-1
POREFLOW Sample Output[a]

Depth (cm)	Temperature (°C)	Pore Press (atm)	Saturation (fraction)	Net Flow (kg/hr-m**2)	H_2O Vapor (mole frac)	Vapor Press (atm)	Water Volume (cm**3/gm)	Water Mass (kg)
0.	300.00	1.	0.	-0.5238E+01	0.	0.	1.463	0.
0.010	269.48	12.98	0.007	0.8387E-01	0.912	12.978	1.345	0.2723E-03
0.030	217.35	21.77	0.058	-0.1129E+02	0.980	21.766	1.216	0.2379E-02
0.050	185.17	11.19	0.157	0.3018E+01	0.415	11.125	1.159	0.6777E-02
0.070	161.01	6.59	0.132	0.1271E+01	0.120	6.251	1.122	0.5895E-02
0.090	141.83	4.66	0.121	0.7071E+00	0.046	3.747	1.095	0.5506E-02
0.110	125.92	3.81	0.114	0.2667E+00	0.028	2.348	1.074	0.5321E-02
0.130	112.30	3.26	0.111	0.1222E+00	0.023	1.519	1.057	0.5248E-02
0.150	100.41	2.82	0.109	0.8864E-01	0.021	1.008	1.043	0.5217E-02
0.170	89.89	2.44	0.107	0.7992E-01	0.021	0.684	1.031	0.5201E-02
0.190	80.54	2.13	0.106	0.7426E-01	0.022	0.473	1.021	0.5193E-02
0.210	72.22	1.87	0.105	0.6670E-01	0.023	0.335	1.012	0.5188E-02
0.230	64.84	1.66	0.104	0.5724E-01	0.024	0.242	1.004	0.5185E-02
0.250	58.33	1.50	0.103	0.4720E-01	0.026	0.180	0.997	0.5184E-02
0.270	52.65	1.38	0.103	0.3775E-01	0.027	0.137	0.992	0.5183E-02
0.290	47.72	1.28	0.102	0.2958E-01	0.028	0.107	0.987	0.5183E-02
0.310	43.50	1.21	0.102	0.2287E-01	0.029	0.087	0.983	0.5182E-02
0.330	39.91	1.16	0.101	0.1755E-01	0.029	0.072	0.979	0.5182E-02
0.350	36.91	1.12	0.101	0.1343E-01	0.030	0.061	0.976	0.5182E-02
0.370	34.41	1.09	0.101	0.1028E-01	0.030	0.053	0.974	0.5182E-02
0.390	32.37	1.07	0.101	0.7878E-02	0.030	0.048	0.972	0.5182E-02
0.410	30.71	1.05	0.101	0.6054E-02	0.031	0.043	0.970	0.5182E-02
0.430	29.38	1.04	0.100	0.4666E-02	0.031	0.040	0.969	0.5182E-02
0.450	28.33	1.03	0.100	0.3602E-02	0.031	0.038	0.968	0.5182E-02
0.470	27.50	1.02	0.100	0.2781E-02	0.031	0.036	0.967	0.5182E-02
0.490	26.86	1.02	0.100	0.2144E-02	0.031	0.035	0.967	0.5182E-02
0.510	26.37	1.01	0.100	0.1647E-02	0.031	0.034	0.966	0.5182E-02
0.530	26.00	1.01	0.100	0.1259E-02	0.031	0.033	0.966	0.5182E-02
0.550	25.72	1.01	0.100	0.9632E-03	0.031	0.033	0.966	0.5182E-02
0.570	25.52	1.00	0.100	0.7201E-03	0.031	0.032	0.966	0.5182E-02
0.590	25.37	1.00	0.100	0.3708E-03	0.031	0.032	0.965	0.5182E-02
0.610	25.26	1.00	0.100	0.1570E-02	0.031	0.032	0.965	0.5182E-02
0.630	25.18	1.00	0.100	0.0000E+00	0.031	0.032	0.965	0.5182E-02
0.650	25.12	1.00	0.100	0.0000E+00	0.031	0.031	0.965	0.5182E-02
0.670	25.08	1.00	0.100	0.0000E+00	0.031	0.031	0.965	0.5182E-02
0.690	25.06	1.00	0.100	0.0000E+00	0.031	0.031	0.965	0.5182E-02
0.710	25.04	1.00	0.100	0.0000E+00	0.031	0.031	0.965	0.5182E-02
0.730	25.03	1.00	0.100	0.0000E+00	0.031	0.031	0.965	0.5182E-02
0.750	25.02	1.00	0.100	0.0000E+00	0.031	0.031	0.965	0.5182E-02
0.770	25.01	1.00	0.100	0.0000E+00	0.031	0.031	0.965	0.5182E-02
0.790	25.01	1.00	0.100	0.0000E+00	0.031	0.031	0.965	0.5182E-02
0.810	25.00	1.00	0.100	0.0000E+00	0.031	0.031	0.965	0.5182E-02
0.830	25.00	1.00	0.100	0.0000E+00	0.031	0.031	0.965	0.5182E-02
0.850	25.00	1.00	0.100	0.0000E+00	0.031	0.031	0.965	0.5182E-02
0.870	25.00	1.00	0.100	0.0000E+00	0.031	0.031	0.965	0.5182E-02
0.890	25.00	1.00	0.100	0.0000E+00	0.031	0.031	0.965	0.5182E-02
0.910	25.00	1.00	0.100	0.0000E+00	0.031	0.031	0.965	0.5182E-02
0.930	25.00	1.00	0.100	0.0000E+00	0.031	0.031	0.965	0.5182E-02
0.950	25.00	1.00	0.100	0.0000E+00	0.031	0.031	0.965	0.5182E-02
0.970	25.00	1.00	0.100	0.0000E+00	0.031	0.031	0.965	0.5182E-02
0.990	25.00	1.00	0.100	0.0000E+00	0.031	0.031	0.965	0.5182E-02

[a]Moisture migration through a heated concrete slab:
- Portland cement
- Brooksville Aggregate with 20% flyash
- W/C ratio = 0.38
- Age = 6 months
- Porosity = 0.25

Ambient (initial) condition:
- Temperature = 25°K
- Pressure = 1.00 ATM
- Pore saturation = 0.100
- Slab thickness = 0.1000E+01 CM

Appendix B

MEASURING CONCRETE FLOW RATES

Concrete flow characteristics were determined experimentally by Dr. M.C. McVay of the University of Florida under contract to the Air Force Civil Engineering Support Agency. This appendix consists of excerpts from his report (McVay and Rish, 1993).

The initial plan was to conduct both air and steam flow tests. To eliminate the possibility of adding moisture, nitrogen, which makes up about 78 percent of air, was used instead. Similarly, to prevent condensation of steam within the pores, superheated steam was used for the steam tests.

EXPERIMENTAL APPARATUS

Since concrete is relatively impervious, a large diameter concrete specimen was necessary to obtain a measurable flow rate. A large diameter specimen also reduces the error caused by side wall effects. Consequently, a 12.7-cm diameter by 5.1-cm long specimen was selected. Flow was to be constrained to one dimension and, therefore, the side of the specimen had to be sealed. For the nitrogen tests, the specimen was sealed inside an acrylic tube as shown in Figure B-1. For the steam tests, repeatable results were achieved by using a 12.78-cm inside diameter steel pipe around the specimen and Dexter Hysol's high temperature epoxy within the gap. The low pressure side of the specimen was supported by a 1.27-cm perforated aluminum plate. The top and bottom of the steel pipe were sealed to 30.5-cm diameter by 2.6-cm thick aluminum plates. These plates were used to provide large heat sources to superheat steam coming from the boiler, as well as to maintain constant temperatures across the circular plane of the specimen.

For the steam flow tests, the specimen, in its container, was placed in an oven, as shown in Figure B-2, so it could be heated prior to beginning the experiments. Also shown in this figure are the boiler (heated with an electric furnace), condenser, and scale to measure mass flow rate. Both the temperature and pressure of the steam entering the oven were continuously monitored as were the temperatures of the specimen and superheated steam in the oven. For each of the steam tests, the oven had to be maintained at a temperature hotter than the boiler to ensure that the steam achieved a superheated state.

The nitrogen flow experiments were conducted by tying into the steam supply line with a high pressure hose connected to a regulated bottle of nitrogen. The nitrogen, after passing through the specimen, was collected underwater in a burette.

FLOW TESTS

To determine the amount of either gas flowing through the concrete, the upstream pressure was set, and the flow rate monitored. The downstream pressure was maintained at ambient. After steady state was reached, the total flow passing through the concrete specimen

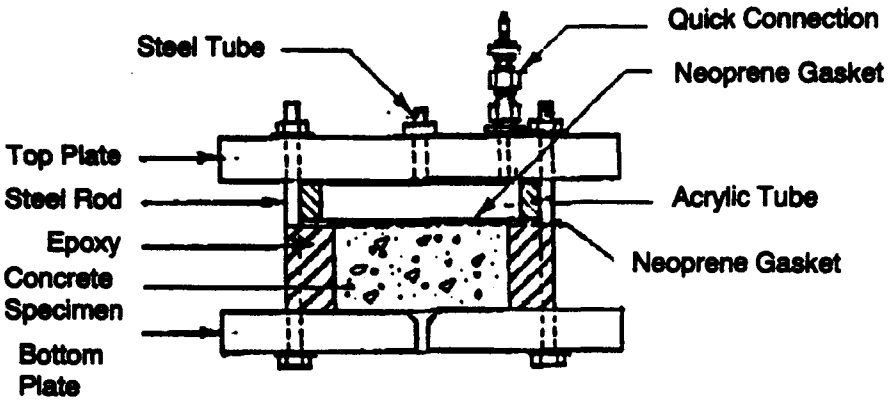

Figure B-1
Nitrogen flow test apparatus.

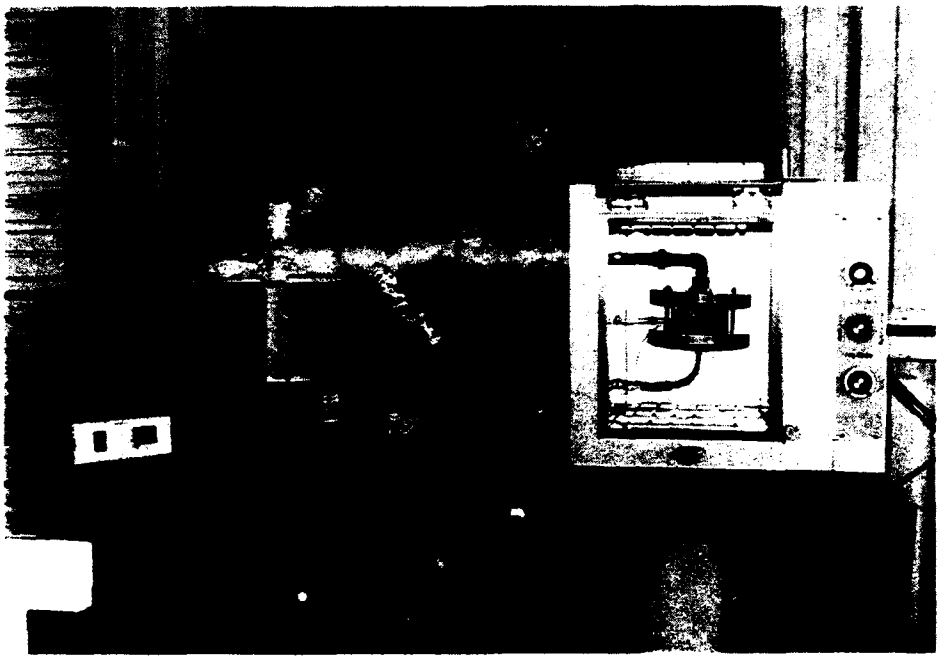

Figure B-2
Specimen placed in an oven for the steam flow tests.

was recorded over a period of several hours to guarantee a representative average. Flow rates were acquired by simply dividing the total measured flow by the total time. The tests were repeated for different upstream pressures up to a maximum of 22 atmospheres.

SPECIMEN PREPARATION

Three different concrete mixes were tested. Specimens constructed of cement mortar were prepared according to ASTM Specification C-139. This required a water-to-cement ratio of 0.4, and a sand-to-cement ratio of 2.5 by weight. Quartz sand was used as the fine aggregate, and no additives such as a plasticizer were used. The specimens were cured for 7 days by submersion in water. After curing, the specimens were dried of their evaporable water by placing them in a convection oven at 110°C and monitoring their weight loss. The drying took approximately 3 days. Porosities of the dried samples averaged about 17.5 percent. After drying, the nitrogen and steam flow tests were conducted.

The two other concrete mixes were similarly prepared, and a limestone aggregate was added. Nitrogen flow tests were conducted on specimens made with the very porous Brooksville limestone and also with the less porous Calara limestone.

Appendix C

EXPERIMENTAL EXAMINATION OF THE EFFECTS OF MOISTURE IN HEATED AIRFIELD CONCRETE

By

C. David Gaughen

SAMPLE PREPARATION

The mix design met the requirements outlined in the Naval Facilities Engineering Command guide specification (NFGS-02520C) for "Portland Cement Concrete Pavement for Roads and Airfields." Type I/II portland cement with both San Gabriel sand and number 57 round rock coarse aggregate was used. Samples were cast from one batch into 2- by 2-foot by 3-inch wood forms and placed in a fog room for 28 days at 70°F. After 28 days, seven beams had an average flexural strength of 830 psi.

When cured, samples were cut into 2.75- by 3- by 3-inch cubes using a masonry saw. The original surface had a coarse burlap drag finish, and the first quarter inch of portland cement concrete was removed with a masonry saw. This procedure gave the surface of each sample a smooth appearance which facilitated photographic documentation. Samples were divided into two groups that were subjected to different environments. The first group was placed in a Blue-M circulating air oven at 50°C for 1 week, and, for an additional week, the temperature was increased to 70°C (dry samples). The second group was placed in a bucket of deionized water for 3 weeks (saturated samples).

TEST PROCEDURE

Saturated and dry samples were subjected to cyclic heating typically caused by an F/A-18 auxiliary power unit (APU) in its ready to load (RTL) mode and VSTOL aircraft during takeoff and landing. Each cycle had a duration of 5 minutes. Figure C-1 shows concrete surface temperature versus time for both actual and experimental heating of an F/A-18 APU operating in the RTL mode. The smooth curve shows actual heating from field data (Ref C-1) and the triangles show experimental heating used in the laboratory. Figure C-2 shows concrete surface temperature versus time for both actual and experimental heating of VSTOL during takeoff and landing. The smooth curve shows actual heating from field data collected in this study and the triangles show heating used in the laboratory.

Figure C-3 shows the apparatus used to experimentally generate these heating rates. The heating source used to simulate the F/A-18 APU was a SEELYE Si-1500C/D heat gun. A methane Bunsen burner was used to simulate a VSTOL. To record the temperature of each sample upon heating, a Dickson model IR550 (infrared temperature measuring instrument) was used. An Olympus SZIIITR microscope system was used to take photographs.

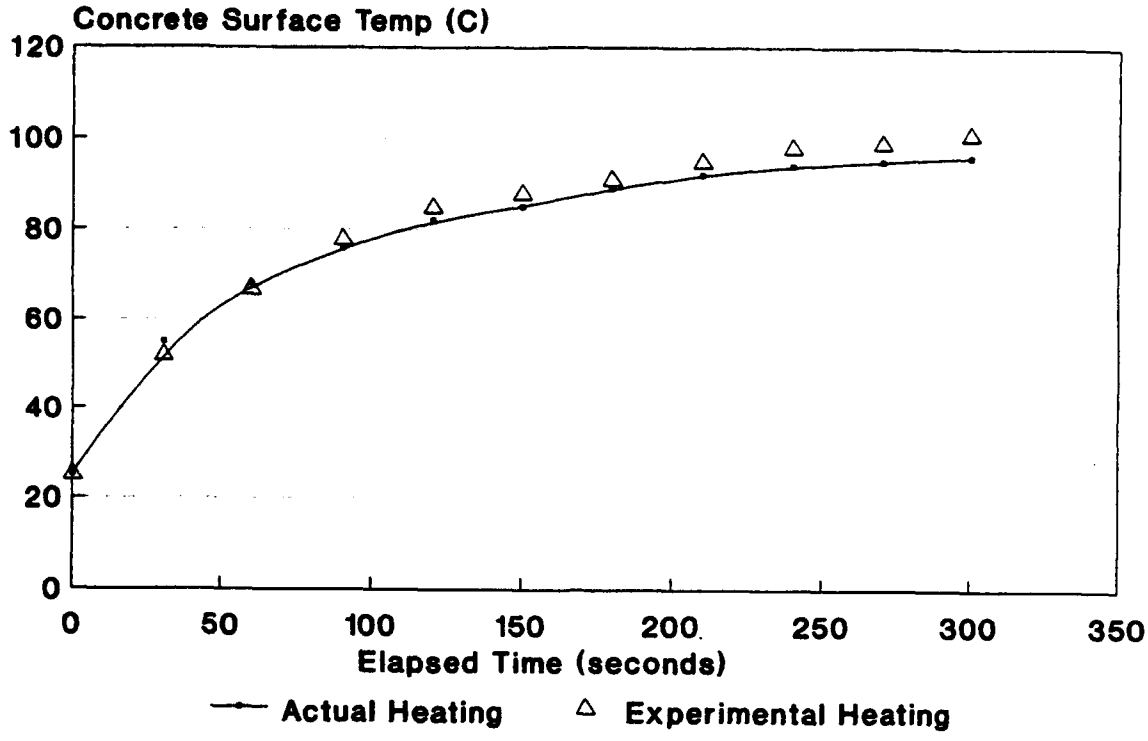

Figure C-1
Actual and experimental heating of F/A-18 APU operating in the RTL mode.

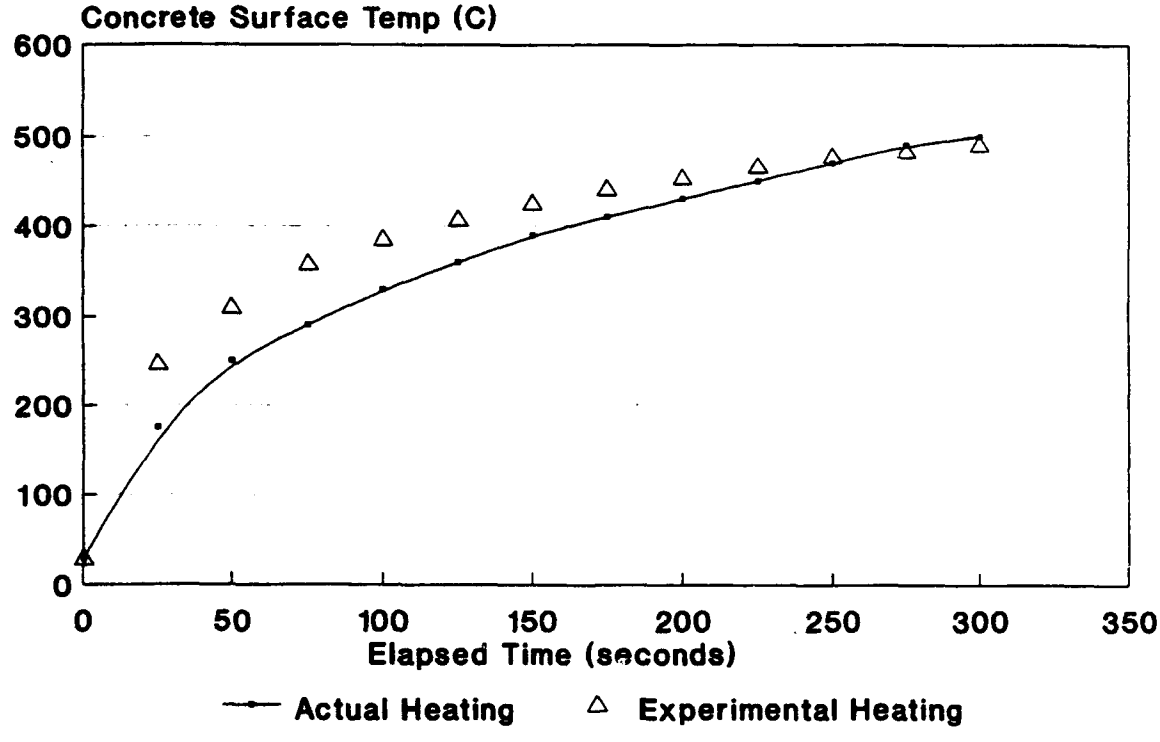

Figure C-2
Actual and experimental heating of V/STOL during takeoff and landing.

Both saturated and dry samples were heated at the rates shown in Figures C-1 and C-2. Samples would either be heated once or cycled six times using these rates. After each cycle, samples would cool to ambient temperature before an additional cycle would begin. If more than one cycle was desired on a saturated sample, it would be resaturated by submersion in deionized water for a minimum of 10 minutes. The table below shows the number of samples, sample type, number of cycles, and cycle type used in this experiment.

Number of Samples	Sample Type	Number of Cycles	Cycle Type
2	Dry	1	F/A-18
2	Saturated	1	
4	Dry	6	
4	Saturated	6	
2	Dry	1	VSTOL
4	Saturated	1	
2	Dry	6	
2	Saturated	6	

RESULTS

Figure C-4 shows the surface of a saturated sample before cycling. A thin layer of white deposits consisting of calcium hydroxide, calcium carbonate, and other solids exits on each surface of the saturated samples. When water passes through concrete it may dissolve some of the readily soluble calcium hydroxide (formed during hydration of the cement) and other solids. This leaching of the calcium hydroxide and subsequent carbonation and evaporation is known as efflorescence (Ref C-2). Carbonation occurs when calcium hydroxide reacts with carbon dioxide in air to form calcium carbonate. Figure C-5 shows the surface of a dry sample prior to cycling. It becomes apparent, when compared to Figure C-4, that this sample has an absence of efflorescence.

Explosive spalling, pop-outs, cracking, and scaling did not occur on any of the twelve samples that were subjected to the simulated F/A-18 APU operating in the RTL mode. The observations were consistent for both the dry and saturated samples regardless of the number of cycles (cycles ranged from one to six). However, cycling on the saturated samples appeared to increase the deposits from efflorescence.

Cracking occurred on the majority of the 10 samples subjected to the simulated VSTOL. This was observed predominantly after the first cycle and continued to progress as the number of cycles increased. Figure C-6 is a photograph taken after six VSTOL cycles of the same dry sample and relative area as in Figure C-5. This figure shows slight cracking in the center and in the right corner. Figure C-7 shows slightly larger cracking after six VSTOL cycles on another dry sample. Many of the cracks that were viewed occurred adjacent to a piece of aggregate.

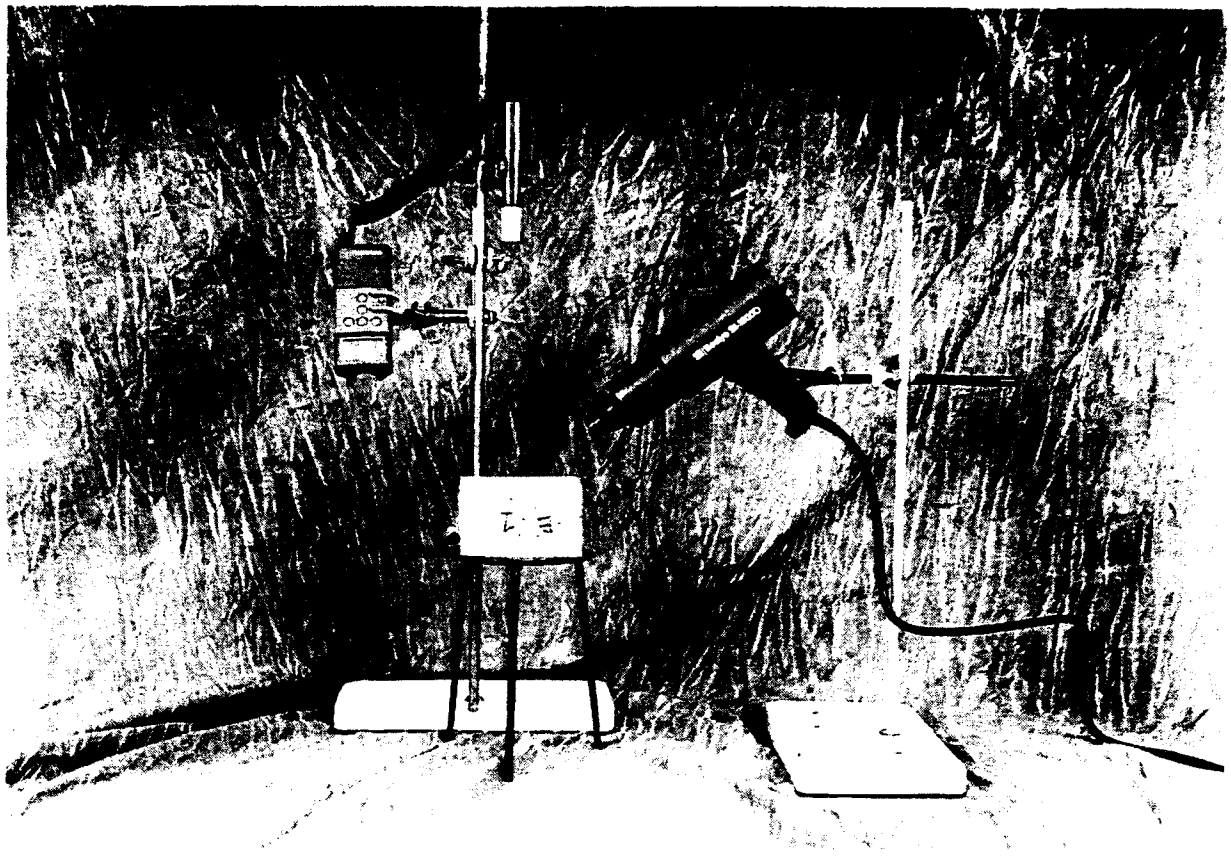

Figure C-3
Apparatus used to simulate heating.

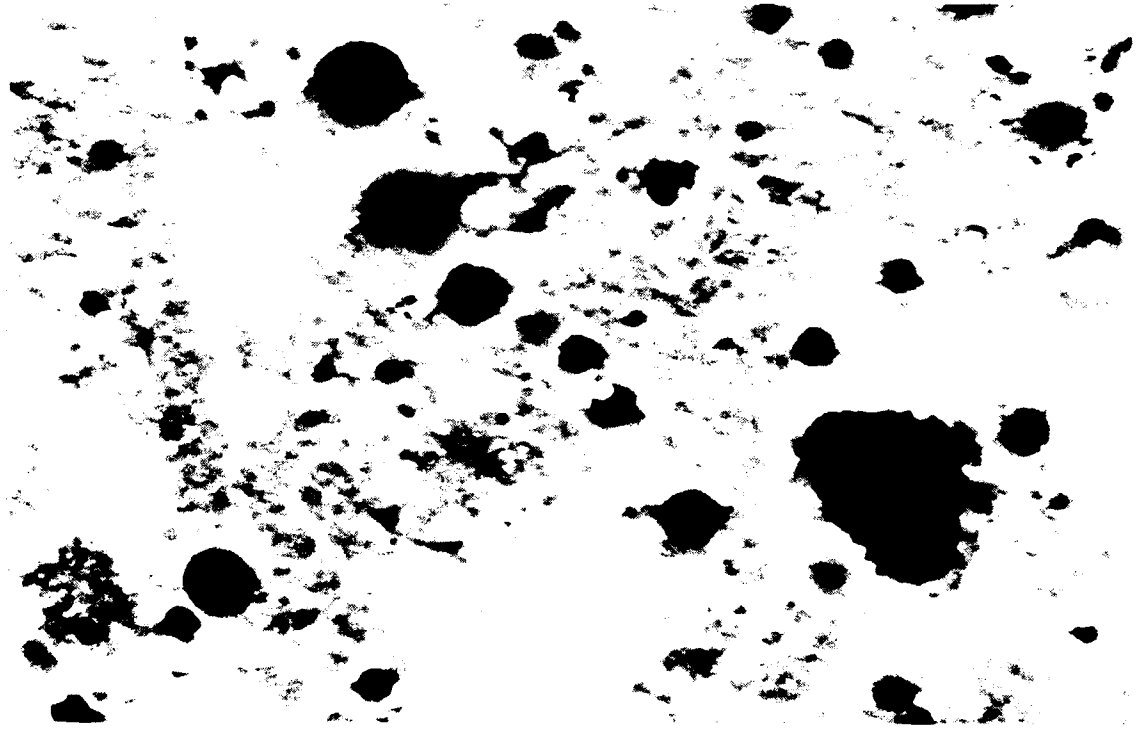

Figure C-4
Saturated sample prior to cycling, 25X. White regions are visible signs of efflorescence.

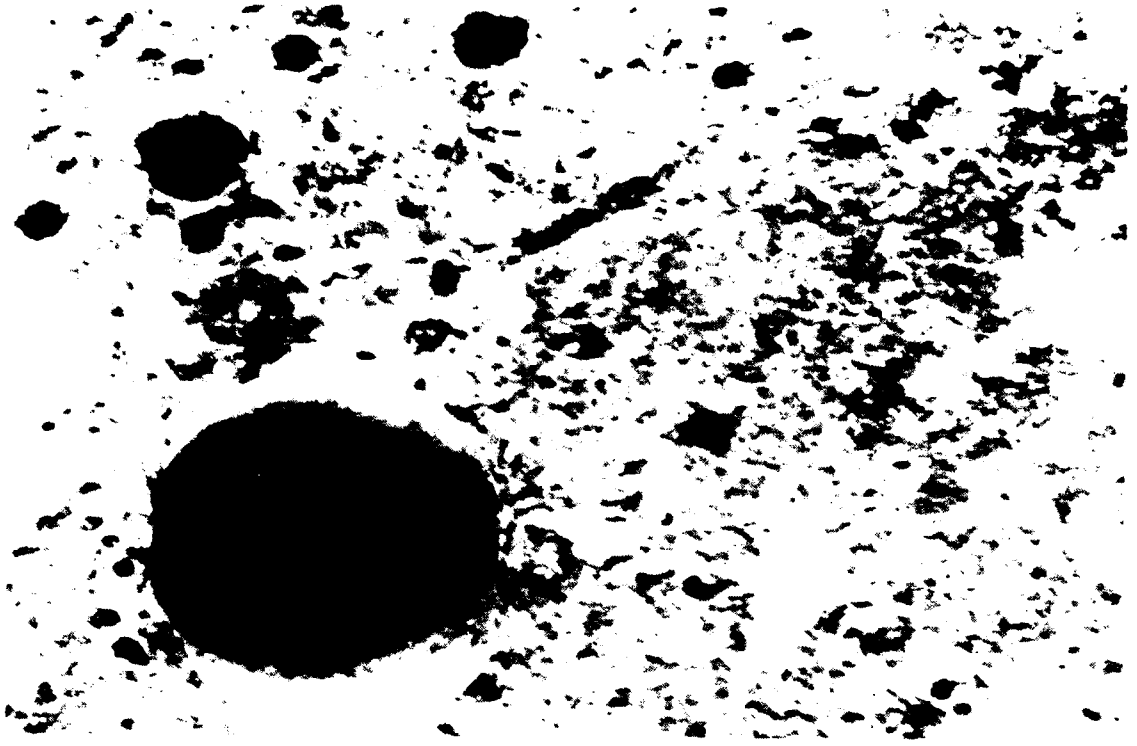

Figure C-5
Dry sample prior to cycling, 25X.

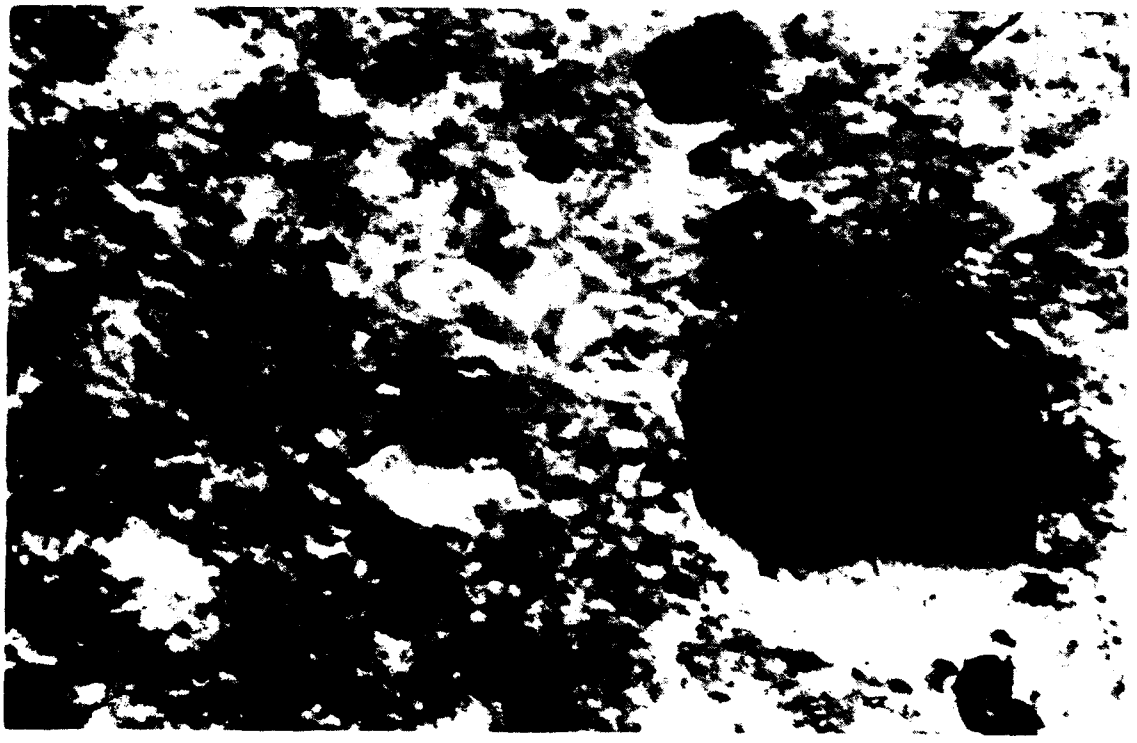

Figure C-6
Dry sample after six V/STOL cycles, 25X.

Explosive spalling occurred only on the saturated samples subjected to the simulated VSTOL. Figure C-8 shows an explosive spall that occurred on the first cycle after 50 seconds of heating. The dark portion in the center of the photograph is where the spall occurred. Figure C-9 shows a portion of the perimeter of the same spall. In this photograph, the concrete appears smooth whereas the region of the spall appears coarse. Figure C-10 shows another perspective of the same spall. This photograph shows a region where the cement paste became suspended above a piece of aggregate. In viewing this spall's crater from 3.3 to 40 times magnification, it was observed that the aggregate remained embedded in the concrete matrix and did not rupture. The sample shown in Figures C-8, C-9, and C-10 was the only sample out of four to exhibit an explosive spall on its cut surface.

Two saturated and one dry sample were subjected to one VSTOL cycle on an uncut surface. Explosive spalling occurred on both saturated samples. Figure C-11 shows one of the explosive spalls. The region of the spall appears coarse and is centrally located. In the spall's crater, a section of clear aggregate is exposed. This uncut surface has cement paste covering all aggregate and most of the entrained air voids. Explosive spalling did not occur on the dry sample.

OBSERVATIONS/COMMENTS

Cracking may have occurred as a result of two phenomena: thermal expansion and thermal shock. Aggregate and cement have different coefficients of thermal expansion. If the expansion rates are not identical, the concrete, upon heating, may relieve internal stress by cracking. In addition, concrete may undergo thermal shock during rapid heating or cooling. This temperature difference between the heated concrete and room temperature may have exceeded the point where cracking occurs in concrete.

The only concrete samples that exhibited explosive spalling were those that were saturated with deionized water and subjected to the VSTOL heating. Two uncut surfaces and one cut surface out of six saturated samples explosively spalled. Therefore, it appears that the most significant contributing factor to this type of spalling was the presence of trapped water in each sample. In addition, upon heating the saturated samples, a steam/water mixture was ejected from entrapped air voids and cracks adjacent to aggregate. This suggests that steam migrates throughout the concrete matrix. Thus, the added pressure from steam may have caused the explosive spalling in the saturated samples.

REFERENCES

C-1. Naval Air Warfare Center. Report SA-162R-91: Evaluation of an F/A-18 auxiliary power unit modified nozzle, by S.W. Houck, D.N. Gordge, and C.A. Hadfield. Patuxent River, MD, Jan 1992.

C-2. George Earl Troxell, Harmer E. Davis, and Joe W. Kelly. Composition and properties of concrete, 2nd edition. New York, NY, McGraw-Hill Book Company, 1968, pp 281.

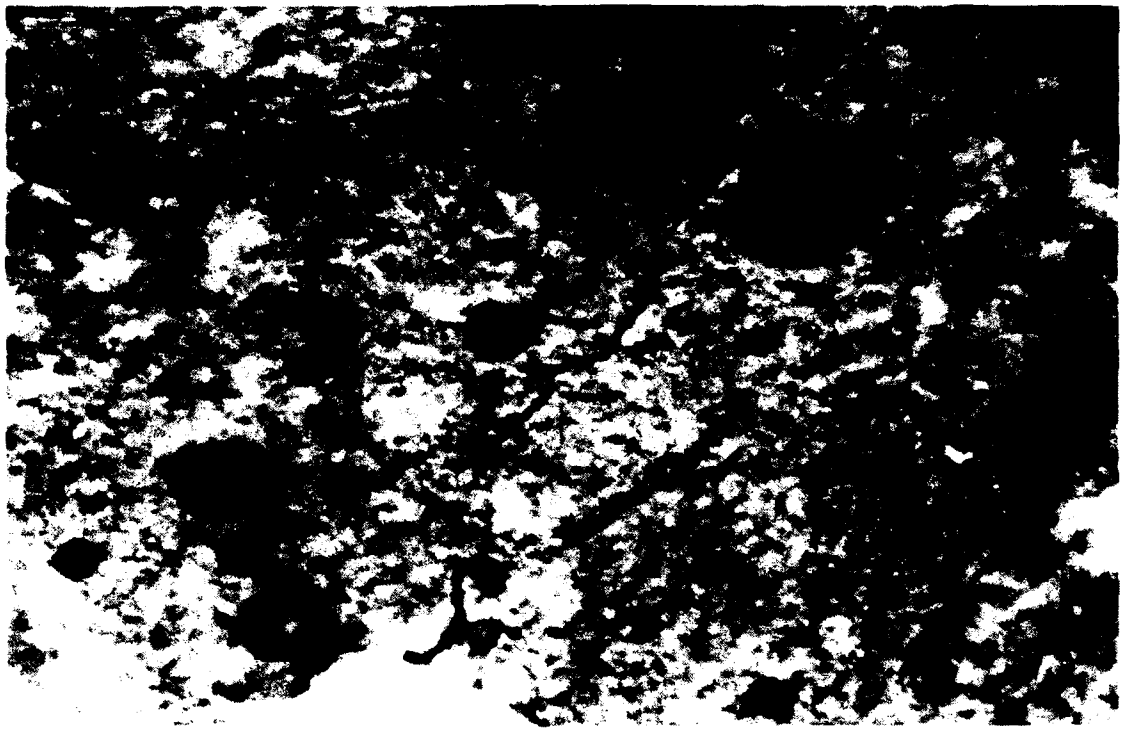

Figure C-7
Dry sample after six V/STOL cycles, 25X.

Figure C-8
Saturated sample showing explosive spall, 3.3X.

Figure C-9
Saturated sample showing concrete and a portion of the explosive spall's perimeter, 15X.

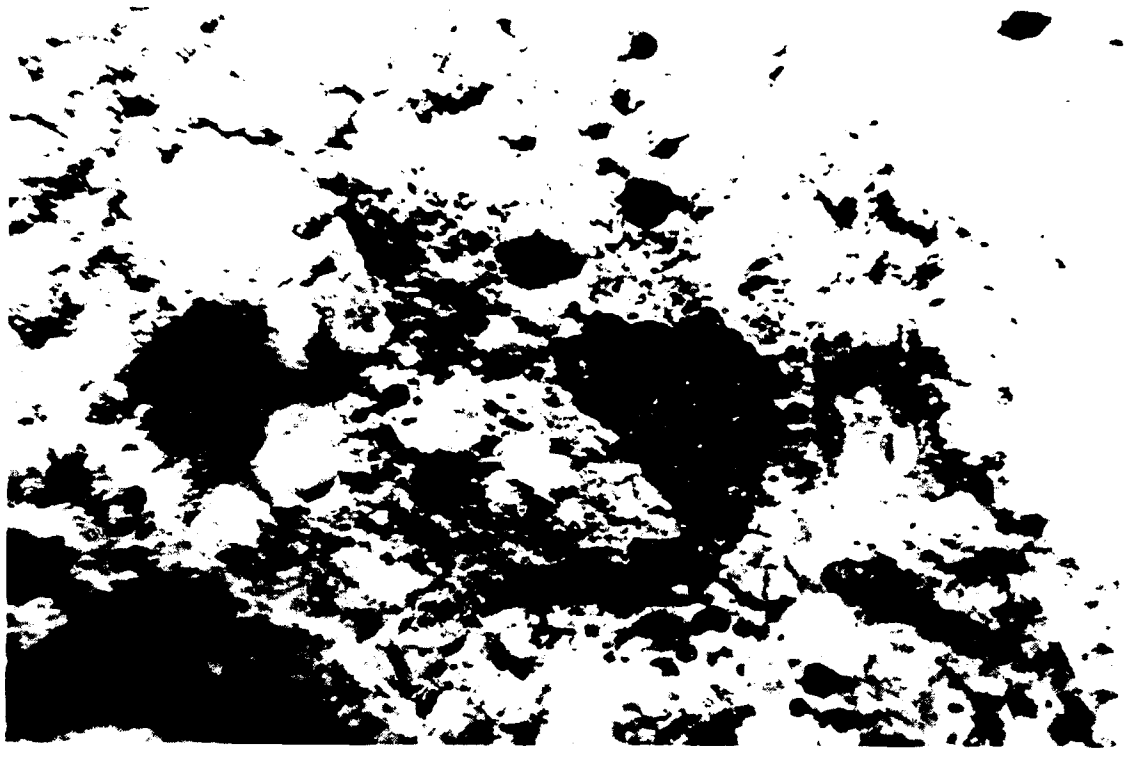

Figure C-10
Saturated sample showing explosive spall crater
with cement paste suspended above central dark aggregate, 15X.

Figure C-11
Saturated sample showing explosive spall on an uncut surface, 15X.

DISTRIBUTION LIST

ARMY CERL / LIB, CHAMPAIGN, IL
ARMY CRREL / CECRL-IC, HANOVER, NH
DTIC / ALEXANDRIA, VA
FAA / ARD 200 (TOMITA), WASHINGTON, DC
LANTNAVFACENGCOM / CODE 15C, NORFOLK, VA; CODE 411, NORFOLK, VA; LIBRARY, NORFOLK, VA
NAVFACENGCOM / CODE 13, ALEXANDRIA, VA; CODE 133, ALEXANDRIA, VA; DEL COLLO, ALEXANDRIA, VA; SKAR, ALEXANDRIA, VA
NAVSCOLCECOFF / CODE C35, PORT HUENEME, CA
NFESC ECDET / CECILIO, WASHINGTON, DC; JONES, WASHINGTON, DC
NORTHNAVFACENGCOM / TECH LIB, LESTER, PA; CODE 164P, SCHIAVINO, LESTER, PA
PACNAVFACENGCOM / CODE 102, PEARL HARBOR, HI; CODE 405, PEARL HARBOR, HI
SOUTHNAVFACENGCOM / CODE 102B, CHARLESTON, SC; CODE 4023, CHARLESTON, SC; LIBRARY, CHARLESTON, SC
SOWESTNAVFACENGCOM / CODE 161, TONG, SAN DIEGO, CA
WES / CODE GP HAMMITT, VICKSBURG, MS; LIBRARY, VICKSBURG, MS
WESTNAVFACENGCOM / CODE 411, SAN BRUNO, CA
WRIGHT LABORATORY / WL/FIVCO-OL, MURFEE, TYNDALL AFB, FL; WL/FIVCO-OL, RISH, TYNDALL AFB, FL